AD NUMBER
AD821823
LIMITATION CHANGES

TO:

Approved for public release; distribution is unlimited.

FROM:

Distribution authorized to U.S. Gov't. agencies and their contractors; Administrative/Operational Use; OCT 1967. Other requests shall be referred to Air Force Weapons Laboratory, Attn: WLDC, Kirtland AFB, NM 87117. This document contains export-controlled technical data.

AUTHORITY

AFWL ltr, 30 Nov 1971

AD821823

AN EXPERIMENTAL INVESTIGATION OF THE DYNAMIC RESPONSE OF MODEL SILO-TYPE STRUCTURES IN COHESIVE SOILS PHASE I, SOIL PROPERTIES

R. E. Olson   J. F. Parola

University of Illinois
Urbana, Illinois
Contract AF 29(601)-6811

TECHNICAL REPORT NO. AFWL-TR-67-16

OCTOBER 1967

AIR FORCE WEAPONS LABORATORY
Research and Technology Division
Air Force Systems Command
Kirtland Air Force Base
New Mexico

Research and Technology Division
AIR FORCE WEAPONS LABORATORY
Air Force Systems Command
Kirtland Air Force Base
New Mexico

AFWL-TR-67-16

AN EXPERIMENTAL INVESTIGATION OF THE DYNAMIC
RESPONSE OF MODEL SILO-TYPE STRUCTURES IN COHESIVE SOILS

PHASE I, SOIL PROPERTIES

R. E. Olson   J. F. Parola
University of Illinois
Urbana, Illinois
Contract AF 29(601)-6811

TECHNICAL REPORT NO. AFWL-TR-67-16

FOREWORD

This report has been reviewed and is approved.

MAYNARD A. PLAMONDON
1LT, USAF
Project Officer

ALLEN F. DILL
CDR, CEC, USNR
Chief, Civil Engineering Branch

GEORGE C. DARBY, JR.
COL, USAF
Chief, Development Division

ABSTRACT

(Distribution Limitation Statement No. 2)

A series of static and dynamic triaxial and one-dimensional compression tests was performed using specimens of Goose Lake clay compacted at a range of water contents from nine percent dry of optimum to three percent wet. This investigation was performed as the first stage of a general investigation of the interaction of cohesive soils and buried silos. The physical properties of the specimens were studied as functions of water content at compaction, stress level, and loading rate. Triaxial compression tests were performed using confining pressures ranging from 10 psi to 1000 psi and times to failure ranging from 3 milliseconds to 50 minutes. Both the compressive strength and the secant modulus increased significantly as the loading rate increased. Undrained one-dimensional compression tests were performed using rise times of 2 milliseconds and 10 seconds, and peak pressures of approximately 200 psi and 400 psi. The stress-strain characteristics were shown to depend on the water content at compaction and the loading rate.

(This page intentionally left blank)

CONTENTS

ILLUSTRATIONS

TABLES

ABBREVIATIONS AND SYMBOLS

γ_d Dry density, lbs/ft^3

w   Water content, %

m   Time, minutes

s   Time, seconds

ms   Time, milliseconds

       Norminal water content, %

t_f Time to failure

σ_3 Total minor principal stress, $lbs/in.^2$

$(\sigma_1 - \sigma_3)_f$ Compressive strength, $lbs/in.^2$

ϵ_f Axial strain at failure, %

E_s Secant modulus at 1% strain, $lbs/in.^2$

M_s Secant modulus at an incremental axial stress, $lbs/in.^2$

σ Total normal stress, $lbs/in.^2$

$\bar{\sigma}$ Effective normal stress, $lbs/in.^2$

μ_w Pore water pressure, $lbs/in.^2$

μ_a Pore air pressure, $lbs/in.^2$

X Bishop's factor, dimensionless

B_a Skempton's pore air pressure coefficient, dimensionless

A_a Skempton's pore air pressure coefficient, dimensionless

B_w Skempton's pore water pressure coefficient, dimensionless

A_w Skempton's pore water pressure coefficient, dimensionless

τ_f Shearing strength, $lbs/in.^2$

$\bar{\sigma}_n$ Effective stress normal to a failure plane, $lbs/in.^2$

$\bar{\phi}$ Effective angle of internal friction, dimensionless

$\bar{c}$ Effective cohesion, $lbs/in.^2$

ϕ_Q Total angle of internal friction determined using unconsolidated-undrained tests, dimensionless

d   Modified cohesion, $lbs/in.^2$

ψ	Modified angle of internal friction, dimensionless
ν_a	Volumetric strain under an all-around stress, %
ν_τ	Volumetric strain during shear, %
ν_t	Total volumetric strain, %
ν_{max}	Maximum volumetric strain corresponding to pressure saturation, %
ν_{dyn}	Assumed volumetric strain at failure in a dynamic test, %
$(\sigma_1 - \sigma_3)_t$	Compressive strength for a time to failure of t, lbs/in.^{2}
$(\sigma_1 - \sigma_3)_{1m}$	Compressive strength for a time to failure of one minute, lbs/in.^{2}
ϵ_a	Axial strain due to application of an equal all-around stress, %

(This page intentionally left blank)

SECTION I

INTRODUCTION

Experimental studies of the interaction of structures with cohesive soils may be performed either in the field on large sized structures or in the laboratory on models. Full-scale field tests are likely to provide the most accurate data, but the time and expense involved in such studies preclude their general use. As a result, attempts are being made to perform laboratory model tests using the largest practicable models.

One of the first problems that enters into such a laboratory study is the selection of a soil. From a theoretical point of view, the soil must possess certain physical properties in order to satisfy modeling laws, due consideration being given to the properties of the modeled structure as well. From a practical point of view, the soil must meet additional requirements. If the soil is to be used in a number of laboratories over some period of time, then a large quantity of reasonably uniform soil should be available. It would be highly desirable to have the soil available in air dried form in bags of about 100 pounds each. The soil should be sufficiently plastic to possess the properties usually associated with cohesive soils but should not be so plastic that specimen preparation techniques are made excessively difficult. If the plasticity is too low, then moisture control may become quite difficult. If the plasticity is too high, time dependent changes in properties will occur.

This investigation represents the first stage in a general model study of the soil-structure interaction problem in cohesive soils. In this first stage, past experience and a literature survey were used to select a soil that would meet the practical requirements previously discussed. A series of triaxial compression and one dimensional compression tests was performed to determine the range in physical properties that could be obtained by varying the compaction water content, the stress level, and the loading rate. Additional variables, such as type of compaction and compaction energy, influence the physical properties of the soil but could not be studied during this initial stage.

1

The various soils that were considered for use in this study are discussed briefly together with the criteria used in finally selecting one of these soils. The index properties of the chosen soil are presented. The remainder of the report is divided into two sections. The triaxial compression study is discussed in the first section and the one-dimensional compression study is covered in the second. In each of these sections, consideration is given to the experimental program, the design and operation of the equipment, the experimental data, and finally to the interpretation of these data.

SECTION II

SOIL SELECTION

Selection of a soil to be used in these experiments was based
on the following criteria:

1. The soil should be cohesive.
2. The soil should be available to others in large
   quantities.
3. The soil should be such that a wide range in physical
   properties of the compacted specimens could be obtained
   by suitable variation in the placement procedure or
   water content.
4. It would be preferable to use a soil that had been used
   on other projects so that some of its properties would
   already be known and previous experience could be used
   to a maximum extent.
5. For economic reasons involved with the preparation of
   large specimens, it would be preferable to use a soil
   that would be available in air dried, powdered, form and
   which would mix with water readily. Further, the soil
   should not have such a high dry strength that air drying
   and repulverization would be excessively difficult.

The soils that were given consideration included the following:
Kaolin Kaolin clays are available from a number of commercial suppliers.
Kaolin clay used for other work at the University of Illinois was
supplied by the Minerals & Chemicals Philipp Corporation, and is known
as pulverized Klondyke clay. Generally, air dry Kaolin clays are avail-
able in bags of about 100 pounds. The clay has usually been water washed
to remove coarse grained constituents, indlucing quartz and mica, and
water scluble salts. The clay is then dried and pulverized so that it
is shipped as a fine, white powder. The untreated clay can also be
obtained but is not likely to be so uniform from one shipment to the
next.

Based on a survey of the literature, it appears that the liquid
limits of commercially supplied kaolins range from about 25 percent to

3

70 percent. However, conversations with others who have used the clay for model tests, together with our own experiences, indicate that kaolin acts as if it were a silt and thus dries quickly, has a very low dry strength, and a low tensile strength when compacted. The clay has proved difficult to work with because it dries so quickly that moisture control is difficult. Further, the clay used in bearing capacity tests on model footings by one investigator, tended to fail in tension rather than in shear and thus did not exhibit properties typical of natural clays.

Montmorillonite There are also a number of commercial suppliers of montmorillonite (bentonite). This clay is widely used as a drilling mud and is thus readily available in large quantities. The montmorillonite that has been used at the University of Illinois was supplied by the American Colloid Company. They supply either sodium or calcium bentonite. The clay is supplied in bags of about 100 pounds, containing pulverized clay of a relatively low water content. Depending on the adsorbed cations, the liquid limit of bentonitic clays ranges from perhaps 150 percent (with many impurities present) to about 800 percent. The clay is very difficult to mix and compact, and its properties change markedly with time after compaction.

Grundite This clay is supplied by the Illinois Clay Products Company. It is supplied in air dried, pulverized, form in bags of about 100 pounds each. The clay is mostly illite but contains a substantial amount of silt- and sand-sized particles. It has a liquid limit of about 60 percent and is classified as a CH in the Unified Soil Classification System. It has a high dry strength and other properties associated with clays of moderately high plasticity. The properties of this clay have previously been studied at the University of Illinois[1] and at Northwestern University[2].

Goose Lake Clay The Goose Lake clay is also supplied by the Illinois Clay Products Company. It is supplied in air dried form in bags of about 100 pounds each. The most common clay mineral is kaolinite with illite as a secondary constituent. The clay is all finer than the #30 sieve and about 34 percent is finer than two microns. It has a liquid limit of about 31 percent. At the present time the Illinois Clay Products Company estimates that they have reserves of Goose Lake clay for

4

about 40 years at the present rate of use. They can supply the clay at $11.25 per ton in 100-pound bags, 30 bags to a pallet, in truckload lots of 30,000 to 36,000 pounds each.

Other Clays A variety of other clays were also considered. There are many suppliers of clay to the ceramic industry. They can provide clay with a wide range in physical properties. Also considered were such natural clays as Boston Blue clay, Vicksburg loess, Vicksburg Buckshot clay, and Fithian Illite because various investigators have reported experiments using these materials. They were not recommended for use on this project because of the difficulties involved in obtaining large quantities of uniform material over a period of years. Processing problems could also be severe with some of these clays.

After consultation with the project monitor, Goose Lake clay was selected as the most suitable for use during this investigation.

5

SECTION III

INDEX PROPERTIES OF GOOSE LAKE CLAY

The index properties of the Goose Lake clay include:

liquid limit	31 percent
plastic limit	17 percent
shrinkage limit	15 percent
specific gravity	2.72

The grain size distribution curve (Figure 1), obtained using standard ASTM procedures (ASTM D421-58 and D422-63) indicates that the soil is 9 percent sand (coarser than 0.06 mm), 57 percent silt (0.06 mm to 0.002 mm), and 34 percent clay (finer than 0.002 mm). Hence the activity[3] is 0.41. In the Unified Soil Classification System the soil is classified as CL.

The standard (ASTM D698-64T) and modified (ASTM D1557-64T) moisture-density curves for Goose Lake clay are shown in Figure 2. The maximum dry densities and optimum water contents are:

Test	Maximum Dry Density, pcf	Optimum Water Content, percent
Standard	112.7	14.5
Modified	124.5	11.3

An X-ray diffraction analysis[4] indicated that the finer-than-two-micron fraction was 20-25 percent quartz, 10-15 percent illite, and about 65 percent kaolinite.
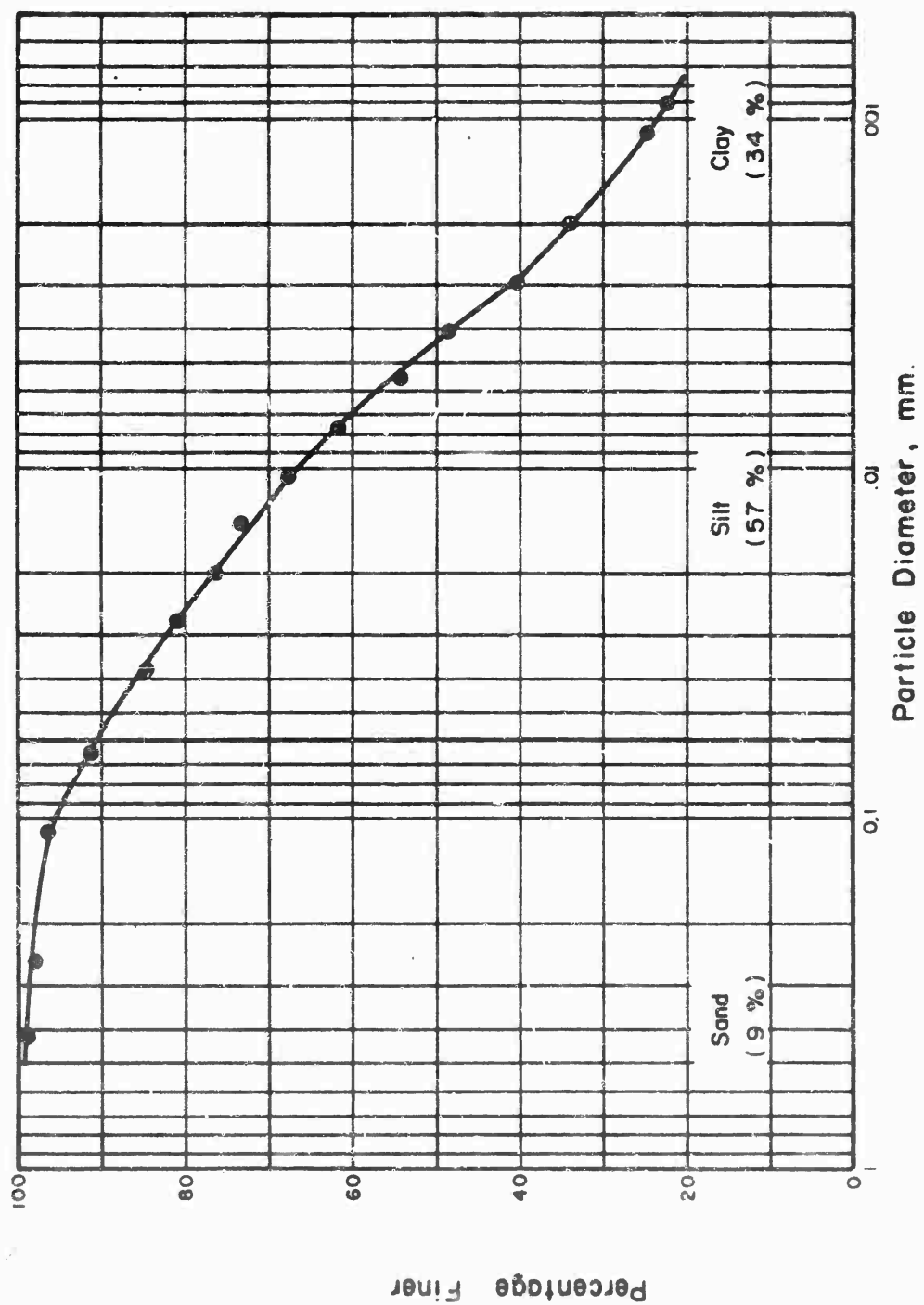
Figure 1. Grain Size Distribution of Goose Lake Clay
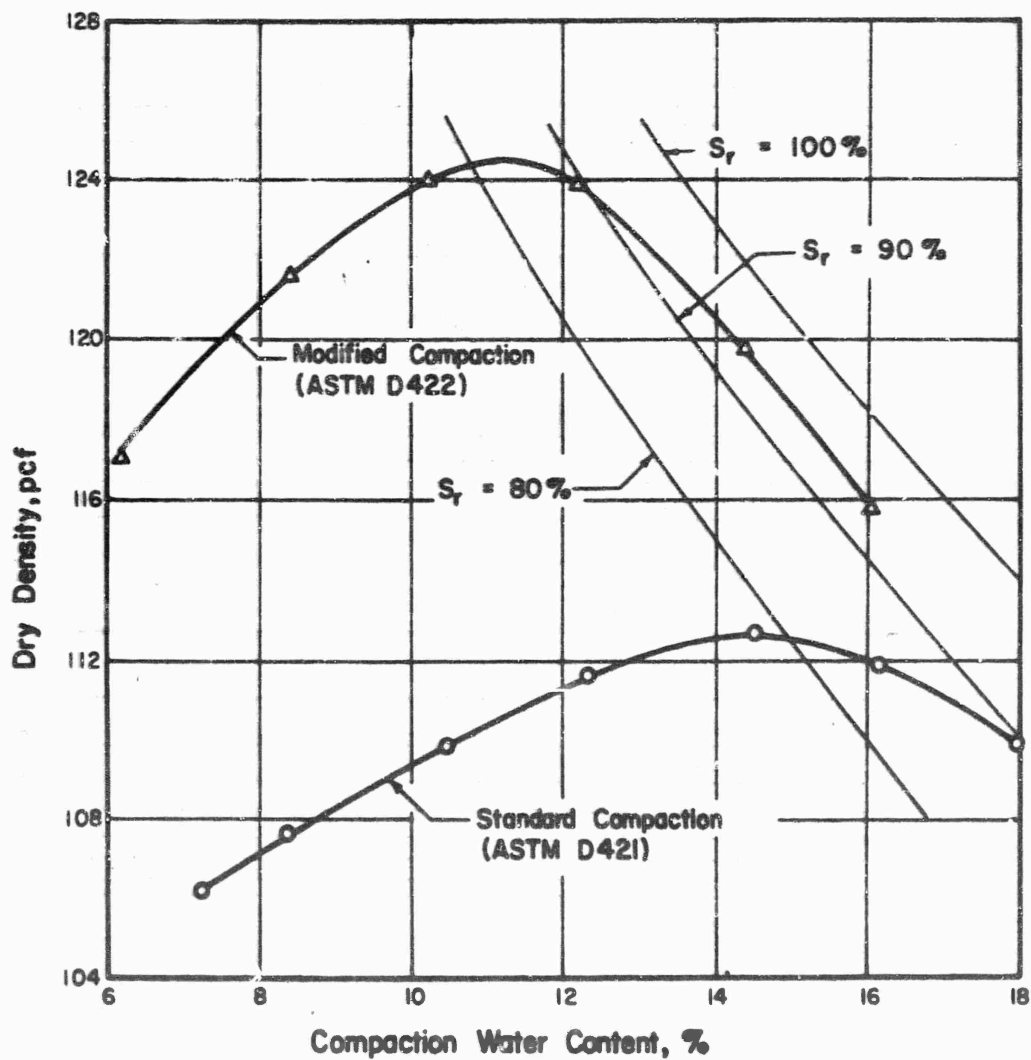
Figure 2. Compaction Curves for Goose Lake Clay

SECTION IV

TRIAXIAL SHEAR TESTS

Apparatus for Triaxial Shear Tests

Compaction equipment. All specimens used in the triaxial
shear testing program were 1.5 inches in diameter and 3.0 inches high
(nominal dimensions). They were prepared by kneading compaction in a
three-part split compaction mold (Figure 3), using a wedge-shaped
compaction foot with a 30-degree apex angle. The compaction pressure
was applied by hand, using a lever arm system (Figure 4). The force
actually applied to the foot was measured by using a proving ring.

Low-pressure static triaxial equipment. As a matter of con-
venience in nomenclature, in subsequent discussions the term low pres-
sure will be used to indicate triaxial tests in which the confining
pressure is 120 psi or less. The term static will be used for tests
in which all stress-strain data could be hand recorded, i.e., for times
to failure longer than perhaps two minutes.

The low-pressure static triaxial compression tests were per-
formed using standard English triaxial cells[5]. Water was used as the
confining fluid. The confining pressure was maintained by using mercury
control apparatuses[5]. Volume change, under the actions of both the
hydrostatic confining pressure and shearing stress, was measured by using
a single buret volume change apparatus. This apparatus consists of a
buret with a water-kerosene interface connected in series between the
self-compensating mercury control apparatus and the triaxial cell so
that any flow of fluid into, or out of, the triaxial cell must cause a
displacement of the interface. The displacement of the interface, cor-
rected for volume change of the equipment, is equal to the volume change
of the soil specimen. Axial loads were applied to the soil specimens at
a constant rate of deformation using a 10-ton mechanically driven press.
The axial force was measured outside the triaxial cell by using a cali-
brated proving ring. All data were hand recorded. Figure 5 shows a
static, low-pressure test in progress.

9

Figure 3. Mold Used in the Preparation of Specimens
for Triaxial Shear Testing

10
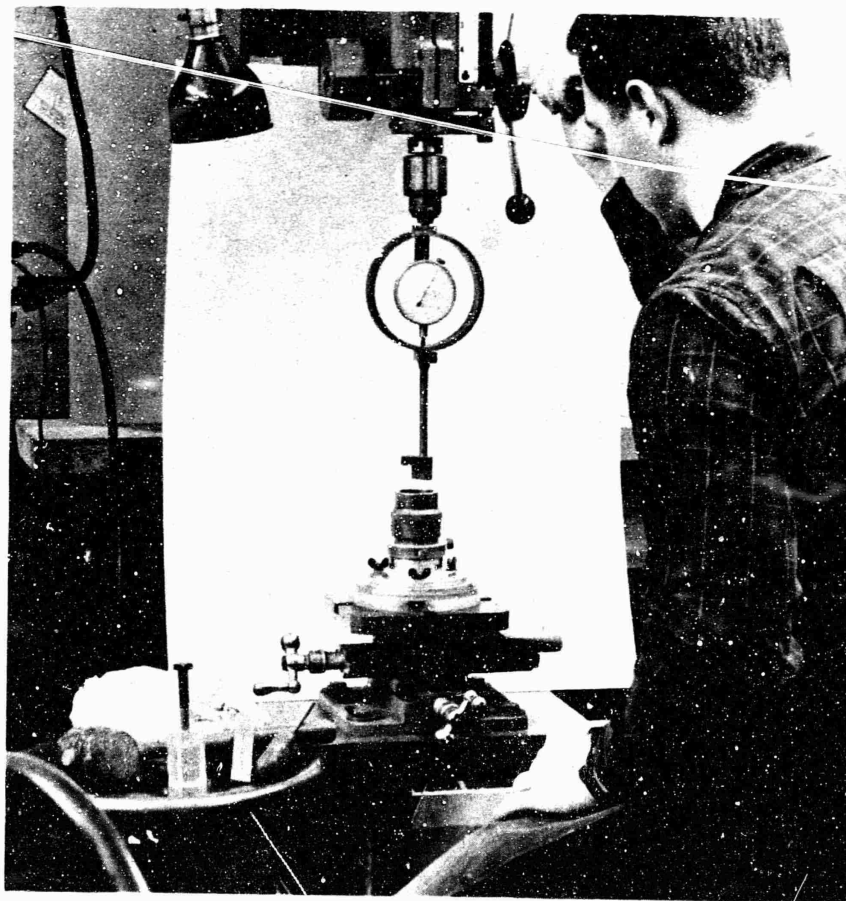
Figure 4. Compaction of a Specimen for Triaxial Shear Testing
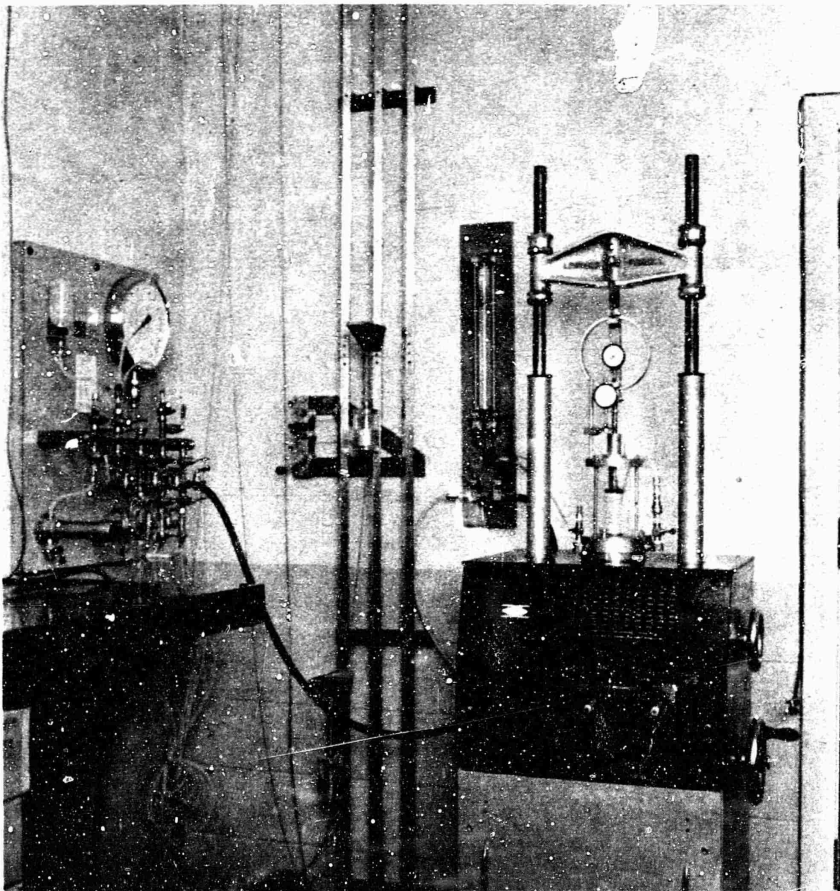
Figure 5. Apparatus for a Static, Low-Pressure
Triaxial Shear Test

<u>High-pressure equipment for static triaxial tests</u>. The term
<u>high pressure</u> is used here for the tests in which the confining pressure
was 400 psi or 1000 psi. The high-pressure static triaxial compression
tests were performed using a cell developed during a previous project[6]
with certain modifications. A cross section through the original cell
is shown in Figure 6. The cell was machined entirely from steel with
the structural parts designed for safe operation at pressures up to
2000 psi.

The axial load is applied to the soil specimen, using a 0.750-
inch diameter stainless steel piston that passes through two ball bush-
ings and a quad-ring seal in the top of the cell. The force applied to
the specimen is measured by using a load cell mounted directly beneath
the specimen. The load cell developed for the previous project[6] con-
sisted of a steel tube with four strain gages mounted on the inside and
wired as a four-arm bridge. This cell had a capacity of about 7000 pounds
and a constant of 5.13 lbs/micro-in./in. It performed quite satisfac-
torily on the previous project because the signals were amplified for
automatic recording. However, for static tests it is convenient to use
a strain indicator to read the load cell. If the strain indicator is
read to within 5 micro-in./in., then the load applied to the specimen
would be known with an accuracy of only about $\pm$ 25 pounds.

To improve the sensitivity, we developed another load cell,
which consisted of three separate load cells spaced 120 deg. apart at
radial distances of about 7/8 inch from the center line of the specimen
(Figure 7). Each of the three load cells was equipped with a full four-
arm strain gage bridge mounted in the 0.1562-inch diameter hole in the
center of the load cell. The three load cells, acting together, had an
operating capacity of 1800 pounds and a constant of 0.276 lbs/micro-
in./in. This triple load cell was used successfully for the static
high-pressure tests.

The axial deformation of the specimen during a shear test was
determined by measuring the relative movement between the loading
piston and the top of the triaxial cell using a dial indicator reading
to 0.001 inch.

The volume change of the specimen due to the application of the
hydrostatic stress, could not be measured directly with this apparatus.

13
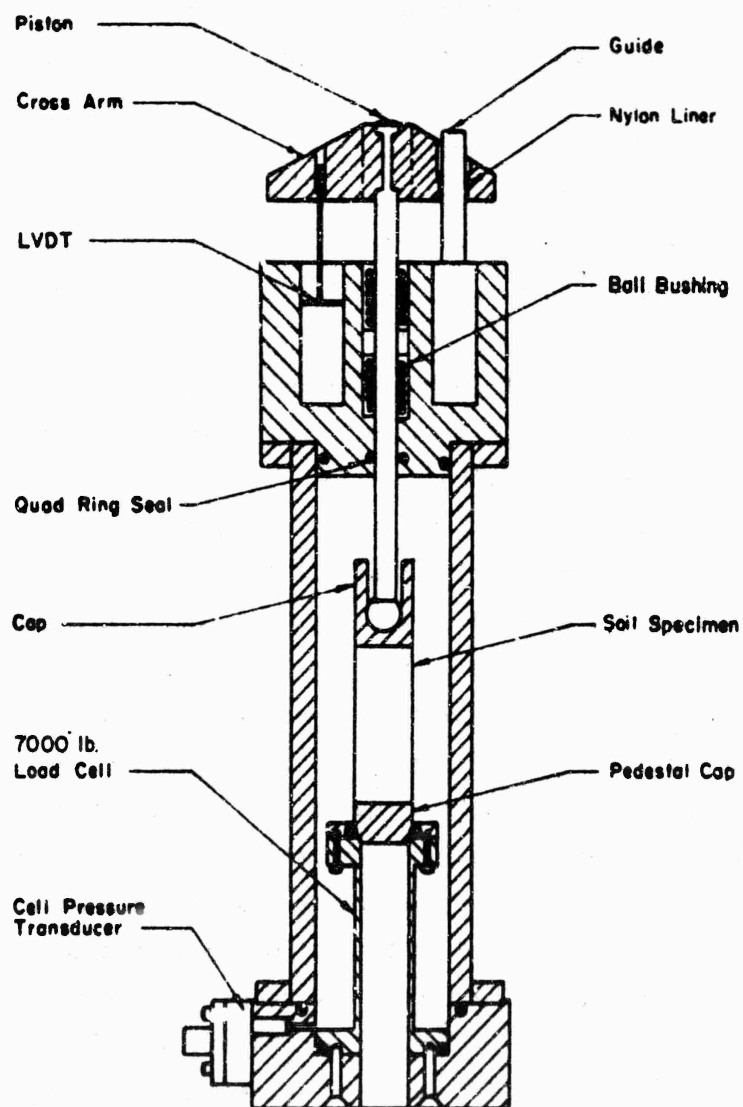
Figure 6. High-Pressure Triaxial Cell
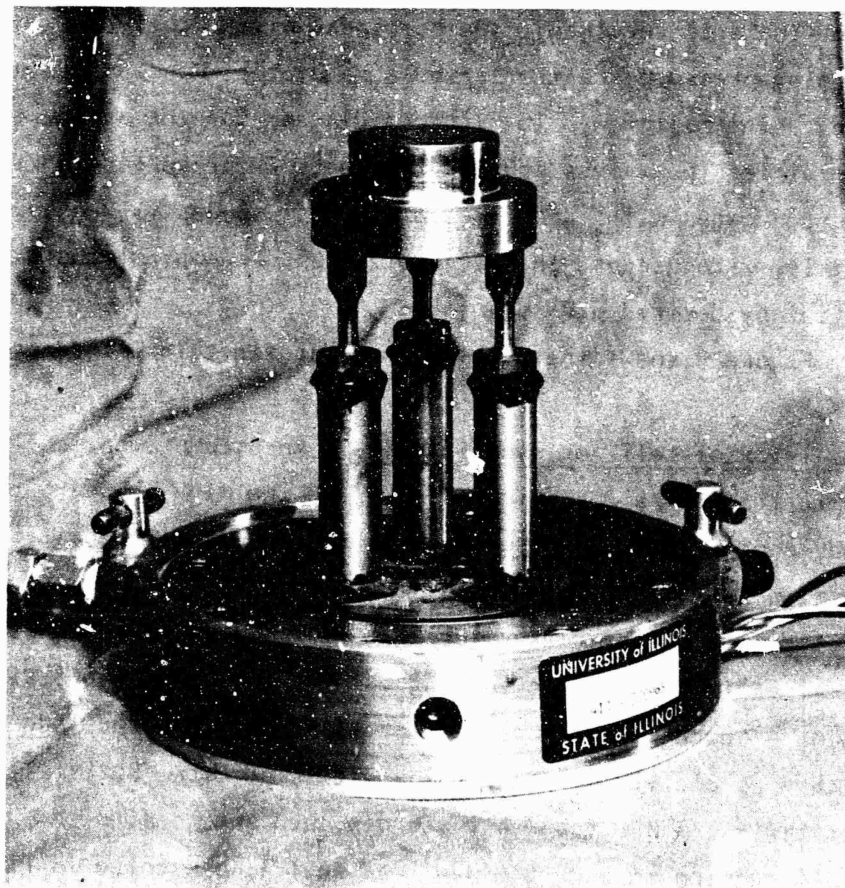
Figure 7. Triple Load Cell for High-Pressure
Triaxial Shear Tests

An approximation was obtained by using the loading piston and deformation dial to measure the axial strain that occurred when the hydrostatic pressure was applied, and then assuming that the volumetric strain was three times the axial strain. There was no provision made for the measurement of volume change during shear.

To prevent gas leakage through the membranes surrounding the soil specimens, the cell was filled with mercury to an elevation above the top of the soil specimen. The remainder of the cell contained air. The confining pressure, controlled by a regulator, was applied above the mercury by using nitrogen. The circuit diagram for the pressure panel board containing the valves and Bourdon gages is presented in Figure 8. Three Bourdon gages with capacities of 100 psi, 600 psi, and 3000 psi, respectively, were used so that accurate pressure control could be achieved in any desired pressure range.

Figure 9 shows the high-pressure static triaxial compression apparatus.

Triaxial cell for dynamic tests. An attempt was made to perform the dynamic triaxial compression tests using the high-pressure cell just discussed, equipped with the sensitive triple load cell. However, in every test there was so much "noise" that the load in the specimen could not be determined with necessary accuracy. It was found that firing the loading valves in the dynamic loading machine (see subsequent discussion) was sending a shock wave through the press and up into the load cells and causing them to oscillate. To eliminate this problem, but still achieve high sensitivity, a new load cell was designed and constructed.

A section through the new load cell is presented in Figure 10. The load-sensing part of this cell has an outside diameter of 1.00 inch and a wall thickness of 0.05 inch. It has a full four-arm bridge using semiconductor strain gages that have a resistance of 125 ohms each and a gage factor of 135. The capacity of this load cell is about 2000 pounds and the constant is 0.0287 lbs/micro-in./in. The constant was unaffected by the application of confining pressures up to 1000 psi. The constant was checked several times during the investigation and was found not to vary. This load cell was used for all tests except a few in which more than 2000 pounds of load was required. The load cell mounted in the base of the triaxial cell is shown in Figure 11.

16
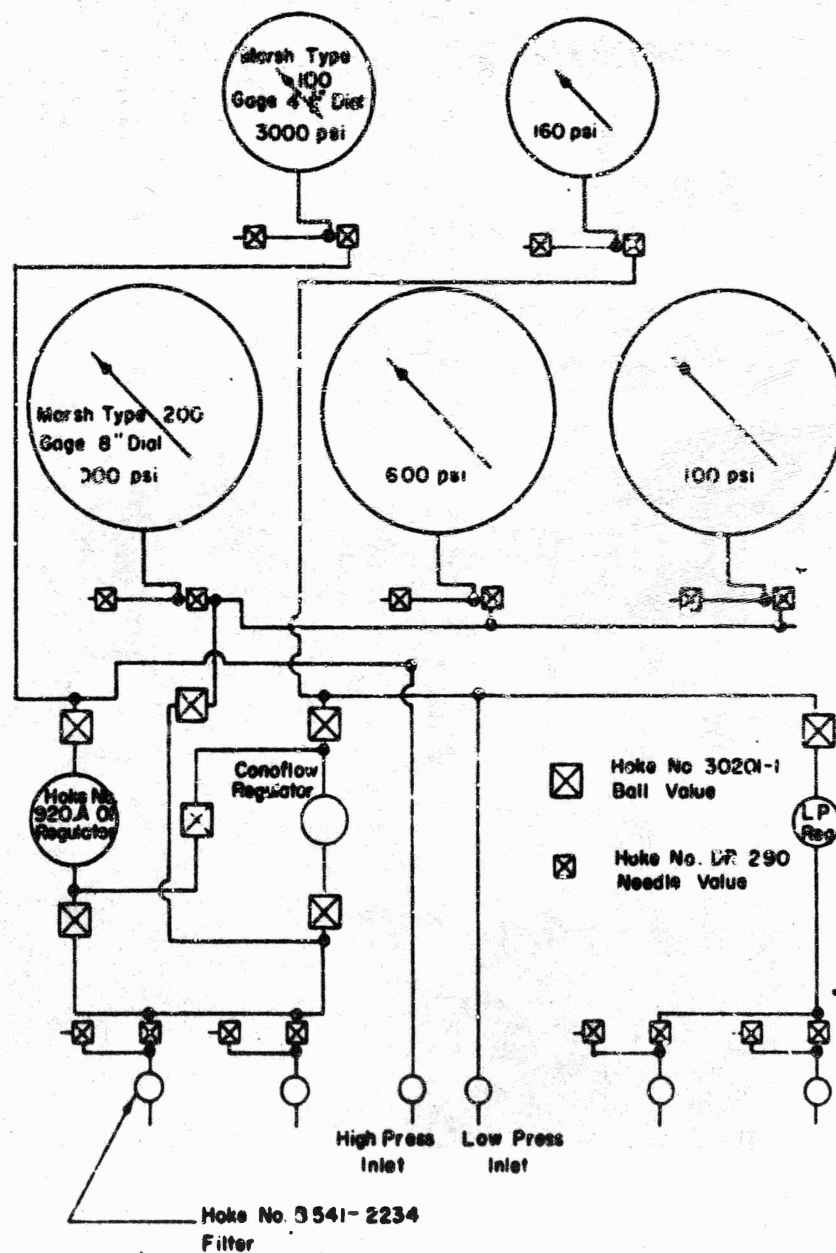
Figure 8. Cell Pressure Panel Board Circuit
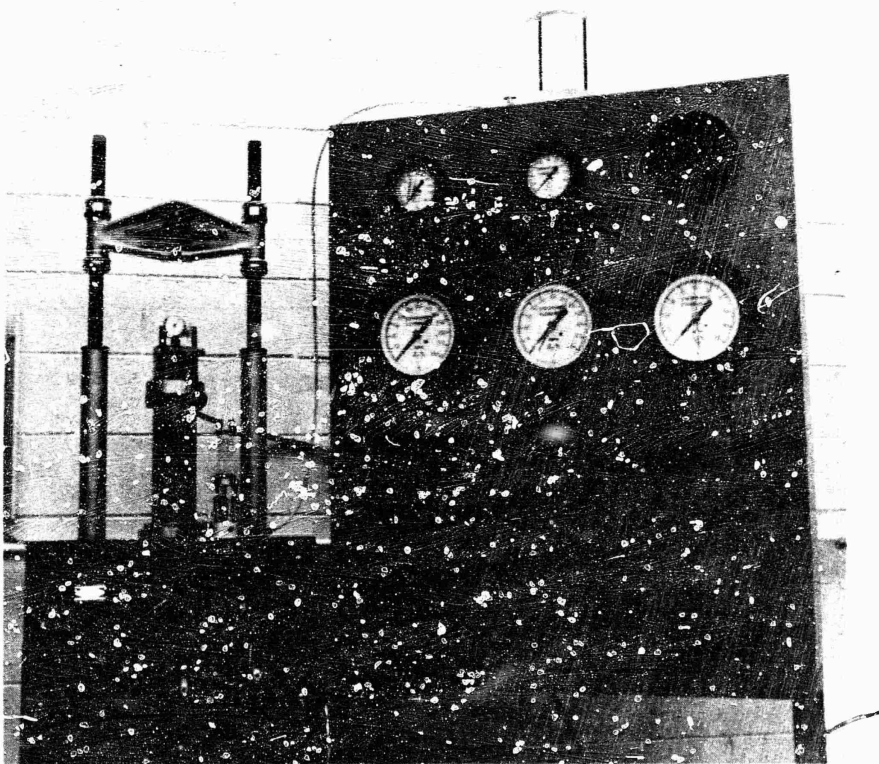
Figure 9. High-Pressure Static Triaxial Shear Apparatus

18

NOTE: All Dimensions In Inches.

Figure 10. 2000-Pound-Capacity Load Cell

Figure 11. Triaxial Cell Used for the Dynamic Tests

The deformation of the soil specimen was measured using a linear variable differential transformer (LVDT) having a travel of plus and minus 0.75 inch. The coils of the LVDT were mounted in the top of the triaxial cell. The core was attached to a cross arm (Figure 11) which, in turn, was rigidly attached to the loading piston. Thus, relative movements between the piston and the top of the cell were measured. However, because the load cell beneath the specimen was relatively incompressible, the LVDT also measured the deformation of the specimen. The upper end of the LVDT core was threaded into the cross arm and thus allowed adjustment of the core just prior to each test. The core was locked in position by a set screw.

For the dynamic tests, the cell was filled with mercury to above the top of the soil specimen during the pressurization stage but was drained just prior to shear.

Dynamic loading press. The loading press used for the dynamic tests was the one developed during a previous project[6]. A schematic drawing of the press is shown in Figure 12. The press consists of four parts: a heavy steel base upon which the triaxial cell is mounted; two heavy Acme threaded shafts that support the "loading machine;" the loading machine; and a cross head with a capsten which is used to position the loading machine.

The essential part of the loading press is the loading machine (item E, Figure 12). A schematic view of the loading machine and the associated hydraulic system is shown in Figure 13. The specimens are loaded by applying a pressure to the "main piston" of the loading machine (Figure 13) and forcing this piston to move downwards at a predetermined rate. The machine may be operated pneumatically or hydraulically. Pneumatic operation yields the higher rates of deformation.

For pneumatic operation, any oil beneath the main piston is exhausted into the upper oil container (Figure 13) so that the space beneath the main piston is occupied only by air. An air pressure is applied to the base of the main piston to force the piston to the top of its travel, and then the space beneath the piston is vented to the atmosphere. The main valve is lowered to the position shown in Figure 13 and is held down by a mechanical device termed a "trigger." The

21
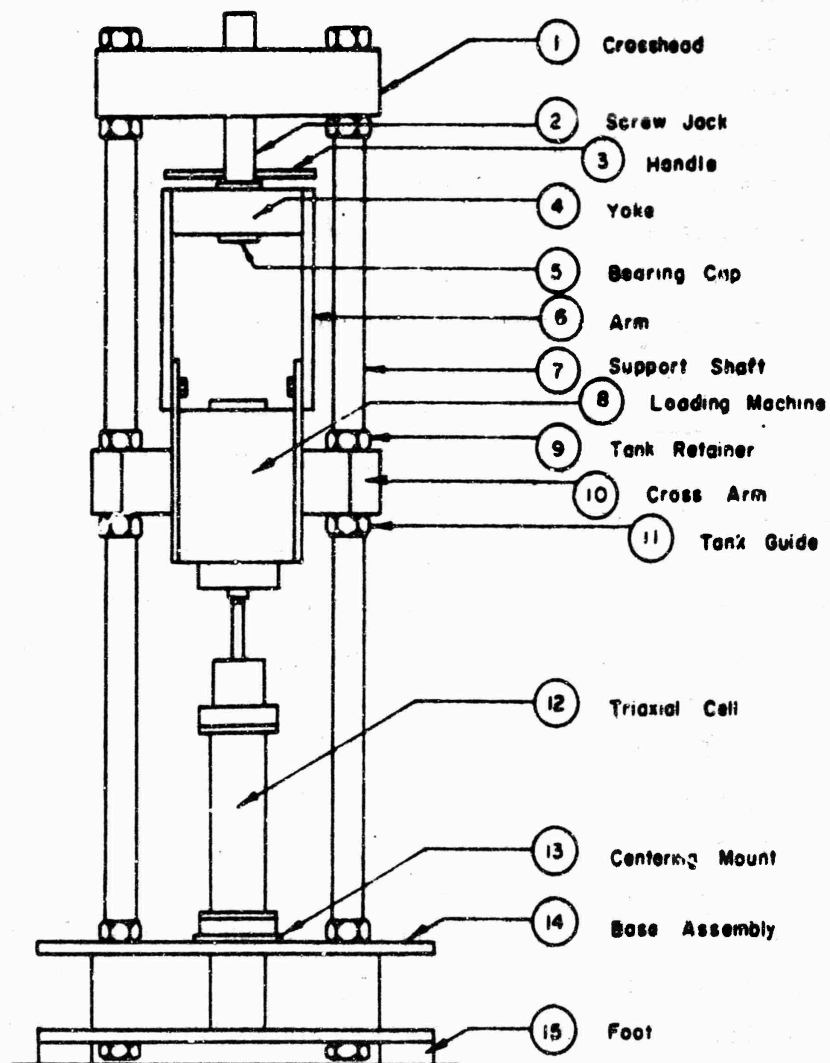
Figure 12. Dynamic Testing Frame

1	Crosshead
2	Screw Jack
3	Handle
4	Yoke
5	Bearing Cup
6	Arm
7	Support Shaft
8	Loading Machine
9	Tank Retainer
10	Cross Arm
11	Tank Guide
12	Triaxial Cell
13	Centering Mount
14	Base Assembly
15	Foot
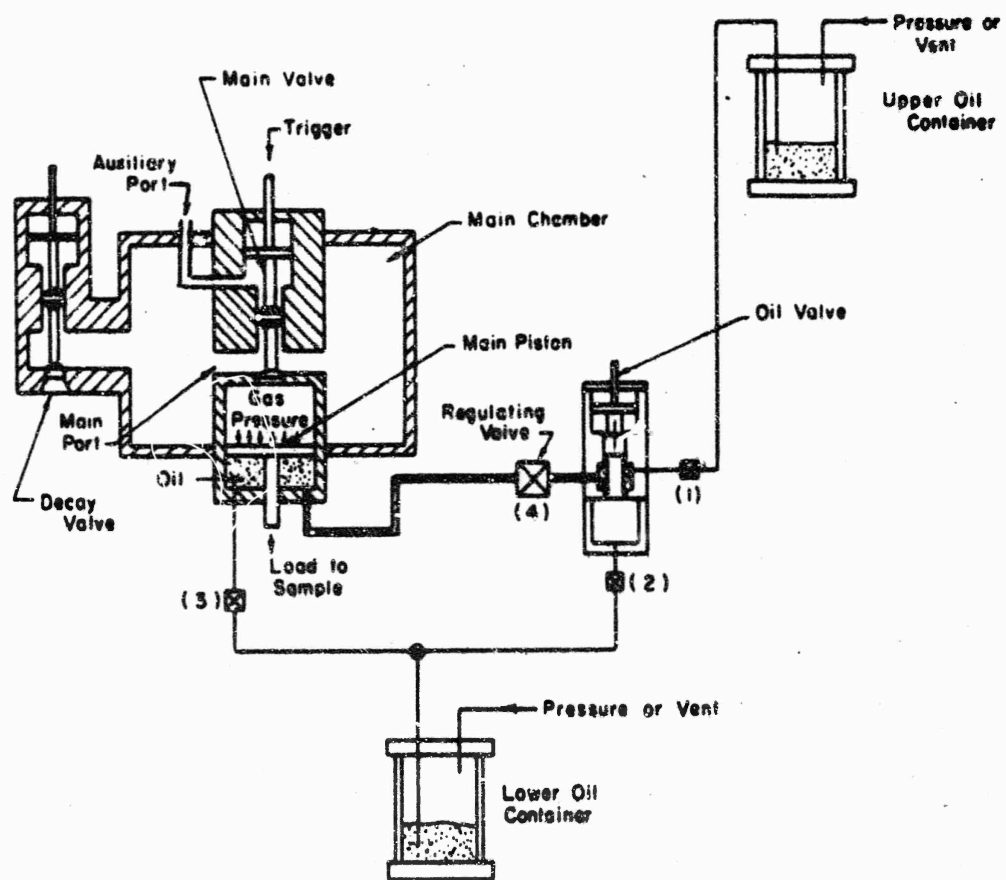
Figure 13. Hydraulic System

"decay valve" is closed. Nitrogen is then let into the main chamber until some predetermined pressure is attained. This pressure is unable to act upon the main piston because the main valve is in the down (closed) position. A nitrogen pressure is applied to the flange on the upper part of the main valve but upwards movement of this valve is prevented by the trigger. The trigger can be released ("fired") by using a solenoid and a mechanical lever system. If a 400-psi pressure is used through the auxiliary port, the main valve accelerates from rest to a velocity of about 400 inches per second during the first 0.5 inch of travel and has attained this terminal velocity before the main ports start to open. Thus, the main ports open over a period of only a few milliseconds. When the main ports open, the nitrogen from the main chamber rushes through the main ports and applies a pressure to the main piston which moves downwards to load the specimen. If the main chamber is filled with nitrogen at 400 psi, a 3-inch high soil specimen can be subjected to 20 percent strain in about 3 1/2 ms. Higher loading rates could be obtained by using helium in place of nitrogen and by replacing the steel main piston with one made of aluminum.

For slower loading rates, the main valve is raised, the space beneath the main piston is filled with oil, the decay valve and oil valves are closed, valves 3 and 1 (Figure 13) are closed, valve 2 is opened, and a gas pressure is applied to the main piston. Thus, the oil is subjected to a pressure in a closed system. When the oil valve is "fired" the oil can escape through the regulating valve (No. 4) and through valve 2 into the lower oil container. The rate of loading of the soil specimen is controlled by the nitrogen pressure applied to the main piston, by the viscosity of the oil, and by the setting of the regulating valve. For this project, times to 20 percent strain of a 3-inch tall soil specimen were in the range from 40 ms to 1 minute when the hydraulic system was used.

Electronic instrumentation. The instrumentation system utilized a 4-channel 20kc carrier amplifier system. Output signals from the load cell and LVDT were simultaneously recorded on paper, using an oscillograph with paper speeds up to 64 inches per second, and an 8-channel FM tape recorder. A timing trace of 10kc was recorded on the

24

magnetic tapes. A preset counter was used to provide a known delay time between the moment when the switch to start a test was thrown, and the moment of firing of the trigger solenoids. The preset counter was used to give the oscillograph and tape recorder sufficient time to accelerate to their proper operating speed. A delay of 300 ms was used. The recording equipment was automatically shut off after some predetermined time. The recording system is shown in Figure 14.

An X-Y plotter was used to plot the magnetic-tape data immediately after the hydraulic tests. For pneumatic tests, the FM tapes were reduced by sampling each recording channel at 1000 locations, evenly spaced, through any desired time range, storing the data in memory, and then typing out the data in any desired combination.

Experimental Procedures

Specimen preparation. The soil to be used for a series of specimens was mixed in a mechanical mixer with a suitable amount of water and stored in a plastic bag for approximately five days before compaction. A water content specimen was taken immediately after mixing. If the water content was outside of the range considered suitable, then either additional moisture was mixed into the soil or else the soil was allowed to air dry by a suitable amount. The soil was remixed by hand inside the plastic bag just prior to compaction of the specimens.

The specimens were prepared by kneading compaction using a nominal foot pressure of 100 psi, 10 layers, and 8 strokes per layer. Each layer was scarified prior to compaction of the next layer to ensure adequate bonding between layers. After compaction, the top and bottom of the specimens were trimmed flush with the mold and then the mold was disassembled. The specimen was weighed to within 0.03 grams and its height and diameter measured using a dial comparator. The specimens were placed in waterproof rubber membranes and stored under water for several days prior to shear.

Performance of low-pressure static tests. The specimens were removed from the water bath. The wet weight of the specimens were obtained and checked with the initial wet weight to ensure against the possibility of leakage during storage. A 1/2-inch wide strip of filter paper was wrapped once around the interface between the soil and each

25
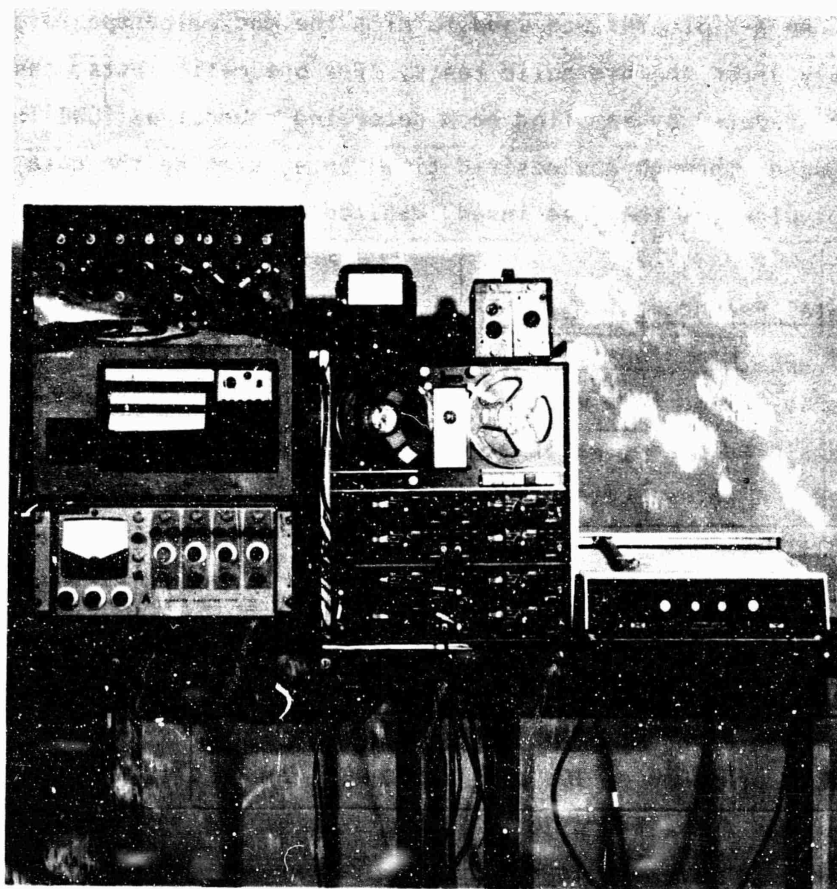
Figure 14. Recording System Used for the Triaxial Shear Tests

end cap to prevent forcing the membrane into this interface, and the specimens were then placed between two rigid plastic discs and surrounded by two thin rubber membranes.

The two pore water pressure connections in the base pedestal of the triaxial cell were thoroughly saturated with water. The soil specimen was placed on the pedestal, with the specimen still sealed between the impervious plastic discs. A metal loading cap containing a stainless steel ball was placed on the top cap. The triaxial cell was then assembled and filled with water in such a way as to exclude all air bubbles. The three nuts used to hold the cell together were tightened using a special torque wrench so that the compressibility of the cell would be reproducible.

A seating pressure of 3 psi was applied by using the mercury control apparatus. The single buret volume change apparatus was then connected in series with the cell. The final cell pressure was applied and the specimen was given 15 minutes to equilibrate. The volume change of the specimen was then obtained as the difference between the measured total volume change and the known volume change of the cell. The height of the specimen was then measured by using a cathetometer.

The loading piston was brought into contact with the loading cap and the axial load was applied at a constant rate of deformation. The load was measured by using a proving ring exterior to the cell. The axial deformation was measured using a dial indicator and the volume change was measured using the single buret apparatus. A test in progress is shown in Figure 5.

At the conclusion of the test the apparatus was dismantled and the entire soil specimen was used to determine the water content.

The data were reduced, and complete stress-strain curves were plotted.

Performance of high-pressure static tests. The base pedestal of the high-pressure cell was not equipped with drainage connections (Figures 6 and 7). Thus, after removal from the water bath and weighing, the specimens were placed directly on the base pedestal. A stainless steel top cap, containing a stainless steel loading ball, was placed on top of the specimen. Filter paper bands, 1/2-inch wide, were lapped over the joints between the specimens and the pedestal and top cap respectively.

27

Two rubber membranes with thicknesses of about 0.002 inch each were rolled over the top cap, specimen and pedestal. The top cap and pedestal were greased with high vacuum silicone grease to aid in sealing. Dual rubber O-rings were used top and bottom to bind the membranes to the cap and pedestal.

The cell was then assembled and placed in the loading press. The loading piston was placed in contact with the loading ball in the top cap and a reading was taken on the dial indicator used to record axial deformation of the specimen. The cell was then filled with mercury to an elevation slightly above the top of the specimen. The pressure panel board was connected to the top of the triaxial cell and the pressure in the cell was increased to the desired level, using nitrogen, and the specimens were given 15 minutes to equilibrate. The loading piston was again pressed into the cell until it made contact with the loading ball and a reading was again taken on the dial indicator. The difference between the two dial indicator readings represented axial compression of the soil specimen (deformation of the cell was found to be negligible). The volumetric strain of the specimen was assumed to be three times the measured axial strain. The volumetric strains were compared with: (1) the volumetric strains actually measured in the low-pressure tests, and (2) the maximum possible volumetric strains corresponding to pressure saturation. In all cases the calculated volumetric strains were reasonable.

The axial load was then applied at a constant rate of deformation. Axial deformations were measured using a dial indicator and the axial load was measured using the load cell mounted beneath the specimen.

After the test, the specimens were removed from the cell and used to determine the average water content. Stress-strain calculations were performed in the usual way except that it was necessary to estimate the volumetric strains that occurred during shear.

<u>Performance of dynamic triaxial compression tests</u>. The first step in the performance of a dynamic test was to prepare the loading press for the particular type of test to be performed. As a safety precaution the main chamber and the triggers were not pressurized at this point.

The top of the triaxial cell was removed from the base and the soil specimen was sealed to the base pedestal following the same procedure as for the static high-pressure tests (Figure 11). The instrumentation system was turned on and calibrated. To calibrate the LVDT, the loading piston was placed in the cell at a position near the center of the displacement range of the test. The LVDT core was locked in place and the circuit was balanced electrically with the core at the center of the linear part of the calibration curve. The piston was raised to the top step of the calibration range and then lowered through four successive distances of 0.250 inch each with the aid of a carefully machined step block, and the output signals from the LVDT were recorded. The recorders were set so that the one inch of travel of the LVDT core approximated full scale of the recorder.

The recorders were calibrated for the load cell by first selecting a resistance approximately equal to the resistance of the load cell circuit when the load cell was subjected to a load somewhat greater than the anticipated test load, and setting the recorders so that this resistance corresponded to nearly full scale. Then a series of smaller resistors were successively switched into the circuit and the traces recorded. Each resistor had previously been calibrated to be equivalent to a certain load in each of the load cells.

The piston of the triaxial cell was raised sufficiently to clear the top cap above the soil specimen and then the cell was assembled. The loading machine was raised and the triaxial cell was placed on the lower platen of the loading press. The cell was centered by a special plate bolted to the lower platen of the press. The piston of the triaxial cell was then lowered to a point just above the top of the loading ball in the top cap, and the loading machine was lowered to contact the top of the piston of the triaxial cell. The cell was filled with mercury to an elevation about one inch above the top of the soil specimen. Nitrogen was allowed to flow into the top of the cell to raise the pressure to 100, 400, or 1000 psi and the specimen was given between 5 and 10 minutes to equilibrate.

During the period when the specimen was equilibrating, the calibration steps were played back from the magnetic tape recorder onto an X-Y plotter to ensure that satisfactory calibrations had been obtained.

29

In a few cases where noise that obscured the calibration steps was encountered, the electrical problems was corrected prior to the test and then the recorders were recalibrated after the test was completed.

The application of the nitrogen cell pressure put a load on the load cell and thus shifted the zero point, usually clear off scale. The recorders were rezeroed as closely as possible and the actual initial reading was recorded. This reading corresponded to a stress difference of zero for the specimen.

The loading machine was then pressurized. The capstan screw on the loading press was used to lower the loading machine, and thus to force the piston down into the triaxial cell. The output of the load cell was switched to a strain indicator. The loading machine was lowered until a seating load of about 1 to 5 percent of the load needed to fail the specimen was applied. The loading machine was then locked in place and the outputs of the LVDT and the load cell were recorded. The last operation prior to performing a high-speed loading test was to drain the mercury to an elevation near the base of the load cell to avoid any change in confining pressure due to the inertia of the mercury. The test was then performed before significant gas leakage through the membranes could occur. For the slowest hydraulic tests the mercury was left in the cell. The loading apparatus, panel board, and triaxial cell just prior to a test are shown in Figure 15.

For a pneumatic test the sequence of operations during the shearing stage was as follows: The instrumentation technician would start the magnetic tape recorder by hand and then close a circuit to start the test. Closing the circuit automatically started the oscillograph, the frequency standard, the goose control unit, and the preset counter. At the end of 300 ms, when the oscillograph had accelerated to its terminal paper speed, the preset counter closed a circuit that discharged a bank of condensers into the solenoid of the main trigger. This trigger was then released, the main valve raised rapidly (several milliseconds), and nitrogen from the main chamber rushed through the ports and onto the main piston of the loading machine. The high nitrogen pressure caused this piston to accelerate rapidly and to travel an inch in about 5 ms. Thus, the soil specimen was deformed 20 percent in approximately 3.5 ms. At the end of its travel, the main piston of the

30
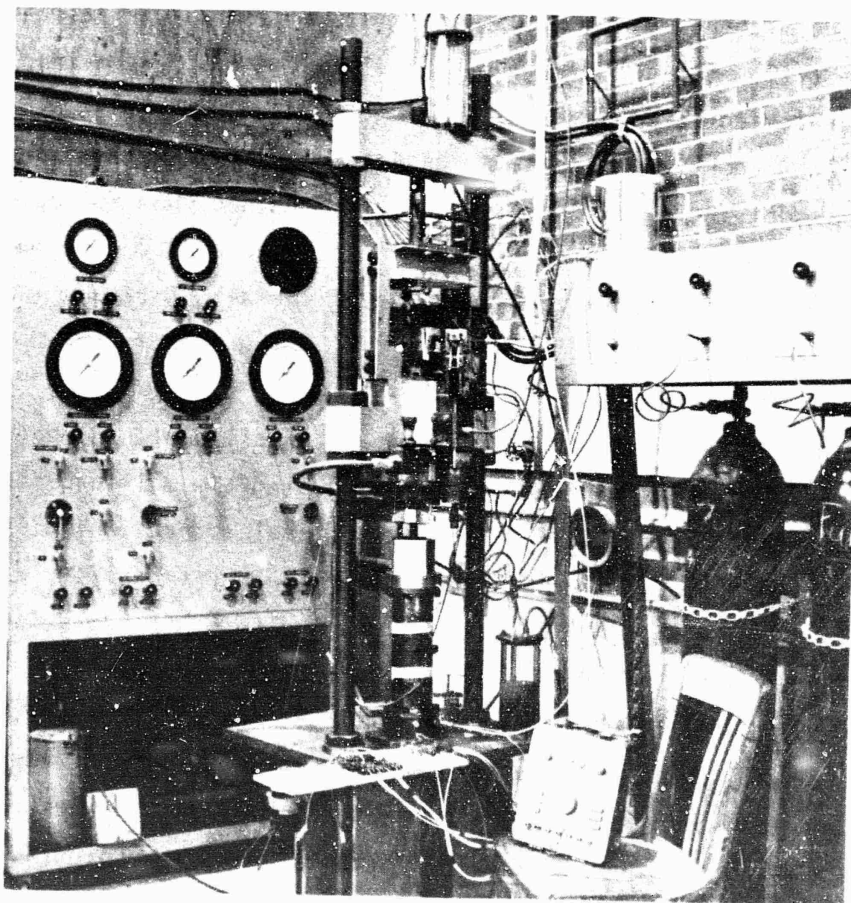
Figure 15. Loading Apparatus, Panel Board, and Triaxial Cell
Just Prior to a Dynamic Shear Test

loading machine struck the end of the cylinder and stopped immediately. During the time the deformation was being applied, the output of the LVDT and load cell were being recorded continuously on both magnetic tape and the oscillograph. At the end of some predetermined time the control unit turned off the recording equipment.

The pressure in the triaxial cell was then released and the remaining mercury was drained back into its reservoir. The pressure in the loading machine was then released and the machine was raised to clear the cell. The cell was dismantled and the entire specimen used as a water content sample.

For the hydraulic tests, essentially the same procedure was followed except that the oil valve was fired rather than the main valve. Further, for these slower tests the magnetic tape record was immediately used to plot a load-deformation curve using the X-Y plotter.

Experimental Results

Moisture-density data. A summary of all pertinent data derived from the triaxial shear tests, including the moisture-density data, is presented in Table I. For each nominal compaction moisture content, the mean compaction moisture content and dry density, and the estimates of their standard deviations are presented in Table II. The moisture-density curve is plotted in Figure 16. The short horizontal and vertical lines through each point, with the hatch marks at the ends, indicate the range of water content and dry density, respectively, containing one standard deviation. The scatter in water contents results from the difficulty of mixing several batches of clay to precisely the same water content. The scatter in density is partly due to the scatter in water content but mostly due to small variations in the dwell time of the compaction foot. The scatter in both water content and density is small and appears to exert a negligible influence on the physical properties of the specimens.

Unconsolidated-undrained shear of unsaturated soil. Before discussing the experimental data, it is useful to review the behavior of unsaturated soils subject to shear. The behavior of the Goose Lake clay under dynamic loading conditions can then be compared with what might be

32

Table I

INDIVIDUAL TEST RESULTS

Test No.	w_n (%)	w (%)	γ (pcf)	t_f (s)	σ_3 (psi)	$(\sigma_1-\sigma_3)_f$ (psi)	ϵ_f (%)	E_s (psi)
1A	$6\frac{1}{2}$	6.4	105.6	370	10	64	2	6,000
2A	$6\frac{1}{2}$	6.4	105.6	1800	40	132	11	7,400
3A	$6\frac{1}{2}$	6.3	105.7	3320	100	276	20	7,000
4A	$6\frac{1}{2}$	6.3	105.3	2870	400	857	20	14,000
5A	$6\frac{1}{2}$	6.4	105.4	2530	1000	1631	18	28,000
6A	$6\frac{1}{2}$	6.4	106.0	114	10	64	2	6,100
7A	$6\frac{1}{2}$	6.4	105.3	550	40	128	11	7,000
8A	$6\frac{1}{2}$	---	104.2	1000	100	264	20	5,800
9A	$6\frac{1}{2}$	6.3	105.7	870	400	850	20	16,500
10A	$6\frac{1}{2}$	6.4	105.8	810	1000	1631	19	31,000
11A	$6\frac{1}{2}$	6.3	105.9	28	10	64	2	6,200
12A	$6\frac{1}{2}$	6.4	105.5	148	40	128	12	6,600
13A	$6\frac{1}{2}$	6.3	105.5	250	100	270	20	7,200
14A	$6\frac{1}{2}$	6.4	105.5	240	400	857	22	18,000
15A	$6\frac{1}{2}$	6.5	105.7	193	1000	1622	18	34,000
16A	$6\frac{1}{2}$	6.4	104.9	14	100	284	19	10,000
17A	$6\frac{1}{2}$	6.2	105.2	3.0	1000	1633	17	48,000
18A	$6\frac{1}{2}$	6.3	104.8	1.2	100	300	20	11,000
19A	$6\frac{1}{2}$	6.2	104.7	0.215	1000	1722	18	52,000
20A	$6\frac{1}{2}$	6.3	105.1	0.200	100	292	19	11,400
21A	$6\frac{1}{2}$	6.1	105.0	0.036	1000	1800	18	57,000
22A	$6\frac{1}{2}$	6.3	105.1	0.037	100	304	18	13,800
23A	$6\frac{1}{2}$	6.2	104.7	0.0017	1000	2211	16	90,000

Table I, Continued

INDIVIDUAL TEST RESULTS

Test No.	w_n (%)	w (%)	γ (pcf)	t_f (s)	σ_3 (psi)	$(\sigma_1 - \sigma_3)_f$ (psi)	ϵ_f (%)	E_s (psi)
1B	$10\frac{1}{2}$	10.4	106.2	520	10	66	3	5,300
2B	$10\frac{1}{2}$	10.4	106.5	2970	40	126	19	5,400
3B	$10\frac{1}{2}$	10.4	106.6	4100	100	222	26	5,000
4B	$10\frac{1}{2}$	10.2	106.9	2870	400	453	20	10,000
5B	$10\frac{1}{2}$	10.2	106.9	2400	1000	519	17	26,000
6B	$10\frac{1}{2}$	10.4	106.9	160	10	66	3	5,300
7B	$10\frac{1}{2}$	10.3	107.2	860	40	128	18	5,700
8B	$10\frac{1}{2}$	10.3	106.9	1200	100	222	25	5,200
9B	$10\frac{1}{2}$	10.3	106.3	830	400	457	19	12,000
10B	$10\frac{1}{2}$	10.3	106.4	690	1000	543	16	27,000
11B	$10\frac{1}{2}$	10.4	106.5	40	10	68	3	5,600
12B	$10\frac{1}{2}$	10.4	106.6	240	40	124	20	5,500
13B	$10\frac{1}{2}$	10.4	106.4	300	100	220	25	5,400
14B	$10\frac{1}{2}$	10.4	106.7	210	400	451	19	12,400
15B	$10\frac{1}{2}$	10.3	106.5	173	1000	558	16	26,000
16B	$10\frac{1}{2}$	10.7	107.0	14	100	228	23	6,800
17B	$10\frac{1}{2}$	10.4	106.8	13	1000	515	16	27,000
18B	$10\frac{1}{2}$	10.7	106.6	1.5	100	232	24	7,800
19B	$10\frac{1}{2}$	10.5	106.7	1.2	1000	549	16	31,000
20B	$10\frac{1}{2}$	10.7	106.5	0.250	100	242	23	8,500
21B	$10\frac{1}{2}$	10.4	106.7	0.220	1000	579	17	33,000
22B	$10\frac{1}{2}$	10.7	106.4	0.042	100	270	22	10,400
23B	$10\frac{1}{2}$	10.5	106.7	0.040	1000	619	18	37,000
24B	$10\frac{1}{2}$	10.7	106.7	0.0031	100	322	24	10,400
25B	$10\frac{1}{2}$	10.4	106.9	0.0030	1000	892	22	51,000

Table I, Continued

INDIVIDUAL TEST RESULTS

Test No.	w_n (%)	w (%)	γ (pcf)	t_f (s)	σ_3 (psi)	$(\sigma_1 - \sigma_3)_f$ (psi)	ε_f (%)	E_s (psi)
1C	13½	13.4	112.7	1580	10	84	11	4,600
2C	13½	13.4	113.0	3550	40	116	23	4,500
3C	13½	13.4	112.0	3450	100	144	22	4,300
4C	13½	13.4	113.6	2650	400	147	18	8,000
5C	13½	13.4	114.0	2950	1000	152	20	7,200
6C	13½	13.5	112.8	480	10	80	10	4,000
7C	13½	13.5	112.6	1040	40	116	22	4,400
8C	13½	13.4	111.7	1080	100	142	23	4,100
9C	13½	13.4	113.6	850	400	154	19	8,500
10C	13½	13.3	113.5	900	1000	156	19	8,000
11C	13½	13.9	111.2	140	10	68	12	3,100
12C	13½	13.5	113.3	250	40	116	21	4,500
13C	13½	13.6	111.5	283	100	142	24	4,300
14C	13½	13.4	113.3	200	400	162	18	8,000
15C	13½	13.4	112.9	235	1000	160	21	9,000
16C	13½	13.5	111.8	14	100	144	22	5,400
17C	13½	13.6	111.3	15	1000	171	19	10,000
18C	13½	13.5	111.6	1.3	100	150	22	6,800
19C	13½	13.5	111.3	1.4	1000	185	21	11,200
20C	13½	13.6	112.1	0.240	100	156	22	7,100
21C	13½	13.5	112.0	0.220	1000	204	19	13,200
22C	13½	13.6	111.9	0.042	100	168	22	7,600
23C	13½	13.6	111.5	0.036	1000	215	18	13,500
24C	13½	13.7	111.6	0.0028	100	222	23	8,700
25C	13½	13.7	111.6	0.0029	1000	291	20	15,000

Table I, Continued

INDIVIDUAL TEST RESULTS

Test No.	w_n (%)	w (%)	γ (pcf)	t_f (s)	σ_3 (psi)	$(\sigma_1-\sigma_3)_f$ (psi)	ϵ_f (%)	E_s (psi)
1D	16	15.9	114.7	4050	10	55.0	22	1750
2D	16	15.7	115.0	4200	40	66.4	22	2400
3D	16	15.7	114.9	3610	100	68.2	24	2950
4D	16	15.8	114.5	3650	1000	68.0	25	2300
5D	16	15.9	115.1	240	10	58.8	21	1900
6D	16	15.8	114.9	370	40	66.5	26	2300
7D	16	15.8	114.9	277	100	71.0	24	2900
8D	16	15.9	114.6	280	1000	69.0	24	2500
9D	16	16.3	113.8	20	100	65.0	26	2300
10D	16	16.2	113.2	18	1000	67.0	24	2700
11D	16	16.2	114.0	1.6	100	70.0	26	2300
12D	16	16.3	113.0	1.6	1000	75.0	25	2500
13D	16	16.4	114.1	0.270	100	74.6	26	2500
14D	16	16.3	113.3	0.270	1000	75.6	25	3000
15D	16	16.2	113.6	0.290	1000	76.4	25	3000
16D	16	16.4	113.6	0.045	100	80.6	24	3000
17D	16	16.4	114.1	0.047	100	82.0	25	3000
18D	16	16.2	113.7	0.045	1000	80.8	24	3200
19D	16	16.4	114.3	0.0027	100	110.0	25	3000
20D	16	16.4	114.0	0.0029	1000	108.0	26	3300

INDIVIDUAL TEST RESULTS

Test No.	w_n (%)	w (%)	γ (pcf)	t_f (s)	σ_3 (psi)	$(\sigma_1-\sigma_3)_f$ (psi)	ϵ_f (%)	E_s (psi)
1E	18	18.0	110.3	4900	10	28.8	30	560
2E	18	18.2	109.9	4450	100	32.6	30	940
3E	18	18.1	109.7	3500	1000	30.8	24	940
4E	18	18.1	109.9	1180	100	33.2	30	1100
5E	18	18.0	110.1	375	10	31.6	30	700
6E	18	18.1	110.3	294	100	34.6	26	1150
7E	18	18.0	110.5	290	1000	34.0	26	900
8E	18	18.2	109.4	21	100	35.2	29	1100
9E	18	18.3	109.6	19	1000	36.0	24	1400
10E	18	18.1	110.0	1.6	100	38.4	27	1200
11E	18	18.3	108.9	1.6	100	37.0	27	1200
12E	18	18.3	109.3	1.6	1000	37.8	24	1400
13E	18	18.4	109.2	1.6	1000	35.6	24	1300
14E	18	18.4	109.7	0.250	100	40.6	26	1300
15E	18	18.4	108.6	0.290	1000	39.4	26	1200
16E	18	18.6	108.8	0.050	100	44.4	27	1400
17E	18	18.4	109.5	0.049	100	44.0	26	1600
18E	18	18.3	109.6	0.053	1000	45.4	26	1700
19E	18	18.3	109.7	0.050	1000	43.6	25	1700
20E	18	18.4	109.9	0.0030	100	49.0	30	900
21E	18	18.4	110.0	0.0027	100	55.2	31	1300
22E	18	18.4	109.6	0.0030	1000	50.0	30	1300
23E	18	18.5	109.7	0.0031	1000	52.4	30	1200

Table II

MOISTURE-DENSITY DATA

Nominal Water Content (%)	Actual Water Content Mean (%)	Actual Water Content S (%)	Dry Density Mean (pcf)	Dry Density S (pcf)	Number of Observations	Degree of Saturation (%)
$6\frac{1}{2}$	6.3	0.1	105.3	0.4	23	28
$10\frac{1}{2}$	10.4	0.2	106.7	0.2	25	48
$13\frac{1}{2}$	13.5	0.1	112.3	0.9	25	72
16	16.1	0.3	114.2	0.6	20	90
18	18.3	0.2	109.7	0.5	23	91
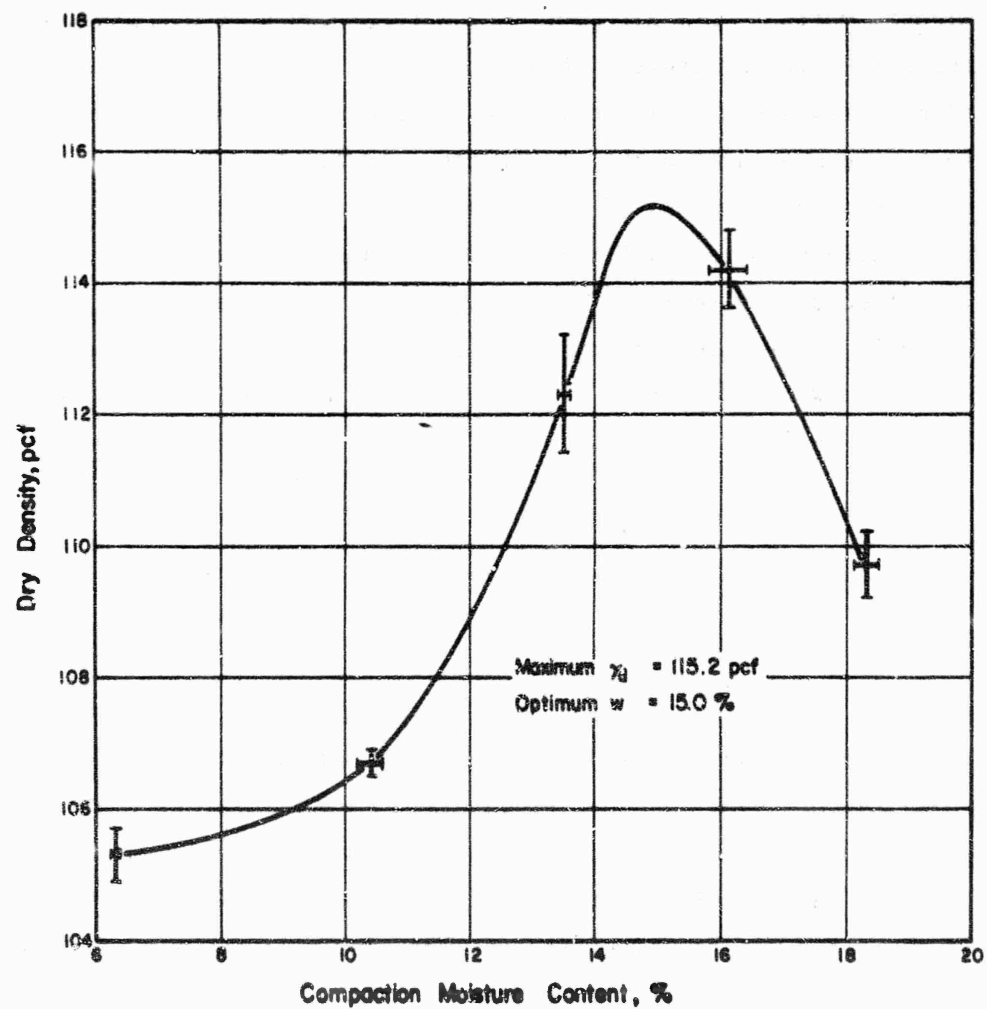
Figure 16.   Moisture-Density Curve for the Specimens Used in the
Triaxial Shear Testing Program

considered typical behavior under static conditions. The review will, of necessity, be brief.

Unsaturated soils are three-phase systems composed of solid mineral matter, pore air, and pore water. The pore air pressure exceeds the pore water pressure. Thus, for soils in which the degree of saturation is low and the air voids are interconnected and at atmospheric pressure, the pressure in the pore water is negative. Negative pore water pressures in specimens of Goose Lake clay, prepared by kneading compaction, were reported by Olson and Langfelder.[1] The data have been replotted as Figure 17. For the water contents used during this project, we would predict the following residual pore water pressures:

Water Content %	Pore Water Pressure psi
6.3	lower than -250
10.4	-190
13.5	-75
16.1	-30
18.3	-10

The pore water pressure in the specimens compacted at a water content of 6.3 percent is certainly more negative than -250 psi and is probably more negative than -1000 psi. An interpretation of such pore water pressures has been presented by Olson and Langfelder.[1]

By definition, the physical properties of soils are controlled by the state of effective stress. The problem remains to develop an equation to yield effective stresses. Bishop[7] proposed an equation of the form:

$$\bar{\sigma} = \sigma - u_w X - u_a (1 - X) \qquad (1)$$

where $\bar{\sigma}$ is the effective stress, σ is the total stress, u_w is the pore water pressure, u_a is the pore air pressure, and X is an experimentally determined parameter whose value was originally assumed to lie between 0 and 1. It now appears that a range from $-\infty$ to $+\infty$ might be more appropriate. If the air voids are continuous and connected to the atmosphere, then $u_a = 0$ and:

$$\bar{\sigma} = \sigma - X u_w \qquad (2)$$

Figure 17. Influence of Compaction Moisture Content
on the Residual Negative Pore Water
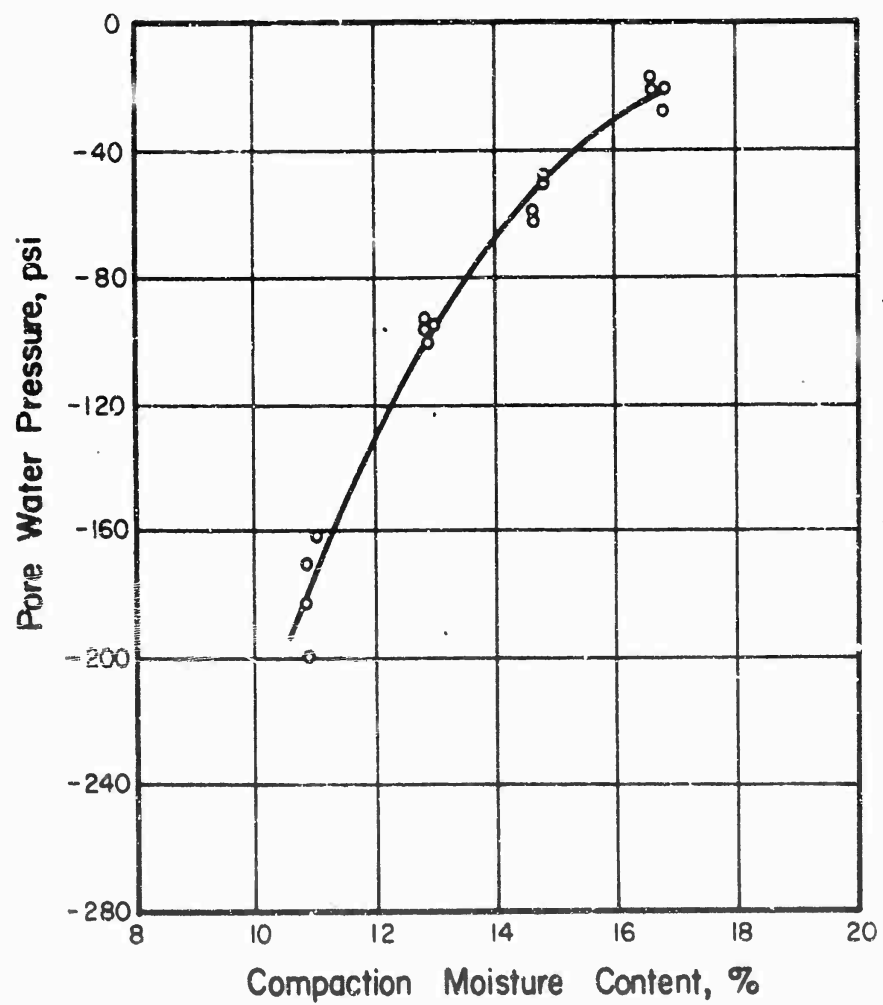Pressure After Compaction

41

The shearing strength of soil is generally expressed as the sum of cohesive and frictional strength:

$$\tau_f = \bar{c} + \bar{\sigma}_n \tan \bar{\phi} \qquad (3)$$

where τ_f is the shearing strength, $\bar{\sigma}_n$ is the effective stress normal to the shear plane, and $\bar{c}$ and $\bar{\phi}$ are the effective cohesion and angle of internal friction respectively. The effective angle of internal friction often decreases slightly as the effective normal stress increases. For uncemented soils it appears that $\bar{c}$ is small and that the strength of the soil is mainly dependent on $\bar{\sigma}_n$ and $\bar{\phi}$.

Although effective-stress shear tests have not been performed using compacted specimens of Goose Lake clay, both $\bar{R}$ (consolidated-undrained with pore pressures measured) and S (consolidated-drained) tests have been performed by using specimens remolded at a water content of 28 percent. For effective stresses in the range of 3 psi to 120 psi, the effective shear parameters were $\bar{c} = 1.5$ psi and $\bar{\phi} = 25\ 1/2$ degrees.

The changes in the pore air and pore water pressure, Δu_a and Δu_w respectively, due to the application of an increment of hydrostatic stress, $\Delta\sigma_3$, and stress difference, can be expressed as follows:[8,9]

$$\Delta u_a = B_a [\Delta\sigma_3 + A_a(\Delta\sigma_1 - \Delta\sigma_3)]$$

$$\Delta u_w = B_w [\Delta\sigma_3 + A_w(\Delta\sigma_1 - \Delta\sigma_3)] \qquad (4)$$

where B_a, A_a, B_w, and A_w are experimentally determined parameters. The coefficient B_w varies from 0 to 1 as the degree of saturation increases from 0 to 100 percent. The relationship is nonlinear and depends on the increment of hydrostatic stress used. Values of the other parameters are still open to conjecture; there are few published data.

The studies performed during this project included only Q-type (unconsolidated-undrained) shear tests. The shapes and relative positions of the Q failure envelopes can be predicted based on the equations and data just presented. Specimens compacted at a water content approaching zero have extremely negative pore water pressures but X approaches zero so the multiple Xu_w, which gives the residual effective stress (Eq. 2 with $\sigma = 0$), also approaches zero. Thus, the unconfined specimens have

42

a negligible effective stress and, accordingly, a negligible unconfined compression strength. Further, applied total stresses will result in negligible changes in the pore air and pore water pressures within the ranges of stress usually of interest to soils engineers. The applied total stress will then be counterbalanced mainly by increases in the effective stress. Accordingly, a plot of strength vs total confining pressure becomes essentially a plot of strength versus effective confining pressure and will be nearly linear, passing very near the origin, with a slope $\emptyset_Q = \bar{\emptyset}$.

The parameter X must increase very rapidly just on the dry side of the optimum point because both the unconfined compression strength and the intercept c_Q maximize just a few percent dry of optimum. It is probable that the large value of c_Q actually represents internal friction developed by the negative pore water pressure according to the equation:

$$c_Q = -Xu_w \tan \bar{\emptyset} \qquad (5)$$

The application of a hydrostatic stress, $\Delta\sigma_3$, will generate a pore water pressure change, Δu_w, according to:

$$\Delta u_w = B_w \Delta\sigma_3 \qquad (6)$$

where B_w will be between 0 and 1. Thus, only part of the applied hydrostatic stress will be taken by effective stress. Accordingly, the strength of the specimens will increase more slowly than for the dry specimens considered previously, i.e., $\emptyset_Q < \bar{\emptyset}$.

Increasing the confining pressure compresses the soil and thus compresses the air voids and increases the degree of saturation. In addition, the increased pore air pressure causes some of the pore air to dissolve in the pore water and thus increases the degree of saturation even further. The higher degrees of saturation cause an increase in B_w so that an increasingly large fraction of the applied confining pressure is taken by the pore water rather than by effective stress. As a result, the failure envelopes have their largest slopes, $\emptyset_Q$, at low values of σ_3 and the slope decreases as σ_3 increases, i.e., the failure envelope is concave towards the confining-pressure axis. If a confining pressure is applied that is large enough to "pressure

saturate" the specimens, then $\phi_Q = 0$ because of the remaining increments of confining pressure are taken by the pore water; there is no further increase in effective stress and therefore no increase in shear strength.

For specimens compacted on the wet side of the optimum water content, the initial degree of saturation is high and a major part of even the first increment of confining pressure is taken by the pore water. Thus ϕ_Q is low, even at small confining pressures and $\phi_Q = 0$ throughout most of the range of confining pressures of interest. The intercept, c_Q is low because the initial negative pore water pressure is low.

Modified failure envelopes. For many years it was common practice to plot standard Mohr diagrams of τ vs σ (or $\bar{\sigma}$) with a semi-circle representing the state of stress in each specimen at failure. The failure envelope then yielded a direct relationship between shearing strength and normal stress. However, the presence of a large number of Mohr circles obscures relationships. Further, it is more convenient to represent each test by a single point rather than by a circle.

Thus, it has become common practice to plot $1/2 \, (\sigma_1 - \sigma_3)$ vs $1/2 \, (\sigma_1 + \sigma_3)$, using either total or effective stresses. The shear parameters in this modified diagram are intercept d and slope ψ. It can easily be shown that:

$$\phi = \sin^{-1} (\tan \psi)$$
$$c = d/\cos \phi \qquad (7)$$

When Q-type tests are performed using specimens of unsaturated soil it is more convenient to plot $\sigma_1 - \sigma_3$ vs σ_3. If we again use d and ψ as the shear parameters, then:

$$\phi = \sin^{-1} \frac{\tan \psi}{2 + \tan \psi}$$
$$c = d \, \frac{1 - \sin \phi}{2 \cos \phi} \qquad (8)$$

Static failure envelopes. Failure envelopes for the static tests are presented in Figure 18. The differences in the compressive strengths for the various tests performed at a given water content and confining pressure, but varying time to failure (static only), was so small that the data points almost completely overlapped. Thus, the points plotted in Figure 18 represent averages of several points which would have plotted nearly on top of each other.

44

For the tests at low water content and high pressure, a problem arose because it was not possible to measure the volumetric strain during shear. These volumetric strains were estimated in the following way: The volumetric strains, v_a, resulting from the application of the hydrostatic confining pressure were plotted vs log σ_3. A similar plot was made for $\sigma_3 \leq 100$ psi for total volumetric strain, v_t, and was extrapolated to higher pressures with the aid of the v_a curve and the known limit to the total volumetric strain, v_{max}, corresponding to complete saturation of the specimen. The data used in these plots, together with the resulting estimated volumetric strains (shown in parentheses), are shown in Table III. These estimated total volumetric strains were used in calculating the cross sectional areas of the specimens and also in estimating the degree of saturation of the specimens at failure.

The failure envelope (Figure 18) for the specimens compacted at a nominal water content of 6-1/2 percent is linear for confining pressures less than 100 psi and the volumetric strains (Table III) are small. At higher confining pressures the failure envelope is distinctly curved, indicating the development of significant pore pressures. The estimated volumetric strains (Table III) also suggest that the soil is approaching saturation at the highest confining pressure and thus that an appreciable curvature should occur in the failure envelope.

The failure envelope for specimens compacted at a nominal water content of 10-1/2 percent is distinctly curved and is nearly flat at a confining pressure of 1000 psi. The estimated volumetric strain at 400 psi of confining pressure is 18.5 percent compared to a limit of 20 percent for complete saturation. At a confining pressure of 1000 psi the specimen has an estimated volumetric strain equal to the limiting value; thus the specimens had apparently reached, or closely approached, the $\emptyset_Q = 0$ condition.

The failure envelopes for the specimens compacted at water contents of 13-1/2 percent and higher become nearly flat at confining pressures between 100 psi and 400 psi, indicating that these specimens became pressure saturated at these pressures. This pressure saturation is confirmed by the volumetric strains shown in Table III.

The static failure envelopes of Goose Lake clay are, therefore of the anticipated shapes and relative positions. The data

45
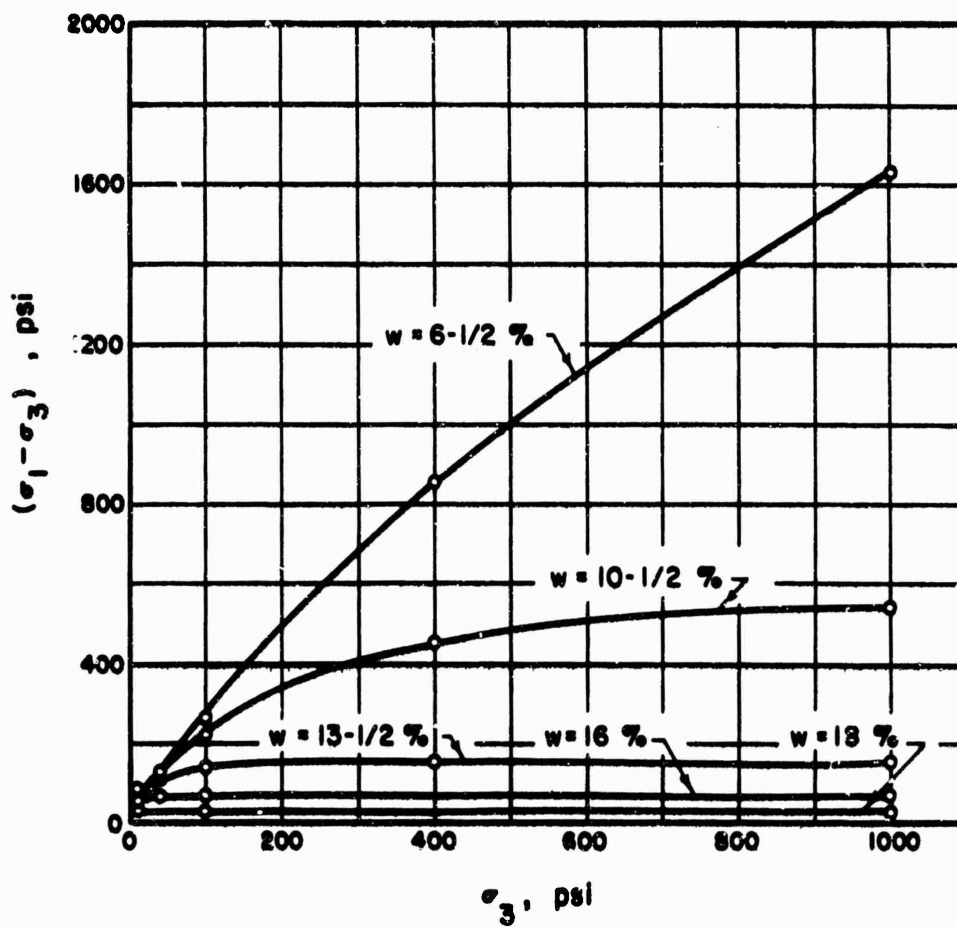
Figure 18.   Static Failure Envelopes for Compacted
             Specimens of Goose Lake Clay

Table III

VOLUMETRIC STRAINS

Nominal Water Contents (%)	Confining Pressure (psi)	ν_a (%)	ν_τ (%)	ν_t (%)	ν_{max} (%)	ν_{dyn} (%)
$6\frac{1}{2}$	10	0.0	-0.9	-0.9	27	--
$6\frac{1}{2}$	40	0.7	1.9	2.6	27	--
$6\frac{1}{2}$	100	3.4	6.6	10.0	27	10
$6\frac{1}{2}$	400	8.7	(12.8)	(21.5)	27	--
$6\frac{1}{2}$	1000	14.8	(10.0)	(24.8)	27	25
$10\frac{1}{2}$	10	0.0	-0.4	-0.4	20	--
$10\frac{1}{2}$	40	1.0	4.4	5.4	20	--
$10\frac{1}{2}$	100	4.0	8.4	12.4	20	12
$10\frac{1}{2}$	400	8.0	(10.5)	(18.5)	20	--
$10\frac{1}{2}$	1000	13.7	(6.1)	(19.8)	20	20
$13\frac{1}{2}$	10	0.2	0.9	1.1	$9\frac{1}{2}$	--
$13\frac{1}{2}$	40	0.8	4.2	5.0	$9\frac{1}{2}$	--
$13\frac{1}{2}$	100	3.9	4.5	8.4	$9\frac{1}{2}$	8
$13\frac{1}{2}$	400	(8.5)	(1.0)	(9.5)	$9\frac{1}{2}$	--
$13\frac{1}{2}$	1000	(9.5)	(0.0)	(9.5)	$9\frac{1}{2}$	$9\frac{1}{2}$
16	10	0.5	0.5	1.0	$3\frac{1}{2}$	--
16	40	1.4	0.8	2.2	$3\frac{1}{2}$	--
16	100	2.7	0.4	3.1	$3\frac{1}{2}$	$3\frac{1}{2}$
18	10	0.8	0.3	1.1	3	--
18	100	2.0	1.0	3.0	3	3
18	1000	(3.0)	(0.0)	(3.0)	3	3

indicate that the strengths of the specimens can be reproduced with high precision and that a wide range in strengths and compressibilities can be obtained by a suitable variation in the compaction water content and the confining pressure.

Influence of strain rate on compressive strength. A variety of diagrams can be used to demonstrate the influence of strain rate on the strength of the specimens. In this report, the compressive strength will be related to the time required to attain the peak value of the stress difference, i.e., to the time to failure, t_f. The compressive strengths have been plotted versus the logarithm of the time to failure in Figure 19 for compaction water contents of 6-1/2, 10-1/2, 13-1/2, 16 and 18 percent, respectively. For the three lowest water contents the strength depended on the confining pressure (Figure 18); thus, separate diagrams were plotted for confining pressures of 100 psi and 1000 psi. At water contents of 16 and 18 percent, the specimens were saturated in the range of confining pressure from 100 psi to 1000 psi; thus, only single curves were plotted and strength tests at a confining pressure of 400 psi were included.

Although the shapes of the curves in Figure 19 vary somewhat from each other, there is no clear effect of either water content or confining pressure on either the shapes of the curves or the amount of increase in strength as the time to failure decreases. In order to obtain a more direct comparison of the curves, the data were normalized by dividing all compressive strengths by the compressive strength corresponding to a time to failure of one minute (the choice of a time to failure of one minute was arbitrary--a time of one minute was previously used by Casagrande and Wilson[10] for their "creep-strength tests"). Separate plots of normalized strength versus log t_f are presented in Figure 20 for confining pressures of 100 psi and 1000 psi. It is clear that the curves all have the same shape and that the dynamic effects are essentially the same for specimens compacted in the range of water content from 10-1/2 percent to 18 percent, i.e., from about 5 percent dry to 3 percent wet of optimum. For lower water contents there is a smaller increase in strength as the time to failure decreases. The normalized strength seems to be only slightly influenced by confining pressure for the specimens compacted on the dry side of optimum, and
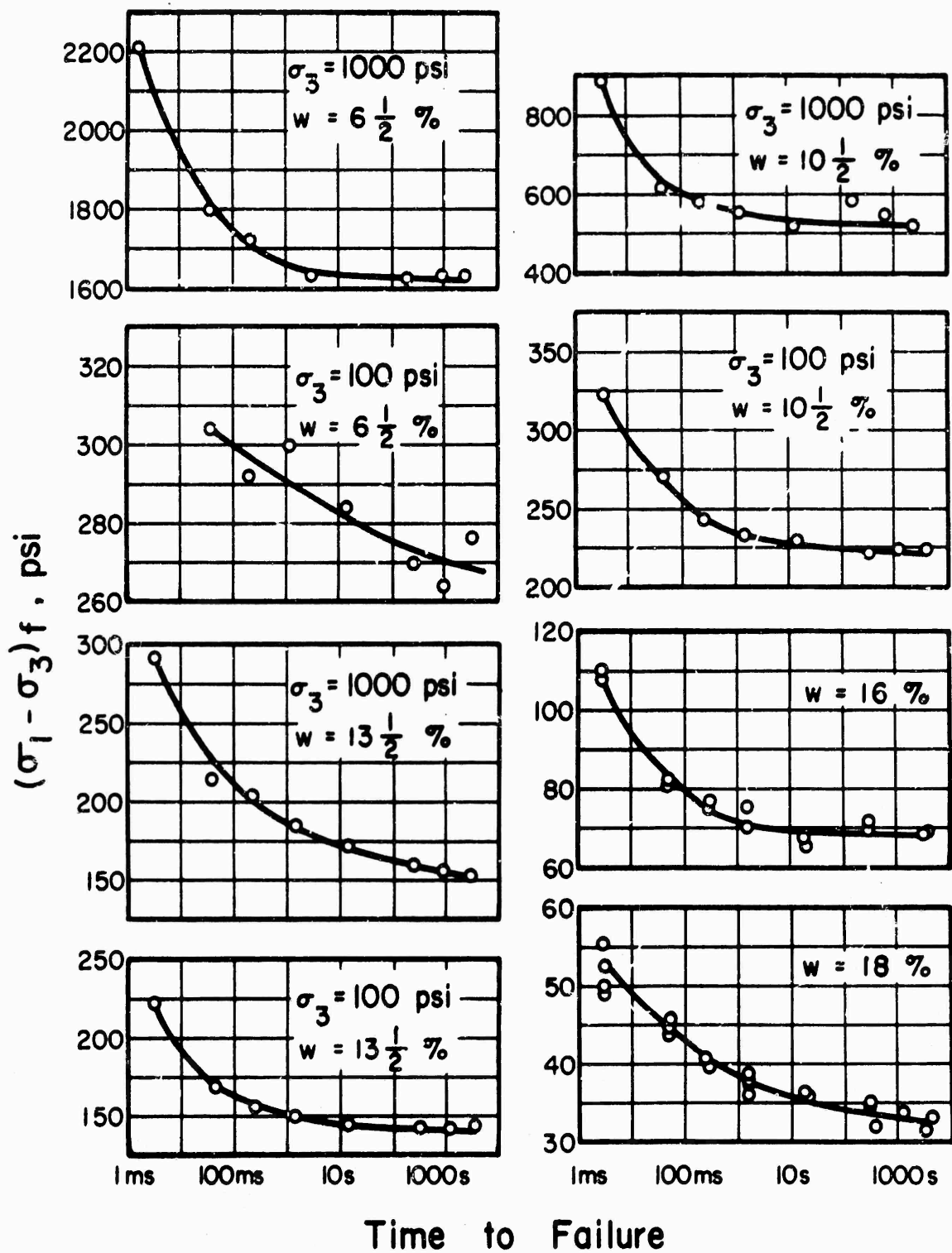
48

Figure 19. Influence of the Time to Failure on the Compressive
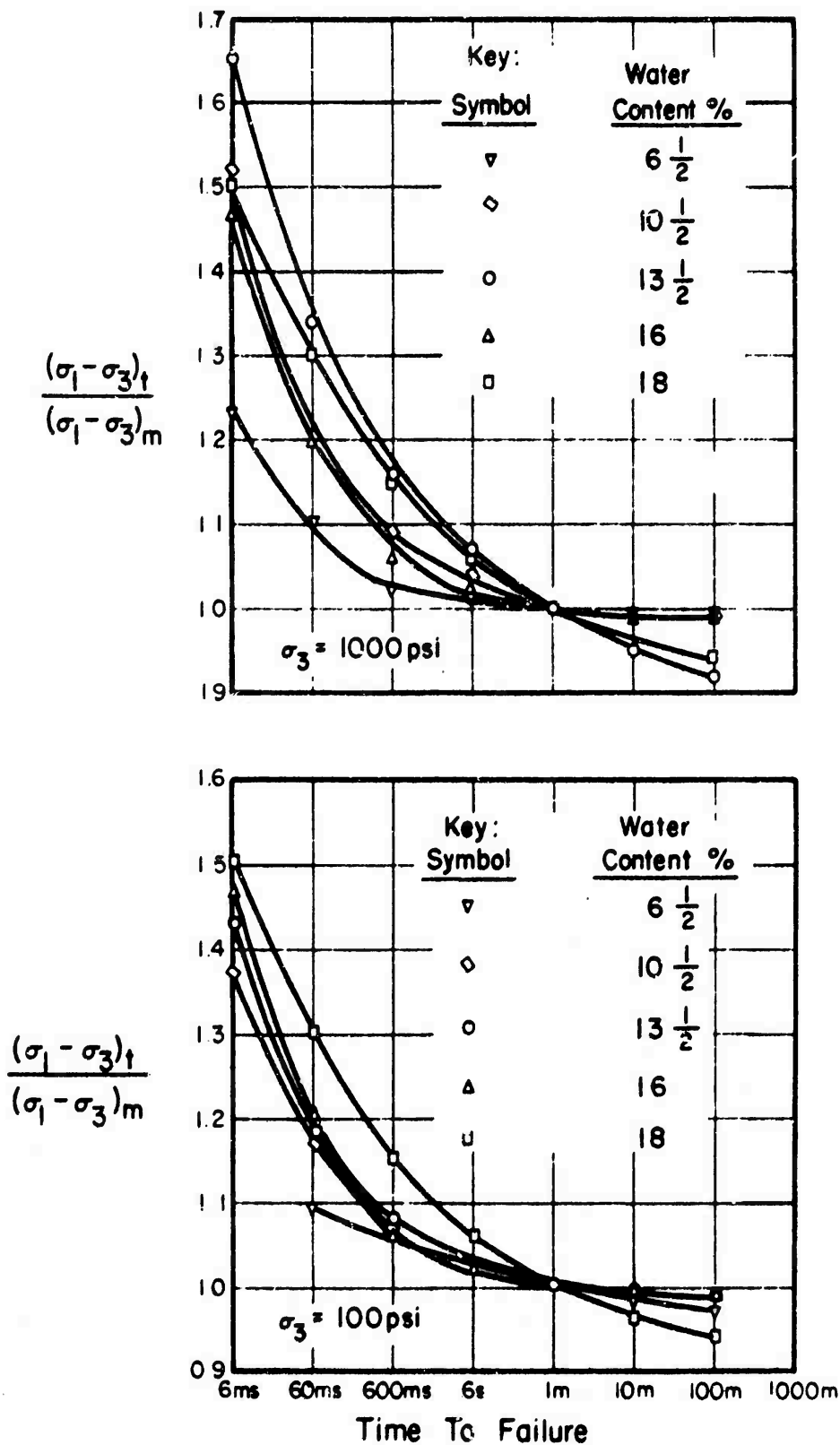Strength of Specimens of Goose Lake Clay

Figure 20. Normalized Strength-Time to Failure Relationships

50

of course, there is no influence for specimens compacted wet of optimum, within the pressure range of 100 psi to 1000 psi. The average normalized strength was calculated for each decade of change in time to failure, using only the specimens whose water contents ranged from 10-1/2 percent to 18 percent. The average normalized strengths are as follows:

Time to Failure	Normalized Strength
100 m	0.95
10 m	0.97
1 m	1.00
6 s	1.04
600 ms	1.10
60 ms	1.22
6 ms	1.44

These data demonstrate that the influence of deformation rate on compressive strength is relatively small for times to failure longer than perhaps 600 ms but increases rapidly for shorter times. To demonstrate this fact more clearly, the percentage increase in strength for each decade of decrease in time to failure, $(\tau_{10t} - \tau_t)/\tau_{10t}$, was calculated. The results are as follows:

Range in Time to Failure	Increase in Strength %
100 m - 10 m	2
10 m - 1 m	3
1 m - 6 s	4
6 s - 600 ms	6
600 ms - 60 ms	11
60 ms - 6 ms	18

Thus, on the average, the increase in strength for the decade from 60 ms down to 6 ms is nine times that for the decade from 100 m to 10 m.

Strains at failure. These strains are of interest in soil-structure interaction problems only as an indication of the brittleness of the soil. The secant modulus is of more use and is discussed later. The failure strains were of special interest in this investigation because it was hoped that the stress-strain characteristics of the chosen soil could be varied between wide limits depending upon the compaction water content or compaction procedure.

51

The strains at the peak value of the stress difference have been plotted versus the logarithm of the confining pressure in Figure 21 for water contents of 6-1/2, 10-1/2, 13-1/2, 16, and 18 percent respectively.

The most remarkable aspect of these diagrams is the small scatter in the data. Usually the strains at failure vary widely and thus attempts at correlation or interpretation are futile. The small scatter in the strains at failure, together with the small scatter of the compressive strength data, indicates that the properties of the Goose Lake clay can be reproduced accurately.

An interesting aspect of the strain data is that the strain at failure is independent of the time to failure. Separate plots will not be presented but a comparison of the data tabulated in Table I with the diagrams (Figure 21) will show no relationship between ϵ_f and t_f.

It is of interest to examine the influence of confining pressure on the strain at failure for each water content. The data for specimens compacted at a water content of 6 1/2 percent will be considered first. The specimens were compacted using a nominal foot pressure of 100 psi. The kneading action of this foot produces a densification equivalent to that obtainable with a hydrostatic effective stress several times greater than the foot pressure. Thus, specimens subjected to only 10 psi of confining pressure in the triaxial cell are subjected to a stress that is much smaller than the equivalent hydrostatic stress applied during compaction. Because there is little change in either the pore air or pore water pressure during shear, for confining pressures less than about 100 psi, these specimens react as if they were overconsolidated specimens subject to drained shear. Accordingly, at low confining pressures, the specimens dilate during shear, and fail at a low axial strain. The deformation tends to be concentrated along a single shearing plane. Increasing the confining pressure caused the specimens to be subjected to stresses closer and closer to the equivalent effective hydrostatic compaction pressure and thus the specimens dilate less during shear and the strain at failure increased. At a hydrostatic stress in the vicinity of 300 psi the specimens might be considered to be normally consolidated in that the equivalent hydrostatic pressure during compaction is likely to be of that magnitude.
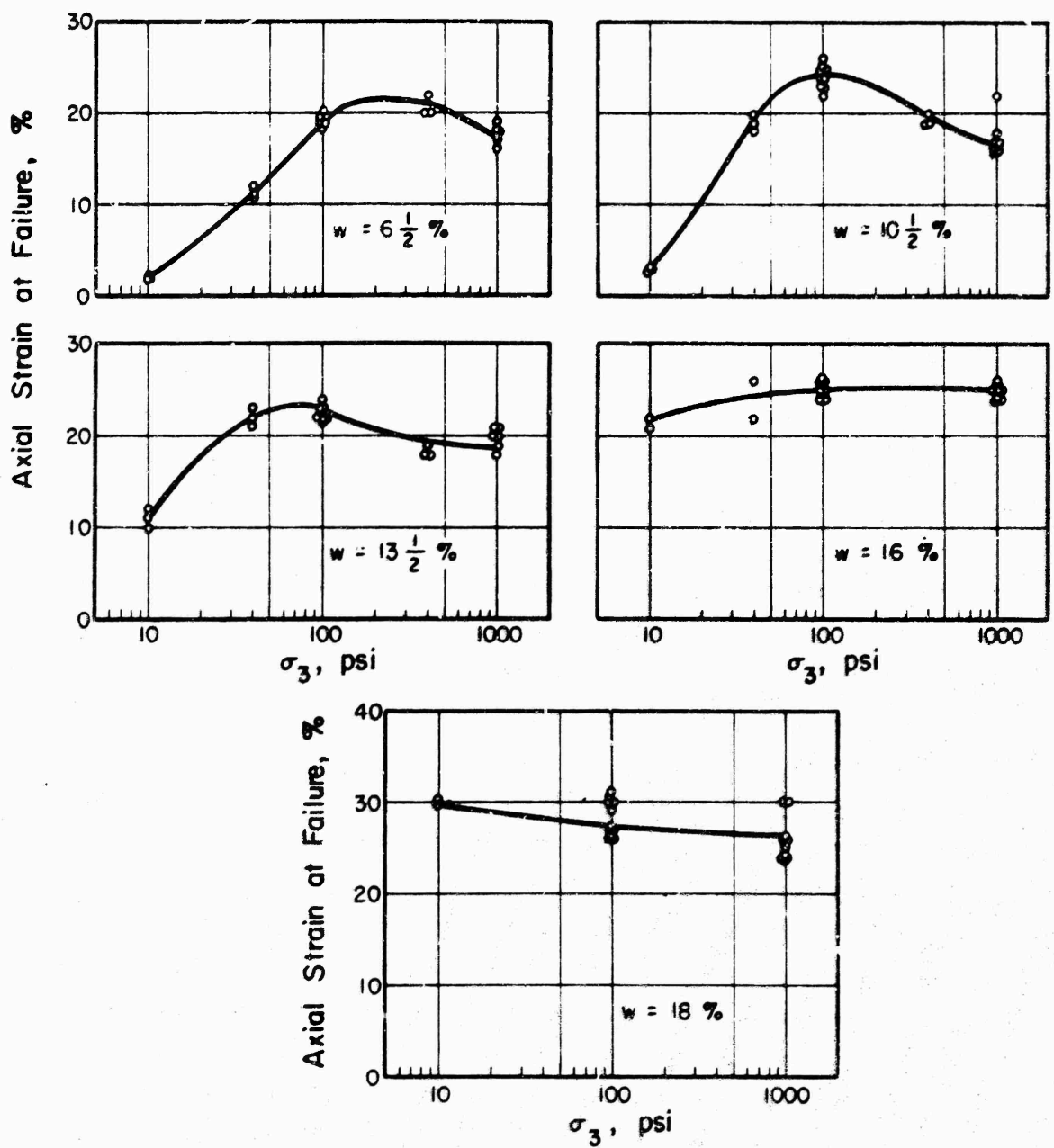
52

Figure 21. Influence of Confining Pressure on the Axial Strain
at Failure of Specimens of Goose Lake Clay

For normally consolidated specimens the strain at the peak stress difference usually decreases as the consolidation pressure increases because of reorientation of the clay particles into face-to-face domains. Thus, the decrease in strain at failure with higher confining pressures was expected.

The opposite extreme from the dry specimens are the ones compacted at a water content of 18 percent. These specimens are nearly saturated even at a confining pressure of 10 psi and are certainly saturated at 100 psi. Thus, for pressures between 100 psi and 1000 psi there can be no effect of total confining pressure on the axial strain at failure because the effective stresses are the same in all of these specimens. All of the specimens compacted at 18-percent water content were soft, strain hardening materials and failed at high axial strains.

Specimens compacted at water contents intermediate between 6-1/2 percent and 18 percent behaved in an intermediate manner. For tests performed at the lowest confining pressures, an increase in the compaction water content resulted in a gradual increase in the axial strain at failure. For tests performed at the highest confining pressures, the axial strains did not vary widely with compaction water content because these specimens were all either saturated, or nearly so, by the high confining pressure.

Secant moduli. Probably the most convenient way of presenting stress-strain data for soil-structure interaction problems is through use of the secant modulus. Tangent moduli are often used but the stress-strain curves obtained from tests with compacted soils are often continuously curved. Thus, the tangent modulus cannot be uniquely defined. Further, experimental errors are most severe at low strains, especially in dynamic tests, and cause excessive scatter. The secant modulus can be defined in a variety of ways. It will be defined here as the ratio of the stress difference, $(\sigma_1 - \sigma_3)$, to the axial strain, ϵ_a; at an axial strain of one percent.

Before examining the data, it is pertinent to point out that it is extremely difficult to determine the secant modulus accurately, and is especially difficult in a dynamic test. In the case of static tests at low pressures, small variations in soil properties, from specimen to specimen, that exert a negligible influence on the compressive

54

strength, exert marked influence on the shape of the stress-strain curve at small strains, and thus influence the secant modulus. Considerable scatter usually results.

In the case of high-pressure tests on soft specimens, the problem of load-cell sensitivity becomes critical. The load cells used on this project were designed to measure the compressive strengths. When a soft specimen was used at a high confining pressure, the load cell was first subjected to a large stress from the confining pressure and then to only a small additional stress as the specimen strained the first one percent. Thus, the stress calculation involved taking the difference between two large numbers and dividing by a small number, 0.01. As a result, secant moduli could not be defined with precision for the specimens compacted at water contents of 16 and 18 percent. For these latter tests, another and even more severe problem occurred because of the application of the seating load. Although great care was used to apply only small seating loads, the fact remains that the sensitivity of the electrical recording system prevents precise determination of the seating loads when this seating load represents less than one percent of the capacity of the load cell, as was the case for the soft specimens. Variations in the seating load that exert a negligible influence on the strains at failure and on the compressive strength, exert considerable influence on the secant modulus. In some cases, significant seating loads were applied and removed during the setting up of the tests involving soft specimens. Such a stress cycle would cause a large increase in the secant modulus. As a result of these problems, the ranges in values of the secant moduli reported here for specimens compacted at water contents of 16 and 18 percent should be correct but attempts to study the influence of strain rate or confining pressure on the moduli will be severely hindered by scatter in the data.

In calculating secant moduli, a correction was applied to the cross sectional area of the specimens for the volumetric strains under the confining pressure but no corrections were applied for volumetric strains during shear. In the cases where this volumetric strain could be measured, i.e., in static tests subjected to pressures of 100 psi or less, the volumetric strain at one percent axial strain, resulting from

the shear, was always one percent or less. The data are certainly not accurate to within one percent and no correction was applied.

The secant moduli are plotting versus the time to failure in Figure 22. For the three lowest water contents, where the sensitivity of the load cells was not a problem, the scatter is remarkably small, smaller than usually obtained even from static tests. The curves show clearly that the secant modulus increases significantly as the rate of deformation increases. Again, the most convenient method of demonstrating the influence of strain rate is to normalize the data. The average curves of Figure 22 were normalized by dividing the secant modulus at various points along the curve by the secant modulus for a time to failure of one minute. The normalized data are plotted in Figure 23. No data are included for the specimens compacted wet of optimum because an average curve could not be drawn through the points. The data in Figure 23 indicate that the dynamic effect is slightly larger for the specimens compacted at the lower water contents and that the confining total stress does not exert a significant influence. The range of data is so small, and nearly random, that a single average curve has been drawn. The normalized secant moduli, and the change in these normalized moduli per decade of change in time to failure, are as follows:

Time to Failure	Normalized Secant Modulus	Increase in Normalized Secant Modulus, %
100 m . . .	0.75	
		 17
10 m . . .	0.88	
		 14
1 m . . .	1.00	
		 16
6 s . . .	1.16	
		 14
600 ms . . .	1.32	
		 14
60 ms . . .	1.51	
		 17
6 ms . . .	1.76	

Thus, on the average, the increase in secant modulus per decade decrease in the time to failure is 15 percent.

The influence of confining pressure on the secant modulus for static tests is shown in Figure 24. For the specimens compacted at a nominal water content of 6-1/2 percent, much of the applied total confining pressure was taken by effective stress within the soil specimen and, as a result, the secant modulus increased markedly with increasing
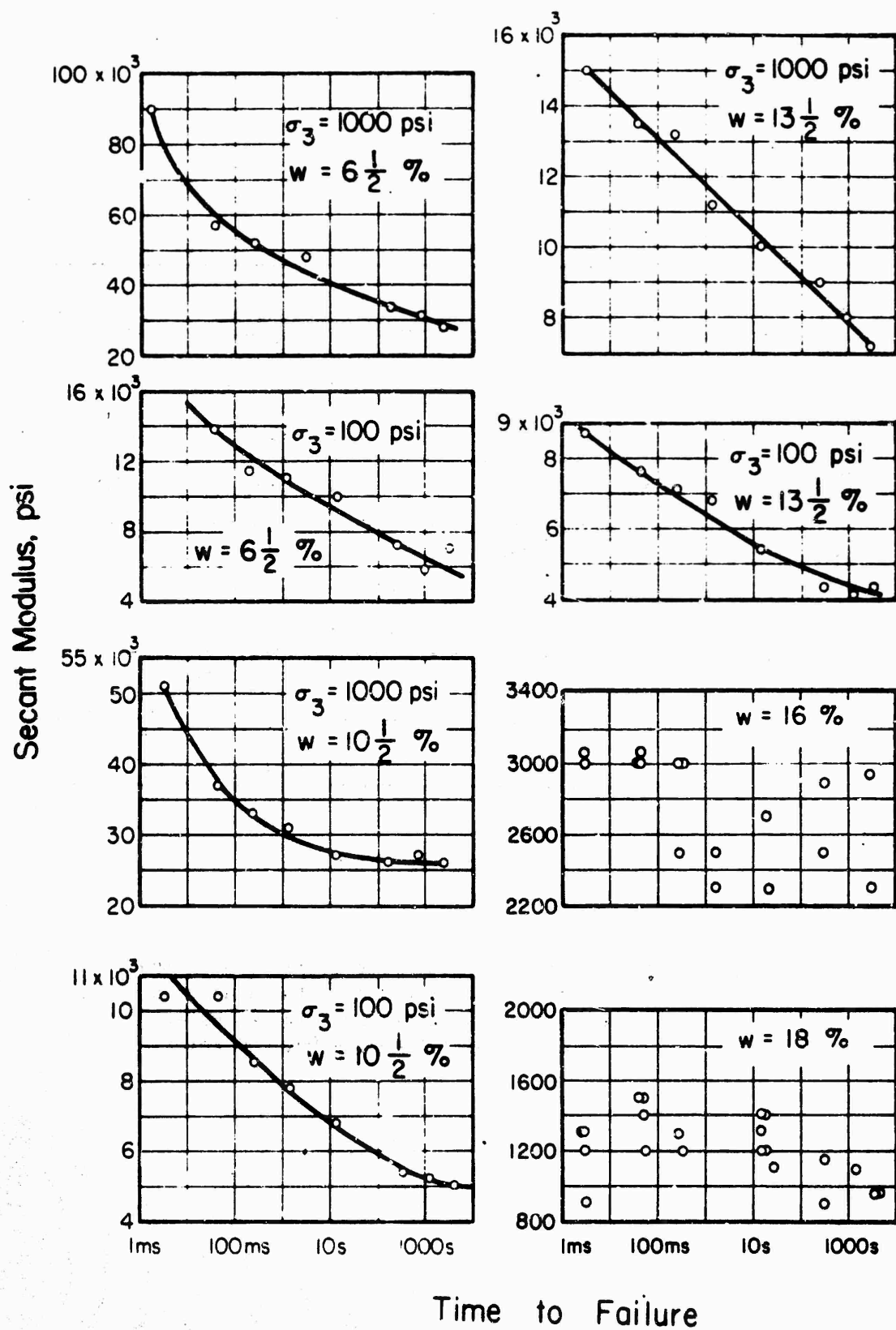
56

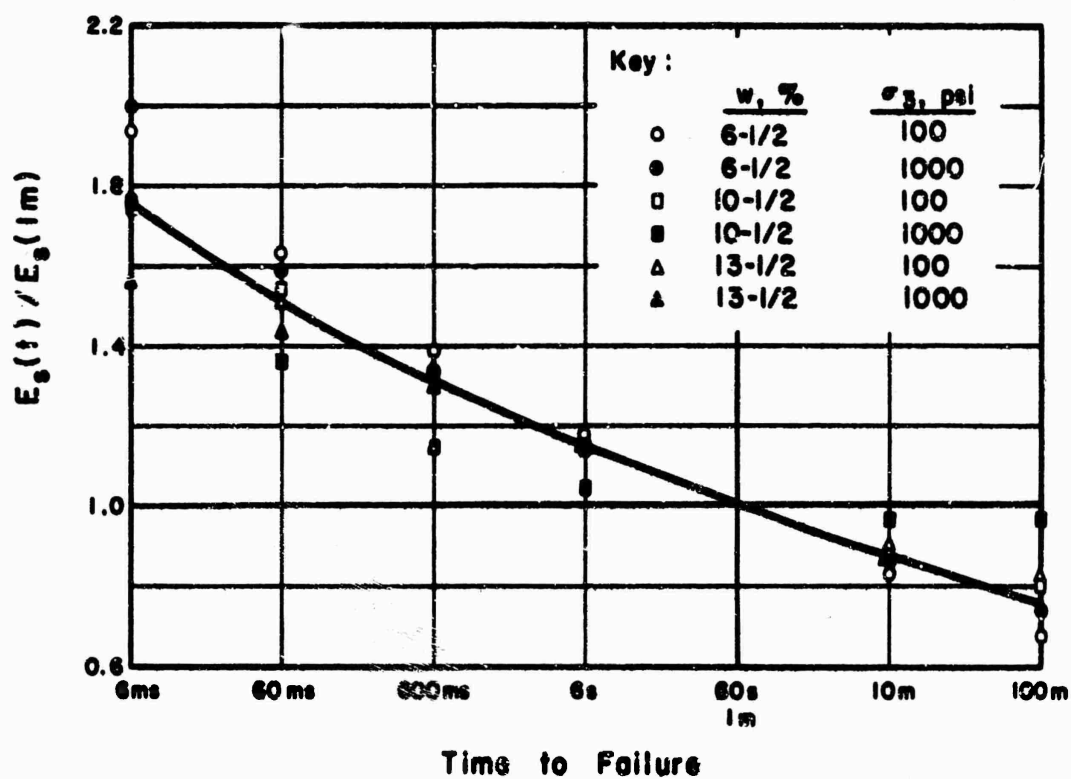Figure 22. Secant Moduli, Defined at One Percent Axial Strain

Figure 23. Influence of the Time to Failure on the Normalized Secant Moduli for Specimens of Goose Lake Clay Compacted at Water Contents Lower than the Optimum Point
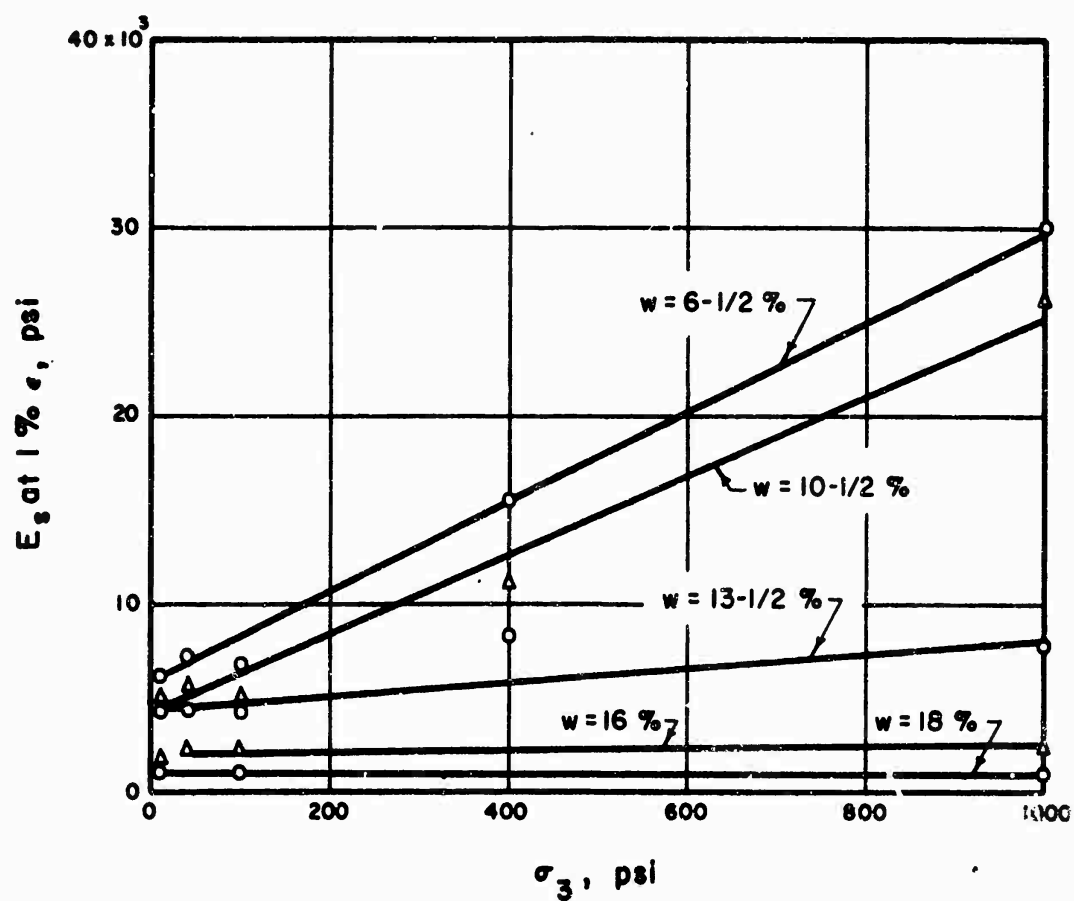
Figure 24. The Influence of Confining Pressure and Compaction Water Content on the Secant Modulus of Compacted Specimens of Goose Lake Clay Subjected to Q-Type Triaxial Compression Tests with a Time to Failure of About 1000 Seconds

confining pressure. Similar, but progressively smaller, rates of
increase occurred for compaction water contents of 10-1/2 and 13-1/2
percent. For specimens compacted at 16 and 18 percent, the specimens
became saturated at confining pressures of the order of 100 psi, as
discussed previously. Thus, any additional applied total stress would
be taken by the pore water and would not be expected to change the
stress-strain properties. Thus, the secant modulus was independent of
confining pressure for pressures greater than about 100 psi. It is
probable that the plots of E_s versus σ_3 would have the same general
shapes as the plots of $(\sigma_1 - \sigma_3)_f$ versus σ_3 (Figure 18) if sufficiently
accurate values of E_s could be obtained.

The influence of compaction water content on the physical
properties of the clay was of considerable interest because it was
hoped that the physical properties could be changed through a wide
range just by altering the compaction water content. The influence of
compaction water content on the secant modulus is shown in Figure 25.
For the specimens compacted on the dry side of optimum, the compaction
procedure effectively preconsolidated the specimens at a stress exceed-
ing 100 psi. Thus, for a confining pressure of only 100 psi the
specimens are effectively overconsolidated and the secant modulus
decreases only slowly as the water content increases. At the optimum
water content the specimens become more plastic and the secant modulus
drops more rapidly. The confining pressure of 1000 psi is consider-
ably more than the pressure applied during compaction. Thus, the
secant modulus decreases rather uniformly as the water content increases,
in response to a gradually increasing degree of saturation. It is
apparent that a considerable range in secant moduli can be obtained by
varying the compaction water content.

Conclusions based on triaxial shear tests. Based on the
triaxial shear testing program just reported, the following conclusions
are drawn:

1. The experimental apparatus performed quite successfully at all
   pressure levels and at all rates of deformation. However, a load
   cell of a different design should be used if secant moduli are
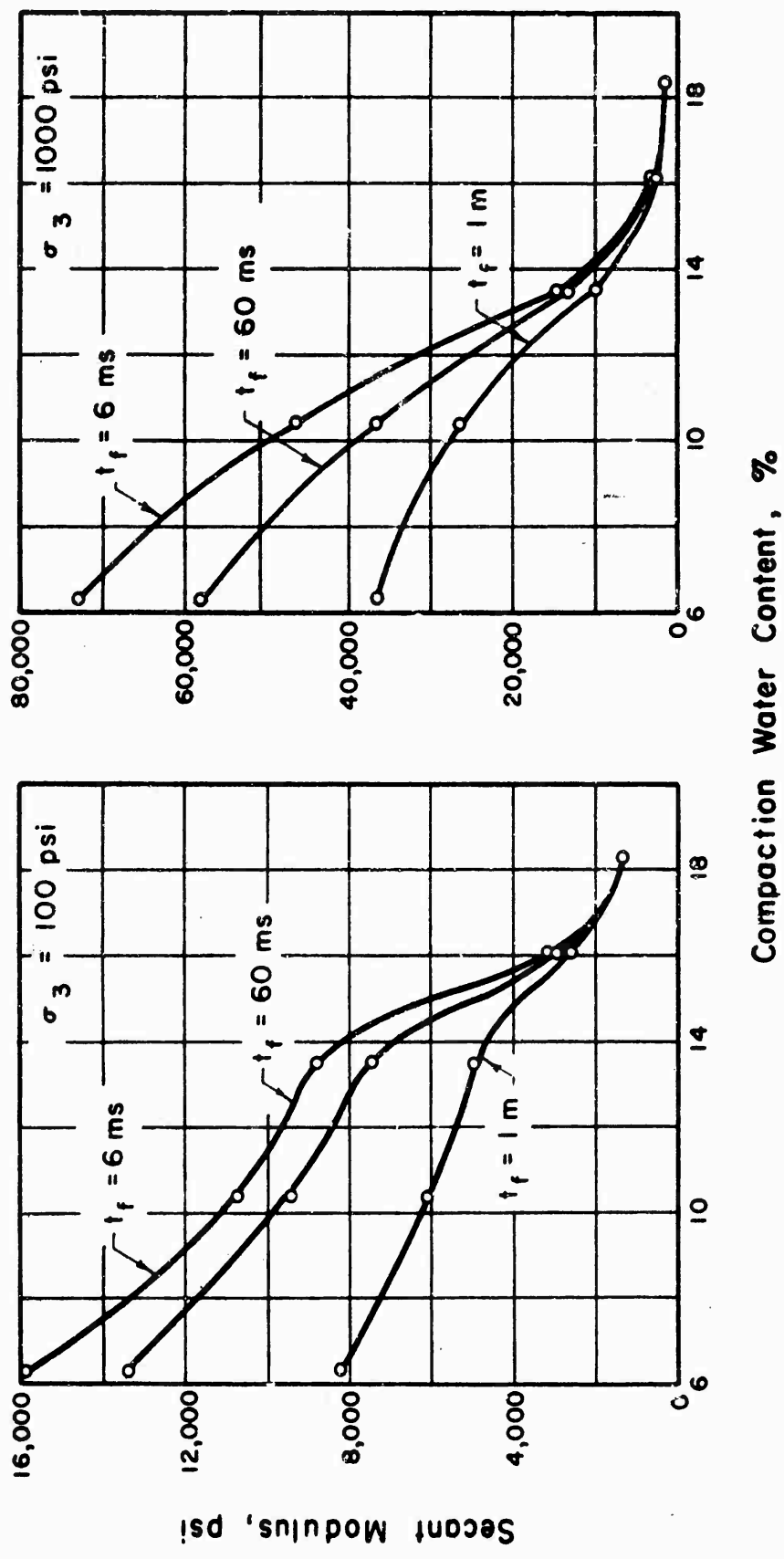   needed for soft specimens.

60

Figure 25. Influence of Compaction Water Content on the Secant Modulus

61

2. The specimen preparation procedures allowed the preparation of large numbers of nearly identical specimens. The physical properties of these specimens were reproducible to a high degree.

3. The failure envelopes obtained from static tests at pressures up to 1000 psi using Q-type (unconsolidated-undrained) triaxial compression tests were concave towards the pressure axis, indicating a gradually increasing value of B_w as the confining pressure increased. The confining pressure required to pressure saturate the specimens (attain the $\emptyset_Q = 0$ condition) decreased as the compaction water content increased. For the specimens compacted 5 percent on the dry side of optimum, a pressure of about 1000 psi was required to attain $\emptyset_Q = 0$ whereas a pressure of less than 100 psi was required for specimens compacted 3 percent wet of optimum.

4. Increasing the deformation rate caused a substantial increase in the compressive shear strength of all specimens. If a time to failure of one minute is used as a standard of comparison, then for specimens compacted at water contents ranging from 5 percent dry of optimum to 3 percent wet, a 10^4 times reduction in the time to failure (down to 6 ms) caused the strength to increase by from 37 percent to 65 percent. The increase was slightly more for specimens subjected to a confining pressure of 1000 psi than for those subjected to 100 psi. This dynamic effect seemed to be smaller for specimens compacted at lower water contents. The average percentage increase in strength, per decade reduction in time to failure, for specimens compacted at water contents from 5 percent below optimum to 3 percent above, ranged from only 2 percent for the t_f range 100m-10m to 18 percent for the range 60ms-6ms. Thus, the dynamic effect was concentrated in the fastest tests.

5. The axial strains at failure depended on the compaction water content and the confining pressure, but not on the rate of deformation. For a confining pressure of 10 psi, the specimens compacted at low water contents dilate during shear and failed at low strains; as low as 1 percent in some specimens. The strain at failure increased as the compaction water content increased. For a confining pressure

of 1000 psi, the specimens compacted at a water content of 8-1/2 percent dry of optimum failed at about 18 percent axial strain, and the strain increased slightly as the compaction water content increased. The specimens compacted 3 percent wet of optimum and subjected to 1000 psi of confining pressure, failed at about 26 percent strain.

6. The secant moduli, defined at 1 percent axial strain, were well defined for the specimens compacted dry of optimum, but were so low for specimens compacted on the wet side of optimum that a problem developed because of the sensitivity of the load cells. For the specimens compacted on the dry side of optimum, the secant modulus increased by from 55 percent to 100 percent when the strain rate was increased by 10^4 times. On the average, there was a 15 percent increase in secant modulus for each ten times reduction in the time to failure. This dynamic effect was not concentrated in the fastest tests as it was for the compressive strengths, but was uniform within a few percent throughout the range of times to failure used during this study.

7. For specimens compacted on the dry side of optimum, the secant modulus increased with confining pressure.

8. For any given time to failure and confining pressure, the secant modulus decreased as the compaction water content increased. For example, for specimens subjected to a confining pressure of 1000 psi and loaded to failure in 6 ms, the secant modulus decreased from about 74,000 psi to 1500 psi as the compaction water content increased from 6 percent to 18 percent.

9. Based on these tests it appears that the strength and stress-strain properties of the Goose Lake clay can be varied between wide limits depending on the compaction water content, the loading rate, and the confining pressure. Further, the properties of the small specimens used in this study can be reproduced with satisfactory accuracy.

63

SECTION V

ON -DIMENSIONAL COMPRESSION TESTS

Introduction

One-dimensional compression tests were performed on specimens of compacted Goose Lake clay that were 4 inches in diameter and one inch thick. The specimens were laterally constrained by a steel ring, one inch high and 0.1 inch thick. The ring was equipped with strain gages so that the stress induced in the ring could be determined. This stress could then be used to calculate the radial stress applied by the soil specimen; which, in turn, could be used to determine the coefficient of earth pressure under conditions of nearly zero lateral strain.

Axial stresses were applied to the soil specimens through a 2-inch thick steel loading cap. The tests were similar to the usual one-dimensional consolidation tests of the fixed ring type except that the compacted soil was loaded under undrained conditions. The upper and lower surfaces of the soil were covered by the impervious steel loading cap and base respectively. The axial deformations of the specimens were measured using linear variable differential transformers (LVDT). The axial load applied to the specimens was measured using a load cell mounted directly above the loading cap.

Attempts were made to load specimens to axial pressures of 200 psi and 400 psi using rise times of either approximately 2 milliseconds or 10 seconds. For convenience of discussion, the tests with a rise time of about 2 milliseconds will be termed dynamic tests and the tests with a rise time of 10 seconds will be termed slow tests. An attempt was made to prepare specimens at approximately the same water contents and densities used for triaxial shear tests.

Apparatus for One-Dimensional Tests

Compaction equipment. To avoid problems associated with the trimming of specimens into the consolidation ring, the soil specimens were compacted directly into the ring. During compaction, the ring was clamped against a polished steel base as indicated in Figure 26. A standard hammer with a weight of 5.5 pounds and a height of fall of
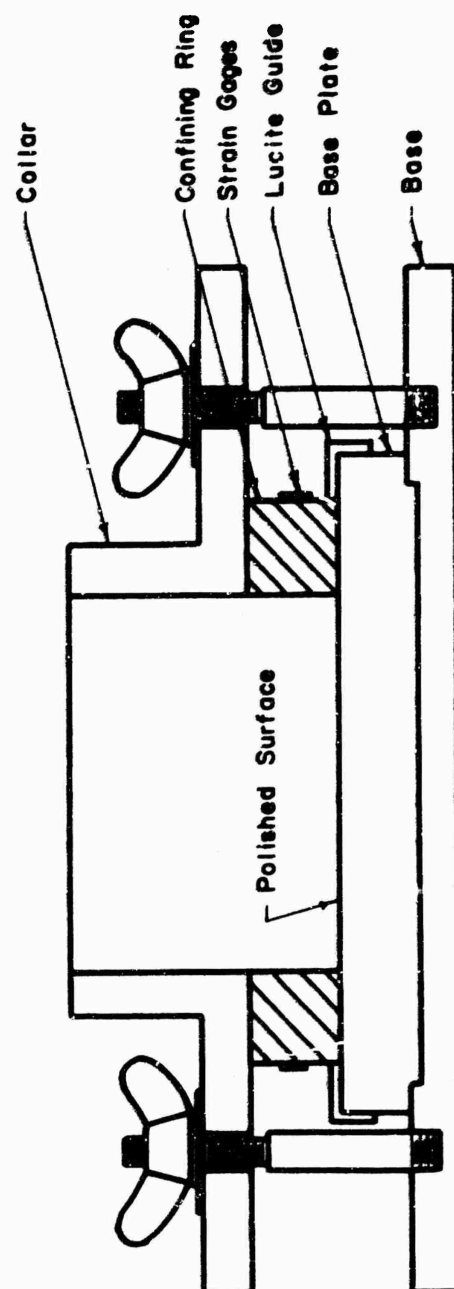
Figure 26. Schematic Cross Section of Apparatus Used for Compaction of One-Dimensional Test Specimens

12 inches was used to compact the specimens. The compaction equipment and the ring are shown in Figure 27.

Compression cell. By analogy with the terminology used for normal one-dimensional consolidation tests, the apparatus not associated with the loading equipment nor with the instrumentation, is termed the compression cell. Front and side views of the partially disassembled compression cell used in these tests are shown in Figures 28 and 29 respectively. The cell consists of the following parts: (1) a steel base with two steel columns for mounting the coils of the LVDTs, (2) a plastic guide used to center the ring, (3) the steel ring containing the soil specimen, (4) an upper plastic guide used to center the loading cap, (5) the steel loading cap, and (6) two plastic blocks containing the LVDT coils.

For these relatively low-pressure tests, a ring with a thickness of 0.1 inch was used. The ring was equipped with electrical strain gages so that the stresses induced in the ring during a loading test could be determined. The ring was calibrated using hydraulic pressure as described by Kane, Davisson, Olson, and Sinnamon.[6] The ring was designed to be used for radial pressures up to 1000 psi. The constant was 0.77 psi radial stress per micro-inch per inch of strain. The ring was centered on the base of the cell using a plastic guide.

During a compression test, the acceleration of the loading cap was determined using a piezoelectric accelerometer, which was mounted rigidly on the edge of the cap (Figure 29).

The axial movement of the loading cap was measured using two LVDTs. The cores of the LVDTs were rigidly connected to diametrically opposed edges of the loading cap (Figure 28). The coils of the LVDTs were sealed into plastic blocks. These blocks were equipped with dove tails so that they could be mounted on the two steel columns shown in Figure 28. The 2 blocks could be slid up and down in the slots and could be fixed rigidly at any location using set screws mounted in the uprights (Figure 29).

In order to calibrate the instrumentation system it was necessary to be able to move the LVDT cores vertically through precisely known distances. The controlled movement was achieved in the following manner: A round-headed machine screw of the 10-32 size was attached to an
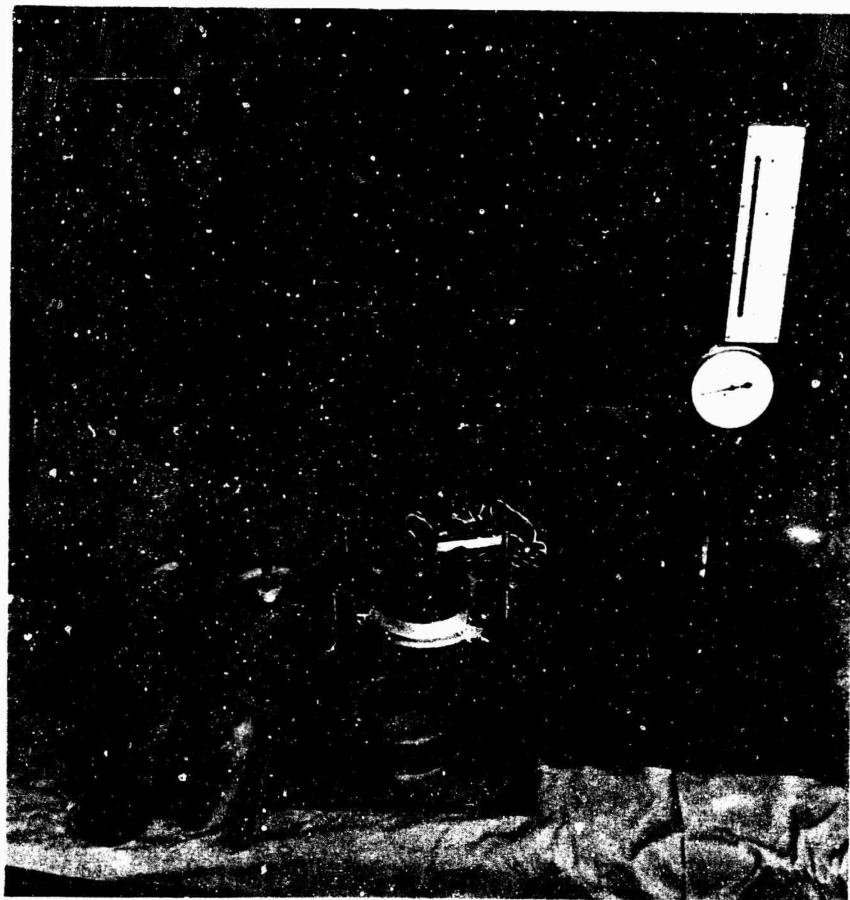
66

Figure 27. Equipment Used in the Preparation of Specimens
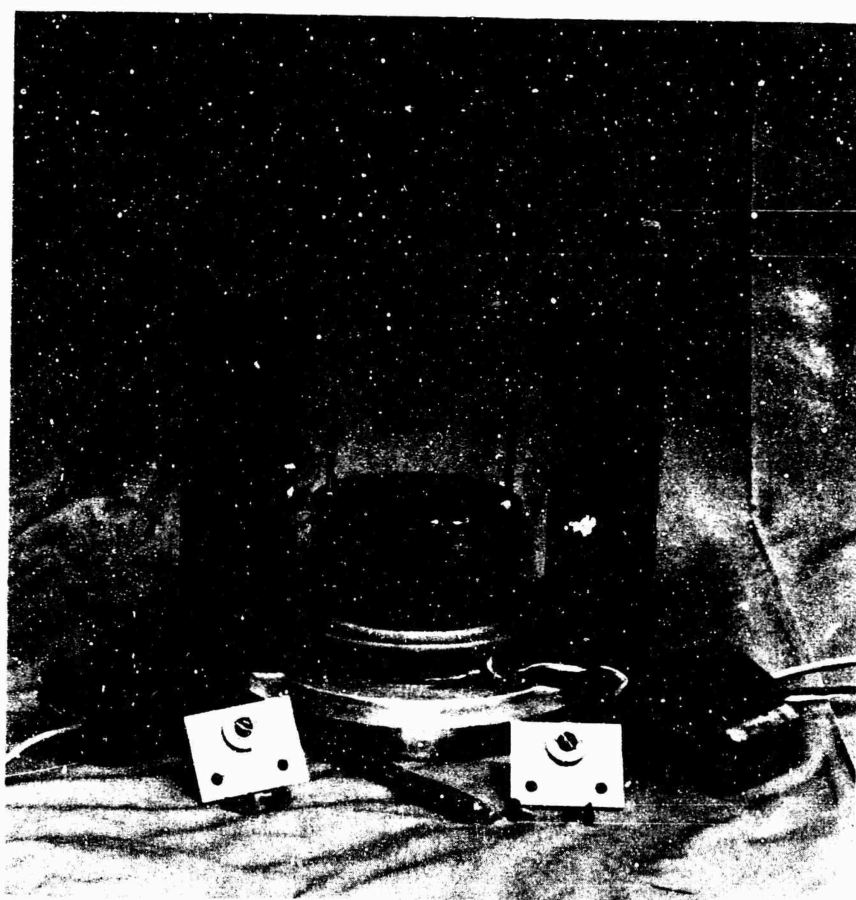for One-Dimensional Compression Tests

Figure 28. Front View of Partially Disassembled Compression
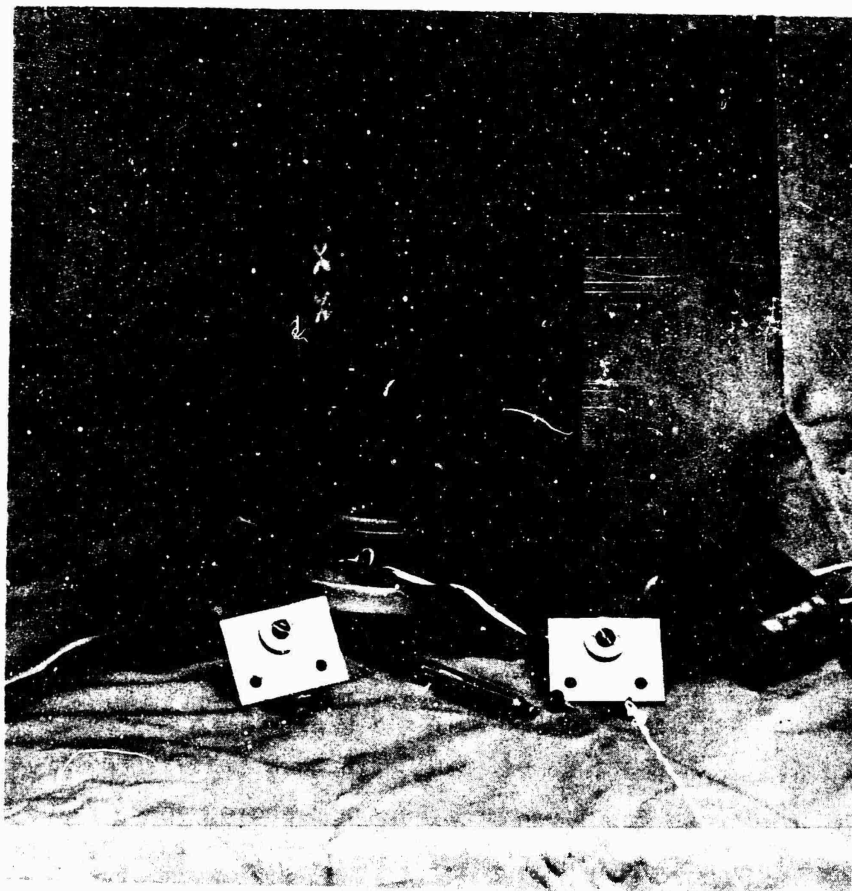Cell Containing a Soil Specimen

Figure 29. Side View of Partially Disassembled Compression
Cell Containing a Soil Specimen

aluminum plate with a collar such that the screw would be free to rotate but could not undergo axial movement relative to the plate. The plate was then attached to the top of one of the steel columns. The plastic block was then raised until the machine screw could be turned into a threaded hole in the block. Rotation of the screw then caused the block, and thus the coil of the LVDT, to move vertically through known distances. The aluminum plates, screws, and blocks are shown disassembled in Figures 28 and 29 and are shown assembled in Figure 30.

Loading Machine. The loading apparatus discussed previously for the triaxial tests was also used for the one-dimensional tests. The machine was operated pneumatically for the "dynamic" tests and hydraulically for the "slow" tests.

For the one-dimensional tests the load cell was mounted on the loading machine. For these tests, the load cell was a solid aluminum cylinder (Figure 30) equipped with electrical-resistance type strain gages. The load cell had a design capacity of 30,000 pounds and a sensitivity of 0.56 psi per micro-inch per inch, where the psi is the pressure applied to a 4-inch diameter soil specimen.

Instrumentation system. The instrumentation system was the same as the one used for the triaxial shear tests with the addition of a charge calibrator and a charge amplifier, which were used to charge and drive the accelerometer. For the hydraulic tests, the data were recorded on magnetic tape and immediately played back onto an X-Y plotter. For the pneumatic tests, the data were transferred from the magnetic tape onto an oscilloscope screen and photographed. The photographs were enlarged and hand reduced to obtain the stress-strain-time curves discussed later.

Experimental Procedure

Specimen preparation. The soil for each series of four tests at a single water content was mixed with water, using batches of 2000 grams of soil each, and stored for 48 hours in sealed plastic bags prior to compaction.

Prior to compaction, the inside wall of the compression ring was coated with silicone high vacuum grease, to reduce ring friction, and the ring was weighed with an accuracy of 0.03 gram. The soil was
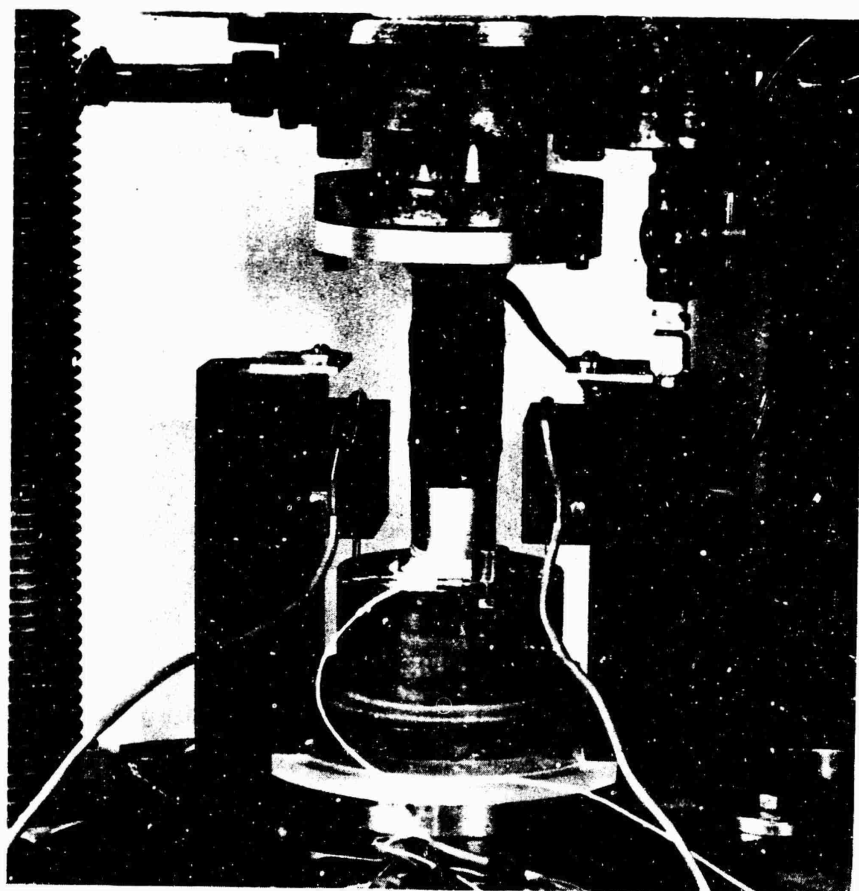
70

Figure 30. One-Dimensional Compression Cell, Fully Assembled and Mounted in the Testing Machine

compacted into the ring in two layers with each layer receiving from six to ten evenly distributed blows from the compaction hammer. Six was the minimum number of blows that would yield a reasonably homogeneous specimen. The surface of the first layer was scarified prior to compaction of the second layer to ensure a firm bond. After compaction, the compaction apparatus was disassembled and the soil was trimmed flush with the faces of the ring. The trimmings were used to determine the compaction water content. The ring and the soil specimen were weighed to within 0.03 gram. A dial comparator was used to measure the actual thickness of the trimmed soil specimen.

The specimen and ring were then placed in the compression cell. Partially assembled cells are shown in Figures 28 and 29.

Test procedures. The assembled compression cell was placed on the lower platen of the dynamic press used for the triaxial testing program. A template, bolted to the base of this machine, ensured precise centering of the apparatus. A small amount of rapid setting cement was placed on top of the steel loading cap and the loading machine was lowered until the base of the load cell had squeezed out all but about 0.10 inch of the cement. The strain gages in the load cell were monitored during this process to ensure that no significant load was applied to the soil specimen. Excess cement was removed and the remaining cement was given 20 to 30 minutes to set. The purpose of the cement was to ensure a uniform seating of the load cell on the loading cap.

The complete compression cell, containing a soil specimen, properly mounted in the press just prior to a test, is shown in Figure 30.

During the time of setting of the cement, the electrical system was calibrated. The recording channels for the LVDTs were calibrated first by moving each of the plastic blocks (Figure 30) vertically through previously selected distances using the 10-32 machine screws. The blocks were then adjusted to their proper initial position and locked firmly in place. Calibration steps were recorded for the axial stress, radial stress, and acceleration using previously calibrated resistors, as for the triaxial tests discussed previously. Calibration steps were recorded on both the oscillograph and the magnetic tape recorder.

After calibration and setting of the cement, a seating stress of approximately 15 psi was applied to the specimens. For the slow tests, the seating stress was applied by lowering the loading machine manually. For the dynamic tests, the seating load was obtained by applying a suitable nitrogen pressure in the main tank prior to closing the main valve. The main valve was then closed and the main tank pressurized for the test. Figure 31 shows the press and compression cell just prior to the performance of a slow test.

The actual performance of a test was performed in the same manner as for triaxial tests. The recording equipment was started about 300 ms prior to firing the machine to ensure that they had attained terminal velocity when the test started. For the hydraulically performed tests, a single setting of the regulating valve was used for all tests. The rise times were of the order of 10 seconds. For the pneumatically performed tests, the rise times were of the order of 2 ms. A dwell time of 30 to 50 seconds was used for all tests. The loads were then decayed to zero over a period of another 30 to 40 seconds.

At the conclusion of each test, the load cell was raised until it no longer contacted the loading cap and the residual deformation was recorded using the LVDTs. The apparatus was dismantled and the dial comparator was used to measure the final thickness of the specimen to provide a check on the LVDTs. A final water content specimen was taken. If any extrusion took place during the test, the extruded material was collected and weighed separately.

Data reduction. For the slow tests, the measured accelerations were less than one "g" and no corrections to the measured axial stress were required. The desired data were then immediately played from the FM tape system onto the X-Y plotter. The recorded radial stresses were later hand corrected for the compression of the specimen.

For dynamic tests, the response time of the X-Y plotter was too long to allow a direct play-back even when the FM system was operated at its slowest rate. Instead, the FM tapes were recorded on the oscillograph tapes for immediate examination, and subsequently on an oscilloscope. Photographs of the oscilloscope screen were enlarged and traced by hand to obtain a permanent record of the test. The oscillograph and oscilloscope records were compared to ensure accuracy. For the dynamic
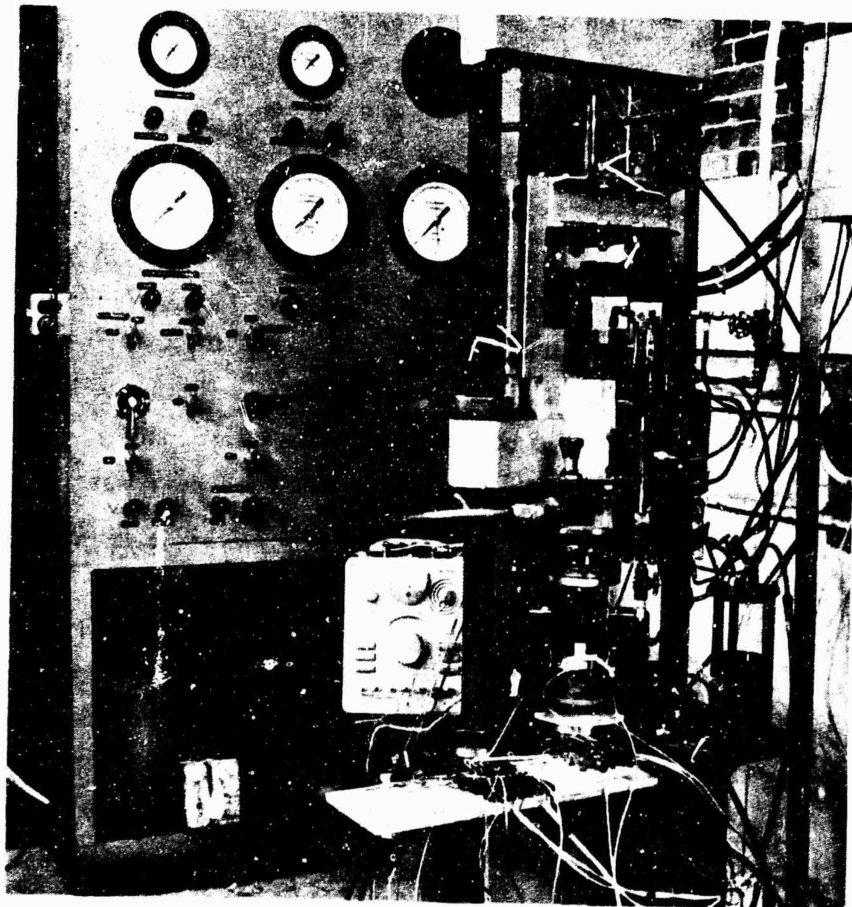
73

Figure 31. Loading Machine and One-Dimensional
Apparatus Prior to a Test

tests, it was necessary to correct the measured axial loads for the inertia of the 7-lb steel loading cap. In some tests at low strains, the inertia of this cap accounted for 50 percent of the total force measured by the load cell.

The data were hand reduced by selecting representative points on the curves and applying the inertial correction to the axial load and the height-of-specimen corrected to the radial stress.

Data Presentation and Discussion

Moisture-density data. The moisture-density data for the specimens used in the one-dimensional compression study are tabulated in Table IV and presented graphically in Figure 32. The scatter in the densities in any one series of tests is considered sufficiently small so that the specimens may be considered identical.

The moisture-density curve obtained from the triaxial shear phase of this project is also shown in Figure 32. For specimens compacted on the wet side of optimum, the two curves are essentially identical. However, on the dry side, the specimens used in the one dimensional tests had significantly higher densities. Attempts to prepare one-dimensional specimens by using either fewer blows per layer or a smaller drop of the hammer led to lower densities but, simultaneously, to non-uniform specimens. Since time was not available for the development of a kneading compaction apparatus similar to the one used for preparing the triaxial specimens, but for the larger sized one-dimensional specimens, it was decided to continue use of drop-hammer type of compaction and accept the difference in the densities.

Stress-strain relationships. Average curves of axial stress versus axial strain, for all of the one-dimensional compression tests, are presented in Figures 33 through 37 and are summarized in Table IV.

The stress-strain curves obtained using the slower loading rates were well defined. A stress-strain curve, with all data points plotted, is shown in Figure 38. The scatter of individual points about the mean line in Figure 38 is representative of the scatter obtained in all of the slow tests.

Scatter of data for the tests in which the rise time was of the order of 2 ms was greater and problems were encountered in recording

75

Table IV

MOISTURE-DENSITY DATA FOR SPECIMENS
USED IN ONE-DIMENSIONAL TESTS

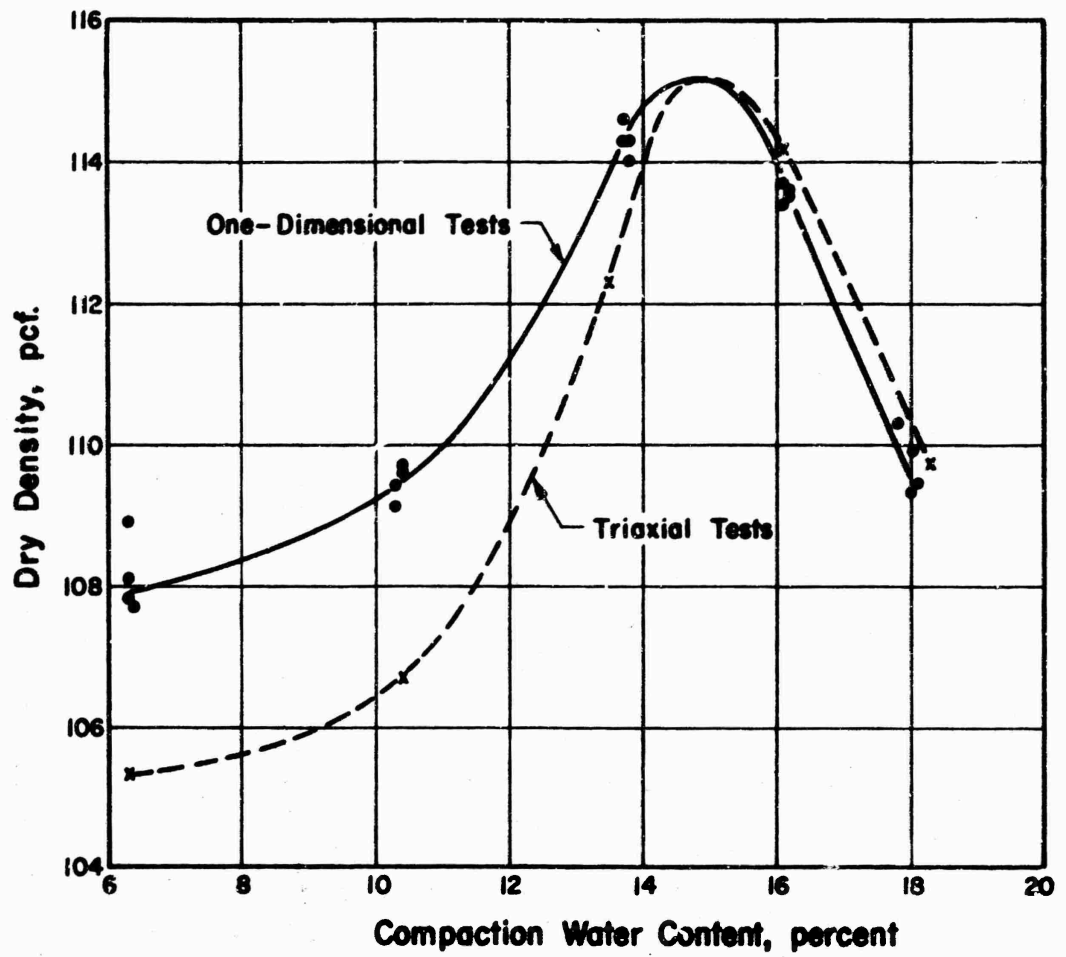| Test No.	Type of Test	Nominal Water Content w_n (%)	Actual Water Content w (%)	Dry Density γ_d (pcf)	Initial Degree of Saturation S_{ro} (%)
1	Slow	$6\frac{1}{2}$	6.3	108.9	31
2	Slow	$6\frac{1}{2}$	6.4	107.7	30
3	Dynamic	$6\frac{1}{2}$	6.3	107.8	30
4	Dynamic	$6\frac{1}{2}$	6.3	108.1	30
5	Slow	$10\frac{1}{2}$	10.3	109.4	51
6	Slow	$10\frac{1}{2}$	10.4	109.6	52
7	Dynamic	$10\frac{1}{2}$	10.3	109.7	51
8	Dynamic	$10\frac{1}{2}$	10.3	109.1	51
9	Slow	$13\frac{1}{2}$	13.8	114.0	77
10	Slow	$13\frac{1}{2}$	13.8	114.3	78
11	Dynamic	$13\frac{1}{2}$	13.7	114.6	77
12	Dynamic	$13\frac{1}{2}$	13.7	114.3	74
13	Slow	16	16.1	113.4	88
14	Slow	16	16.2	113.6	89
15	Dynamic	16	16.2	113.6	89
16	Dynamic	16	16.1	113.7	89
17	Slow	18	18.0	109.3	88
18	Slow	18	18.1	109.4	89
19	Dynamic	18	18.0	109.9	90
20	Dynamic	18	17.8	110.3	89

Figure 32. Moisture-Density Curves
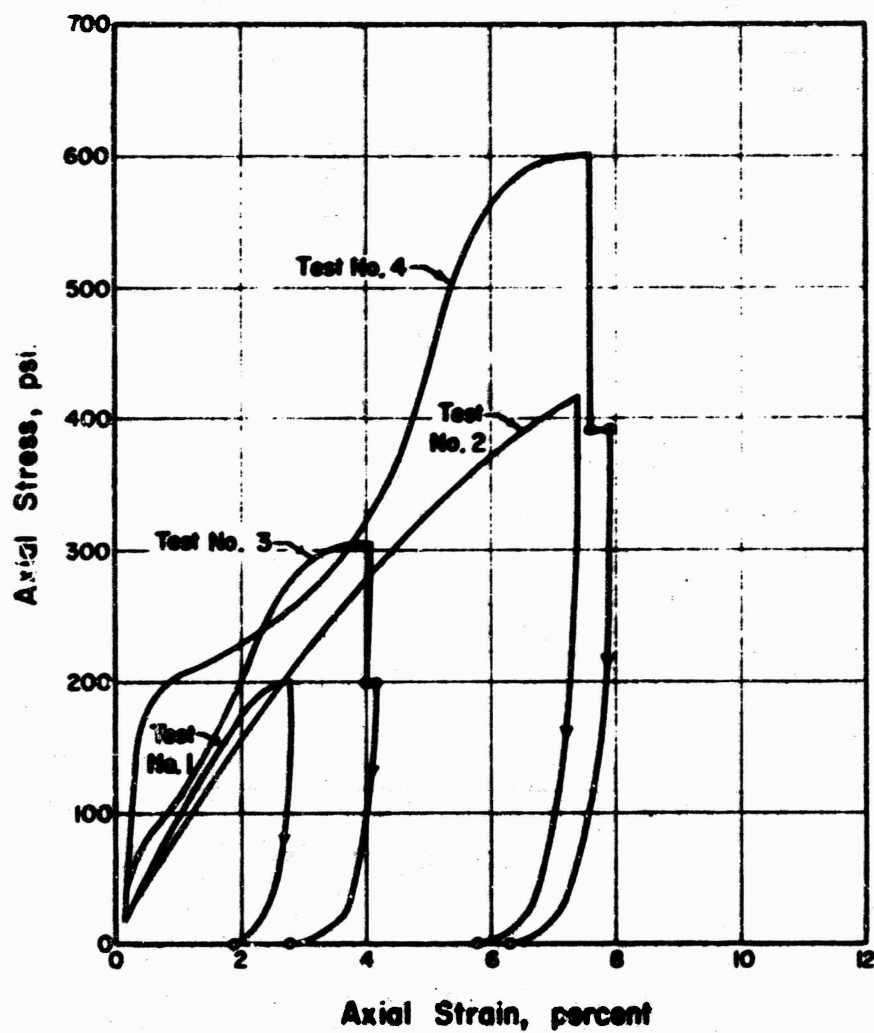
Figure 33. One-Dimensional Stress-Strain Curves for Specimens Compacted at a Water Content of 6-1/2 Percent
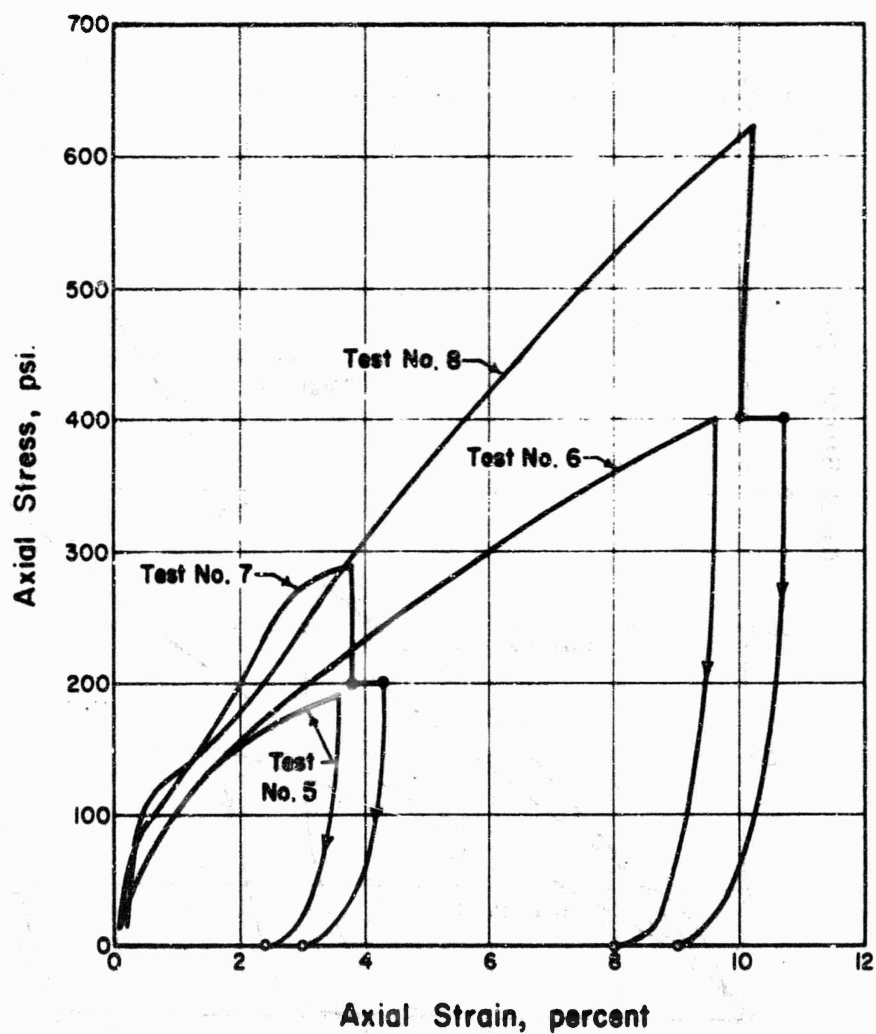
Figure 34. One-Dimensional Stress-Strain Curves for Specimens
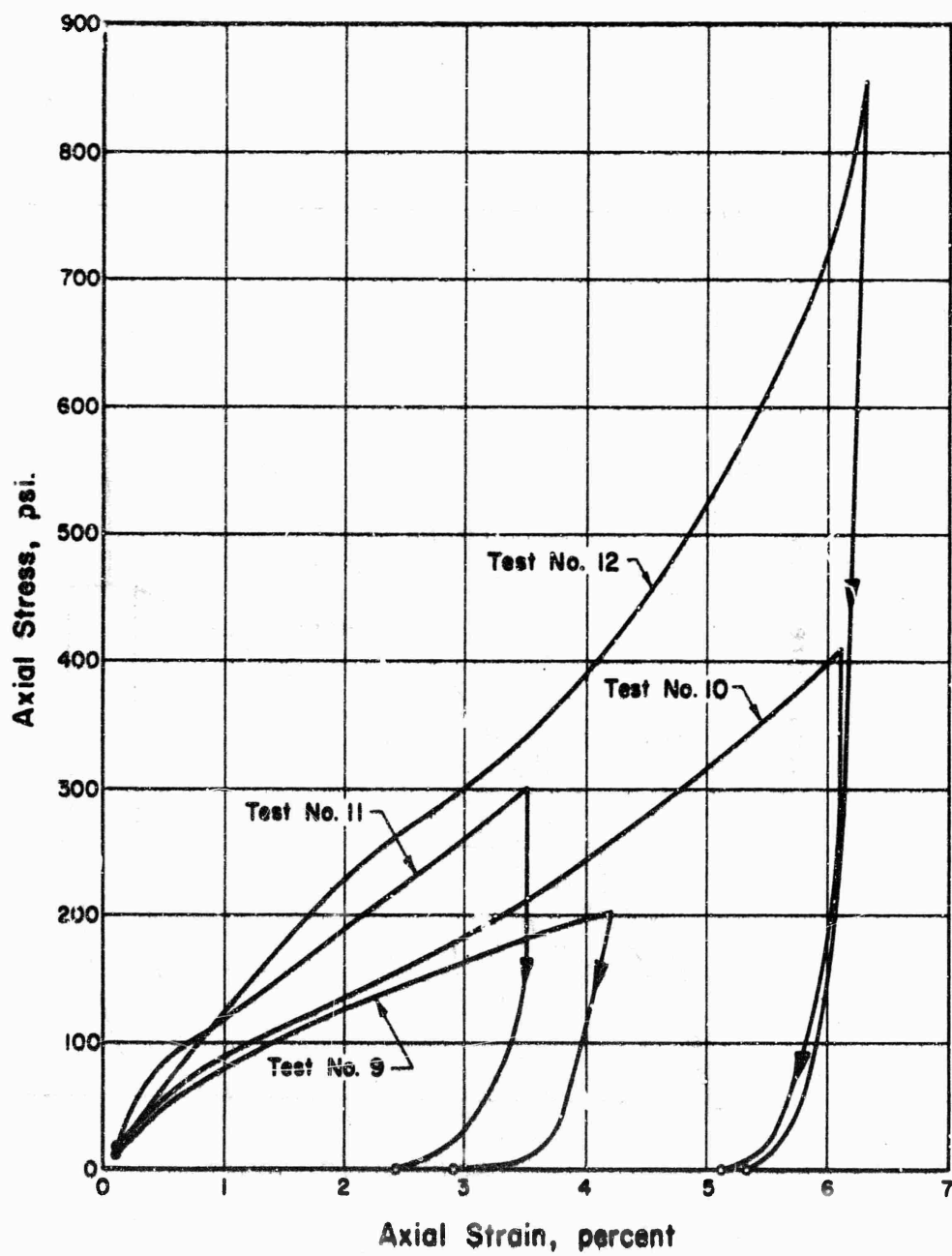Compacted at a Water Content of 10-1/2 Percent

Figure 35. One-Dimensional Stress-Strain Curves for Specimens
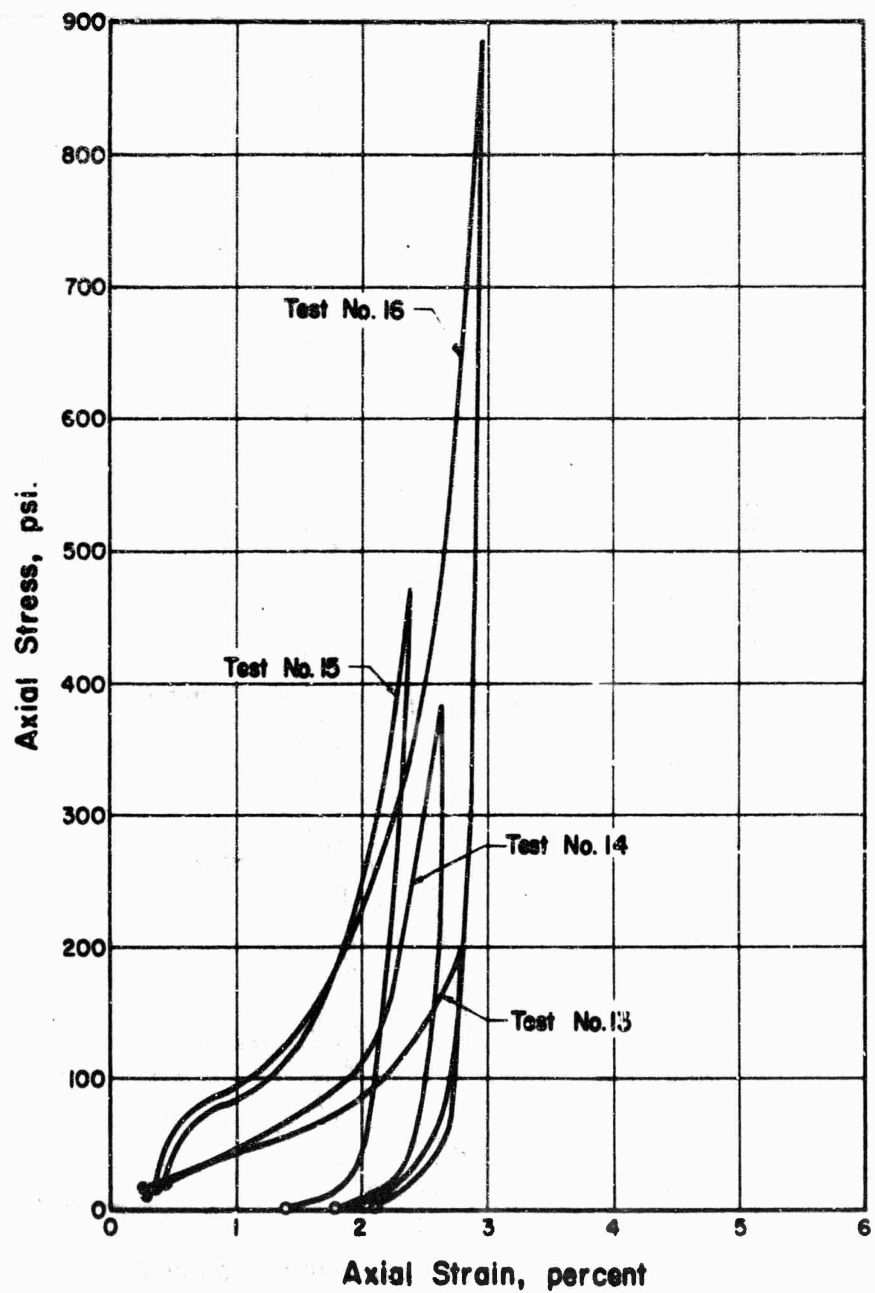Compacted at a Water Content of 13-1/2 Percent

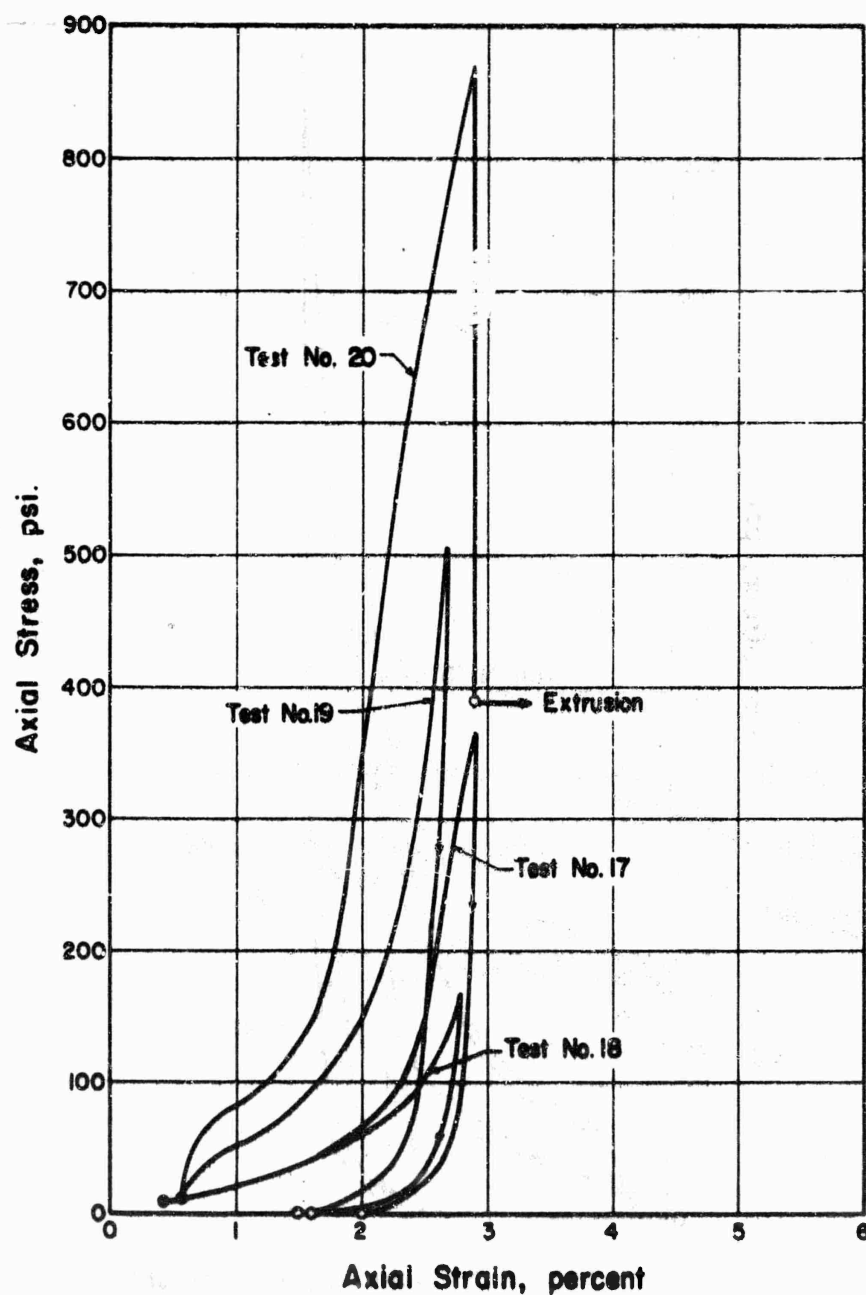Figure 36. One-Dimensional Stress-Strain Curves for Specimens Compacted at a Water Content of 16 Percent

Figure 37. One-Dimensional Stress-Strain Curves for Specimens
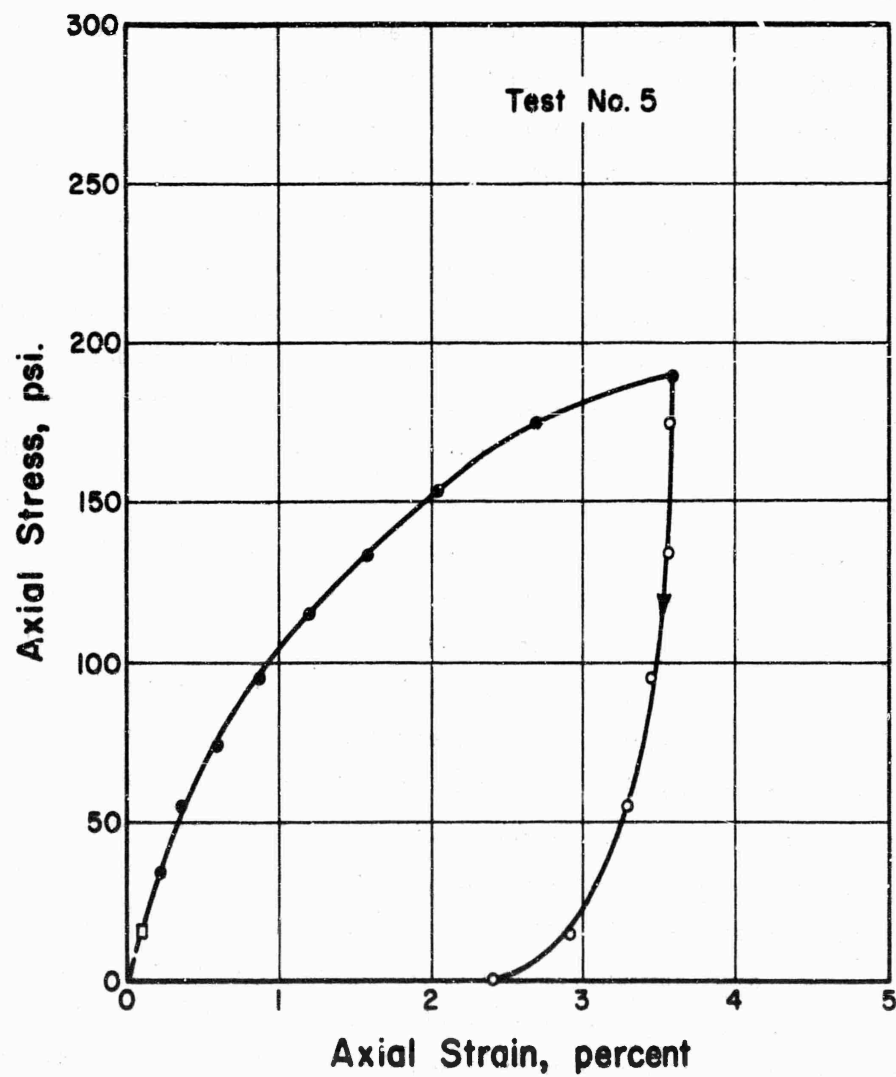Compacted at a Water Content of 18 Percent

Figure 38. Representative Stress-Strain Data for a Slow Test

data for such high loading rates. As an example of the type of data obtained, the tracing of the oscilloscope picture of axial stress versus axial deformation is presented in Figure 39 for Test No. 3. The aspects of this typical curve that warrant special comment are the hatched zones about the seating load and ultimate loads, the steep initial portion of the curve, the variations in stress and strain during the rise time, and the correction for the inertia of the loading cap.

After the test was set up, but before any axial load was applied, the outputs of the LVDTs and the load cell were recorded on the tape recorder. The tape recorder was stopped and the seating load was applied. The tape recorder was restarted and the outputs of the LVDTs and the load cell were recorded. The tape recorder was then stopped and final preparations were made to perform the test. The recorder was started again and the loading machine was fired. When the data from the tape recorder were displayed on the oscilloscope, it was not possible to display just the very short length of tape containing the test. Previous parts of the tape were also recorded. Thus, oscillations of the tape, as it passed over the rollers of the recorder during starting and stopping and normal tape imperfections, caused output fluctuations that are apparent, not real, variations in axial load and deformation. The hatched zone around the seating load represent such fluctuations. The point marked "seating load and deformation" was actually found by playing the magnetic tape data onto an oscillograph so that the time dependency of the output could be distinguished, and picking off the average position of the load and deformation traces after application of the seating load. The displacement of the oscillograph traces due to the application of the seating load was little more than the width of the traces themselves. Thus, the reported seating loads are known with an accuracy of not more than about ± 5 psi and the deformations are not known more closely than about 0.001 inch.

It is believed that most of the small fluctuations in the stress-strain curve (Figure 39) also resulted from small oscillations of the tape. One shipment of magnetic tape was tried but the apparent fluctuations in the various traces were so severe that reasonably accurate soil data could not be obtained. The tapes were discarded and tapes of higher quality were substituted. The scatter immediately decreased
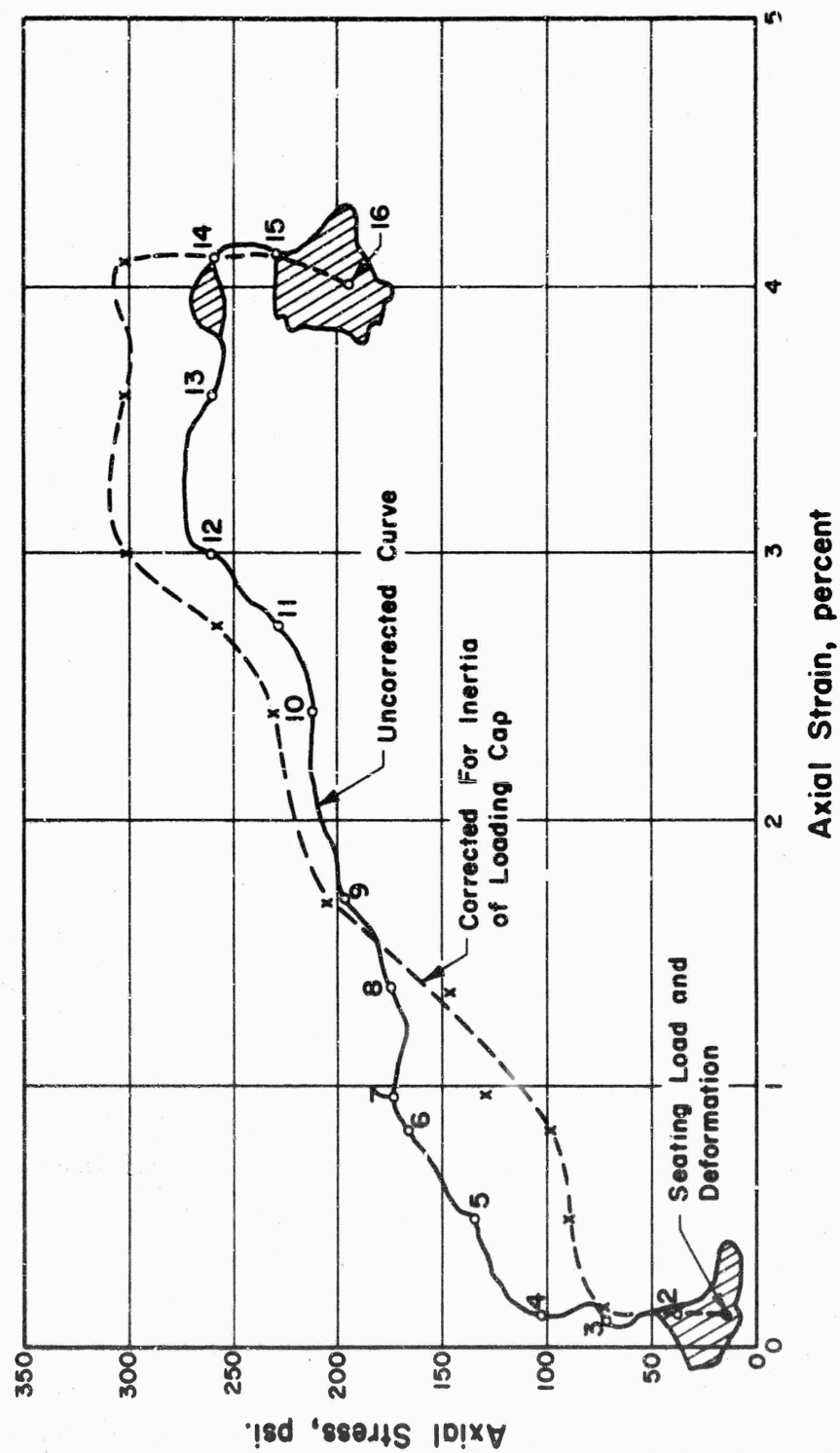
Figure 39. Dynamic Test Data for Test No. 3

85

to the small amount indicated in Figure 39. At the present time, further reduction of the scatter may not be possible without installation of a different type of recording system. It appears, however, that the scatter is not so large as to require such major changes.

The nearly vertical nature of the early part of the stress-strain curve, which occurred for all except one of the dynamic tests, cannot be immediately explained. A copy of the oscillograph tape, made from the magnetic tape, for Test No. 3 is shown in Figure 40. The vertical line used as a base for time measurements was drawn at the point where the axial-load trace first appeared to deviate from a horizontal line. The acceleration trace suddenly indicated finite accelerations starting 0.08 ms later. Radial stresses were first detected at a time of 0.62 ms. The two LVDTs simultaneously began indicating cap movements at a time of 0.74 ms. The accelerometer indicated that the acceleration increased almost linearly from 0 g to 73 g in slightly less than 0.5 ms. Such an acceleration would cause a movement of the cap of less than 0.002 inch and, thus, might go undetected. The acceleration of 73 g's corresponds to a pressure of 40 psi on the cap. The total pressure indicated by the load cell at that point was about 100 psi. Thus, about 40 percent of the apparent load was used to accelerate the heavy steel loading cap. However, the remainder of the load should have been taken by the soil and should have caused deformation. The existence of stress in the soil is shown by the fact that a stress was recorded in the confining ring at a time of 0.62 ms. For a brittle soil with a low degree of saturation, Poisson's ratio would be expected to be quite small for low stress levels. Thus, as suggested by the traces, the soil should take some amount of axial load before a significant amount of radial stress was indicated. The various channels of data therefore confirm each other except for the LVDT channels which indicate a negligible deformation until perhaps 0.2 or 0.3 ms after the specimen began taking axial stress. Because of the fact that the specimens appeared to be taking load without significant deformation, the calculated initial tangent moduli were nearly infinite. For the present, the source of the error is not apparent but it is probably involved with reaction time of the recording equipment, and with the excessively heavy cap used for these tests. Because of these problems, moduli determined during the
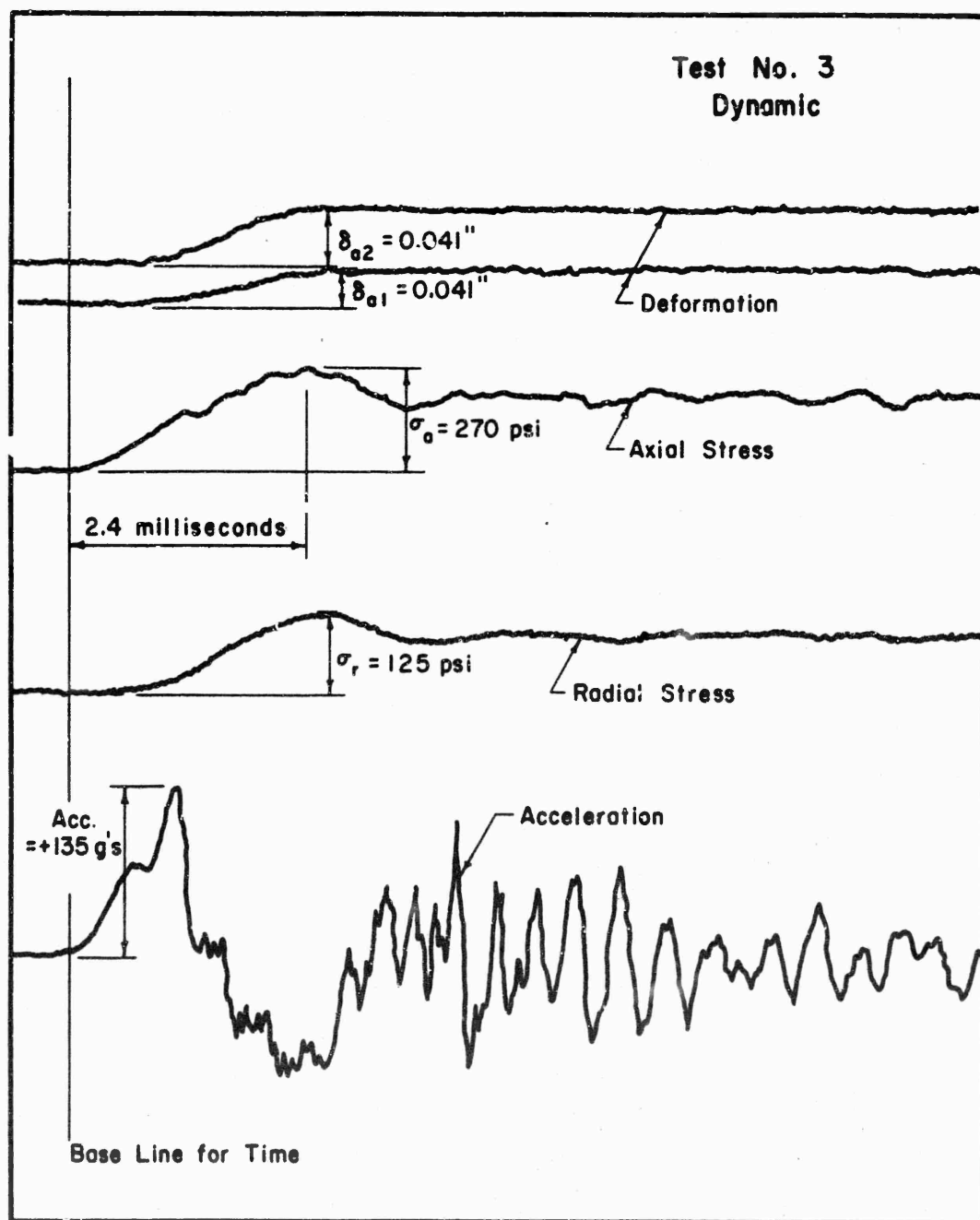
Figure 40. Typical Magnetic Tape Data Recording
f a Dynamic Test

first 1/2 ms will tend to be ignored. Other types of tests are more suitable for measurement of moduli under such low stress levels, and with such rapid rise times.

Referring again to Figure 39, the uncorrected stress-strain curve rose essentially vertically to a stress of 100 psi and then less rapidly to a stress of 190 psi. It is believed that the following small decrease in stress was due to a stress pulse that started at the loading machine when the test was fired and travelled up through the loading machine, down through the frame into the base of the press, and then back up through the specimen into the load cell. This small decrease in stress occurred for all tests subjected to the higher loading rates and, in all cases, occurred about 1/2 ms after the test started.

The measured stress then increased again and rose to a peak value of 270 psi before dropping to 200 psi. The overshoot of 70 psi resulted from the inertia of the loading system.

The minor variations in the stress-strain curve are again believed to result from small oscillations of the tape though some of them may also result from oscillation of the loading press. The hatched zone at a stress of 200 psi represents variations in stress and strain due to a combination of causes, including vibrations in the press.

The recorded stresses were corrected for inertial effects by hand. The loads were read off the curve (Figure 39) at the points indicated by the numbers 1 through 16. These loads were corrected for the inertial resistance of the cap, using the recorded accelerations, and the corrected stresses were replotted versus deformation as the dotted line in Figure 39. The corrected curve is plotted to a convenient scale in Figure 41, and a smooth curve has been drawn through the points. For this particular test, the press was set for a constant pressure of 200 psi. The actual applied stress reached 300 psi because of the inertia of the loading system, and then decreased back to 195 psi. The short horizontal line starting at an axial strain of 4 percent in Figure 41 represents creep at constant load. The creep is quite small because the stress overshoot had prestressed the specimen.
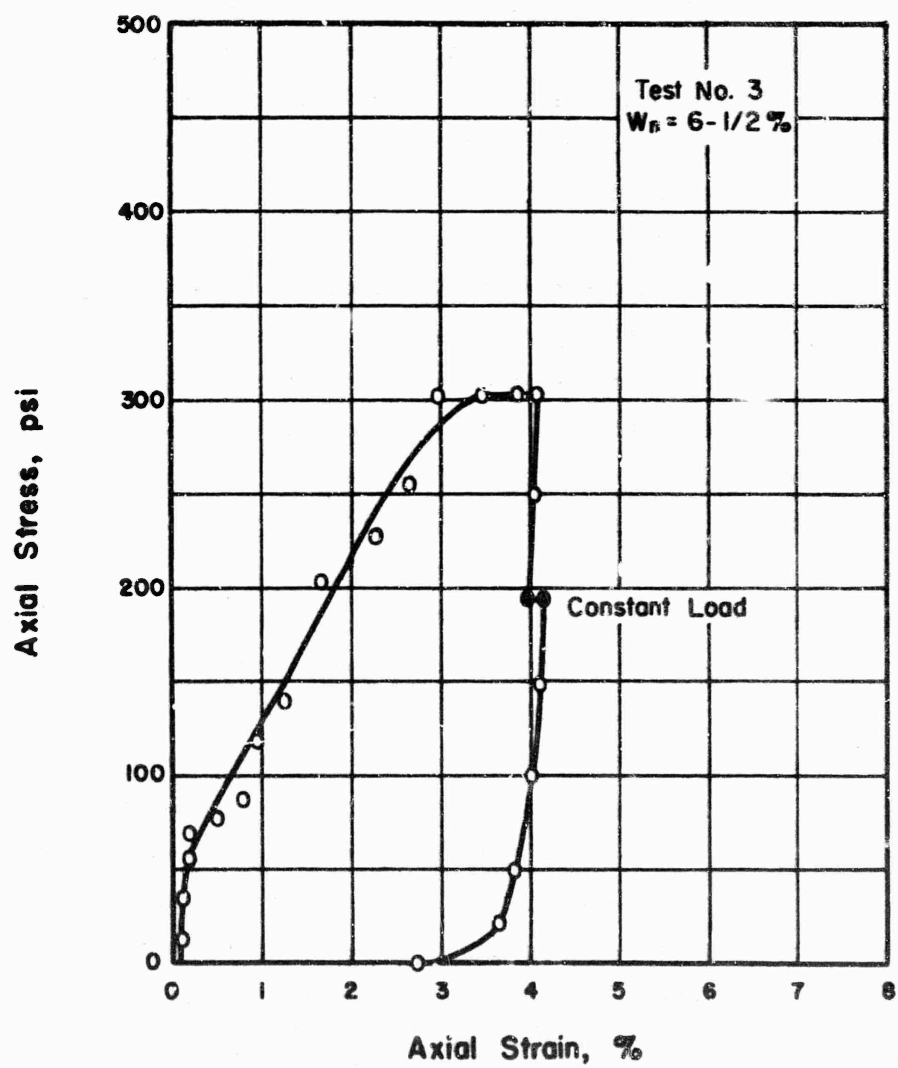
88

Figure 41. Representative Stress-Strain Data for a Dynamic Test

The foregoing procedure was used in the reduction of all data taken from dynamic tests. The scatter of points in Figure 41 is typical of the scatter obtained in all other dynamic tests.

One additional problem occurred in the case of tests performed on specimens compacted at water contents higher than optimum. These specimens withstood the peak loads without difficulty but after the load had decreased to its steady value and remained in place for a few seconds, the soil suddenly began extruding. The tests were stopped as soon as this happened.

The stress-strain curves for the one-dimensional compression tests are of the shapes generally expected. In all cases, the specimens subjected to the most rapid tests underwent smaller strains at any given stress level than did the specimens subjected to the slower rise times. The two slow tests at each water content yield about as identical stress-strain curves in the low-stress range as can be expected. In the dynamic tests, the stress-strain curves at low stresses are of questionalbe accuracy as just discussed. At the higher stresses the curves duplicate each other with reasonable accuracy.

For specimens compacted at water contents of 6-1/2 and 10-1/2 percent, the initial degrees of saturation were so low (Table V) that application of the relatively low stress levels used in this study probably did not cause the generation of large pore air or pore water pressures. It may be noted (Table V) that the strain corresponding to pressure saturation was about 25 percent for the specimens compacted at a water content of 6-1/2 percent, whereas the maximum recorded strain was only 7.6 percent, at a stress of 600 psi. Thus, the changes in pore pressure must have been relatively small.

The one dimensional stress that would produce densification equivalent to that developed by the compaction procedure is unknown, but based on the triaxial test results it must be of the order of 250 psi. For applied stresses smaller than this value, the soil would be loaded along a reloading curve and relatively small deformations would be expected. For higher stresses, the soil should be compressed along the virgin curve with proportionately larger strains occurring. Thus, for low stresses, the stress-strain curves should be concave towards the strain axis (Figure 33). As the stress is increased further, the

90

Table V

SUMMARY OF ONE-DIMENSIONAL
COMPRESSION DATA

Test No.	Seating σ_a (psi)	Seating ϵ_a (%)	Time (s) Rise	Time (s) Dwell	Time (s) Decay	Initial Peak σ_a (psi)	Initial Peak ϵ_a (%)	Initial Peak S_r (%)	Ultimate σ_a (psi)	Ultimate ϵ_a (%)	X_o	Maximum Possible Strain ϵ_a (%)
1	17	0.1	10	49	34	201	2.8	33	201	2.8	0.37	25
2	26	0.1	7	54	36	415	7.4	38	415	7.4	0.51	26
3	14	0.2	0.0024	31	32	303	4.1	34	196	4.2	0.53	26
4	15	0.1	0.0023	32	32	600	7.6	38	390	7.9	0.55	25
5	16	0.1	11	52	36	189	3.6	57	189	3.6	0.38	17
6	13	0.1	8	57	38.	398	9.6	71	398	9.6	0.45	17
7	15	0.1	0.0025	32	33	290	3.8	57	199	4.3	0.53	17
8	16	0.2	0.0028	33	37	620	10.2	72	402	10.7	0.61	17
9	13	0.1	10	54	47	201	4.2	88	201	4.2	0.61	7.6
10	18	0.1	10	52	40	408	6.1	95	408	6.1	0.83	7.3
11	14	0.1	0.0025	31	33	300	3.5	87	194	3.5	-	7.3
12	15	0.1	0.0023	30	38	857	6.3	96	397	6.1	0.94	7.5
13	11	0.3	12	41	47	202	2.8	96	202	2.8	0.99	3.9
14	12	0.3	7	19	46	382	2.7	97	382	2.7	1.00	3.6
15	19	0.4	0.0020	38	30	475	2.4	96	202	2.2	0.97	3.6
16	15	0.4	0.0016	23	37	920	3.0	98	390	2.9	1.00	3.7
17	10	0.4	6	48	41	370	2.9	96	370	2.9	1.00	4.1
18	12	0.6	17	40	40	170	2.8	97	170	2.8	1.00	3.8
19	14	0.6	0.0017	54	32	511	2.7	97	190	2.5	1.00	3.6
20	14	0.6	0.0015	31	40	893	2.8	97	390	2.9	1.00	3.8

compressibility of the soil structure decreases and the stress-strain
curves should pass through an inflection point and become concave
towards the pressure axis.

For the specimens compacted at a water content of 13-1/2
percent, the stress-strain curves (Figure 35) at strains less than
about 3 percent are concave towards the strain axis. The maximum
strain, corresponding to pressure saturation, was 7.6 percent (Table V).
Thus, at 3 percent strain, appreciable pore pressures were developing.
At strains higher than 3 percent, the stress-strain curves became con-
cave towards the strain axis both because of decreasing compressibility
of the soil structure and because of the development of high pore air
and pore water pressures.

For specimens compacted on the wet side of optimum, the volume
of gas voids is relatively small so that the limiting strains, under
undrained conditions are also small. For the specimens used in this
investigation, the limiting axial strains were in the range of 3.6 to
4.0 percent for these specimens (Table V). Thus, the stress-strain
curves become quite steep after about 2 to 3 percent axial strain and
the incremental modulus, $d\sigma_a/d\epsilon_a$, approaches the modulus of water.

In every series of tests at constant water content, the
stress required to achieve some given strain was higher for the dynamic
tests than for the slow tests. The difference is mainly due to the
viscous resistance of the soil structure to volume change. A small
part of the difference may result from the lack of time for the gas
voids to dissolve in the pore water during dynamic tests.

Secant moduli. Secant moduli were defined as the ratio of the
axial stress applied in excess of the seating stress, to the strain in
excess of the strain that occurred when the seating stress was applied,
i.e., the moduli were calculated using the seating load and deflection
as the base of measurement.

The secant moduli have been plotted versus the "incremental
axial stress," defined as the stress applied in excess of the seating
stress, in Figures 42 through 46. The shapes of the modulus-stress
curves follow directly from the shapes of the stress-strain curves,
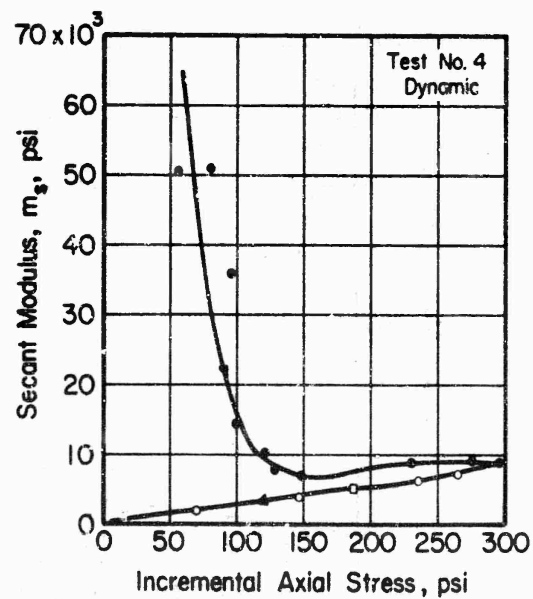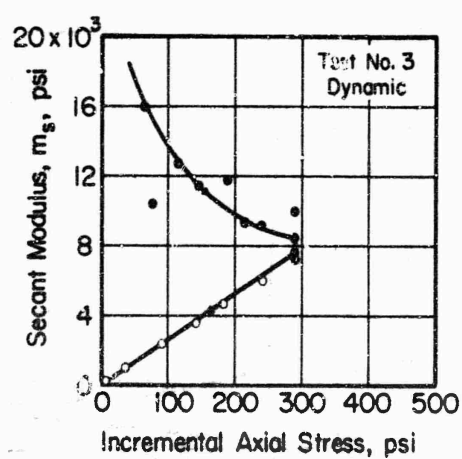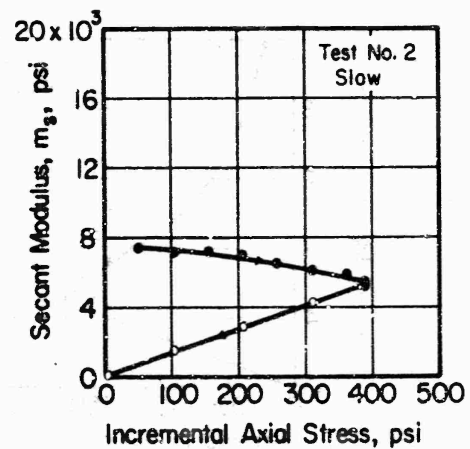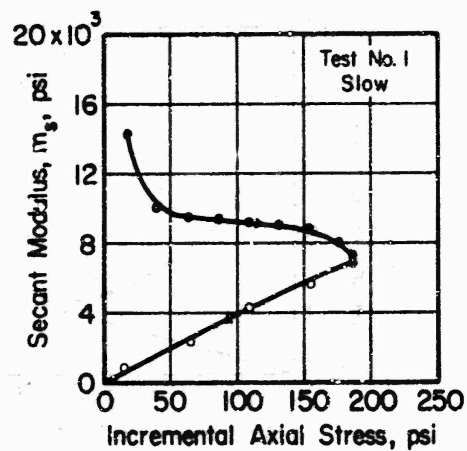just examined, and thus require little additional discussion. It should

92

Figure 42. Relationship Between Secant Modulus and Incremental Axial Stress for Specimens Compacted at a Water Content of 6-1/2 Percent
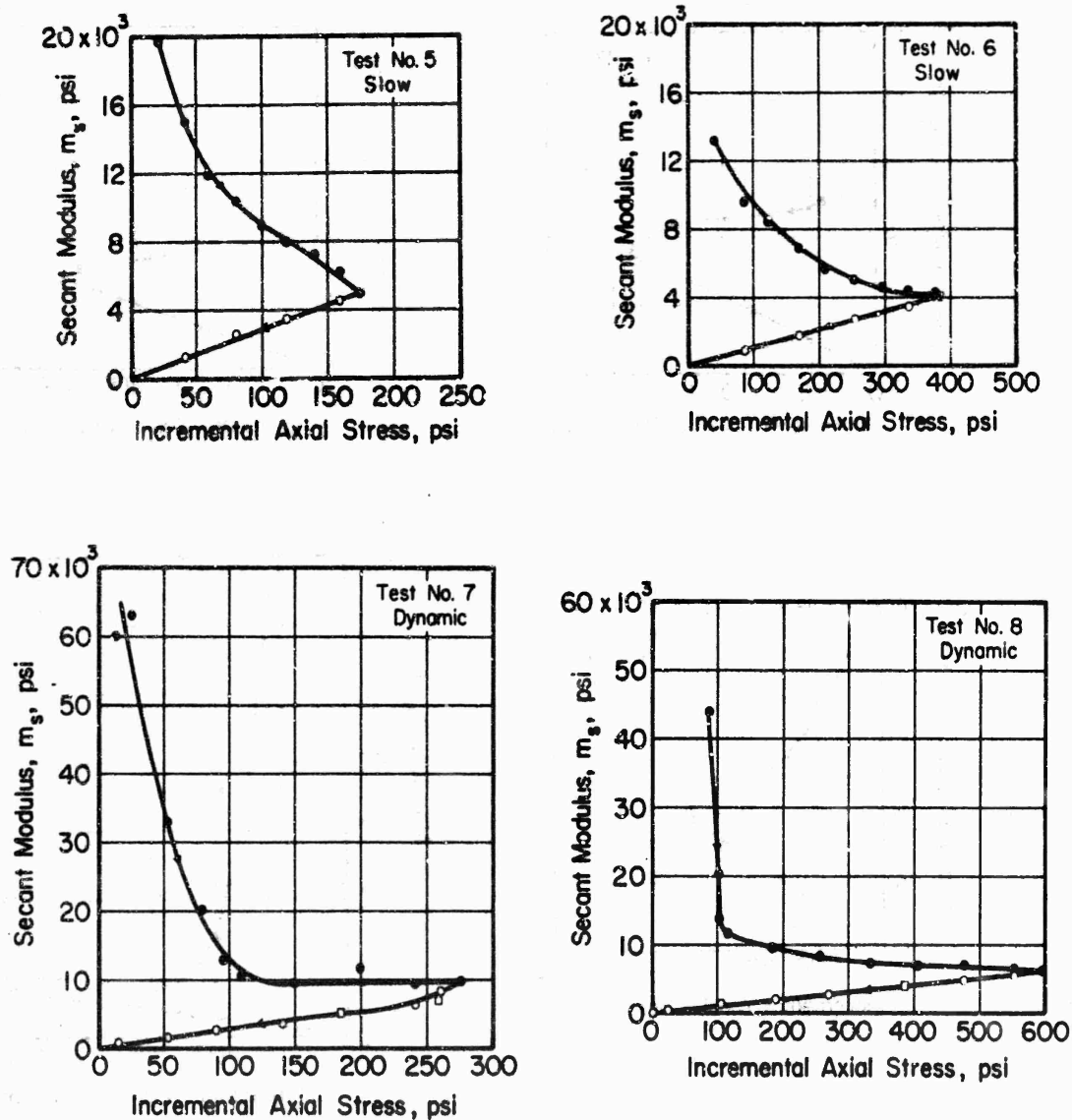
Figure 43. Relationship Between Secant Modulus and Incremental
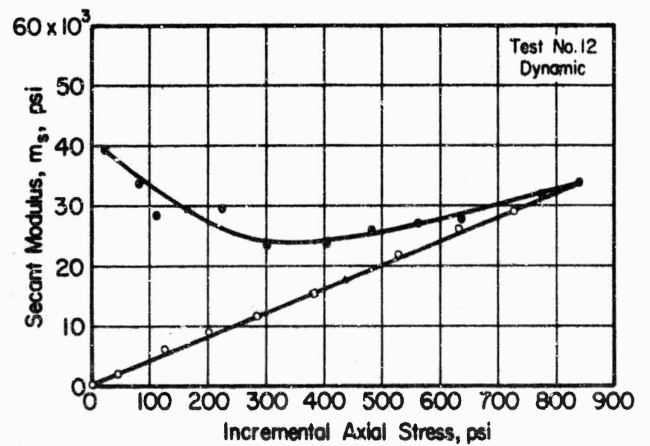Axial Stress for Specimens Compacted at a Water
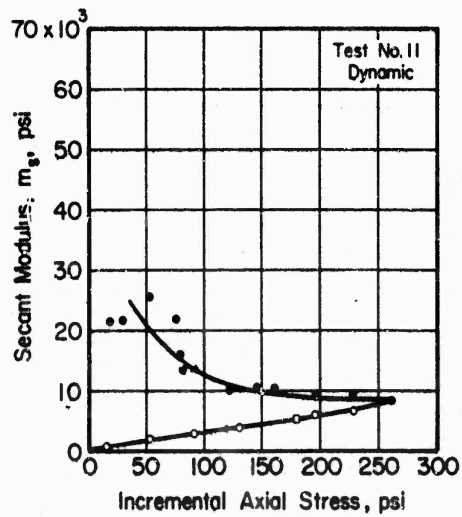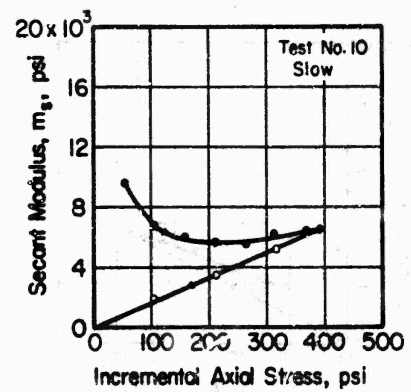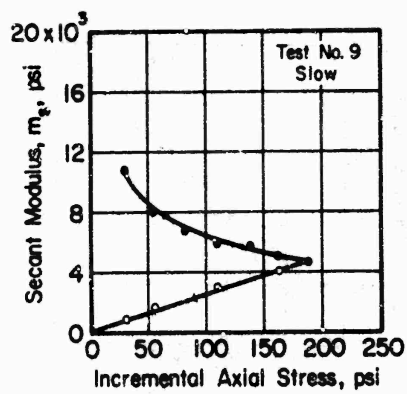Content of 10-1/2 Percent

94

Figure 44. Relationship Between Secant Modulus and Incremental Axial Stress for Specimens Compacted at a Water Content of 13-1/2 Percent
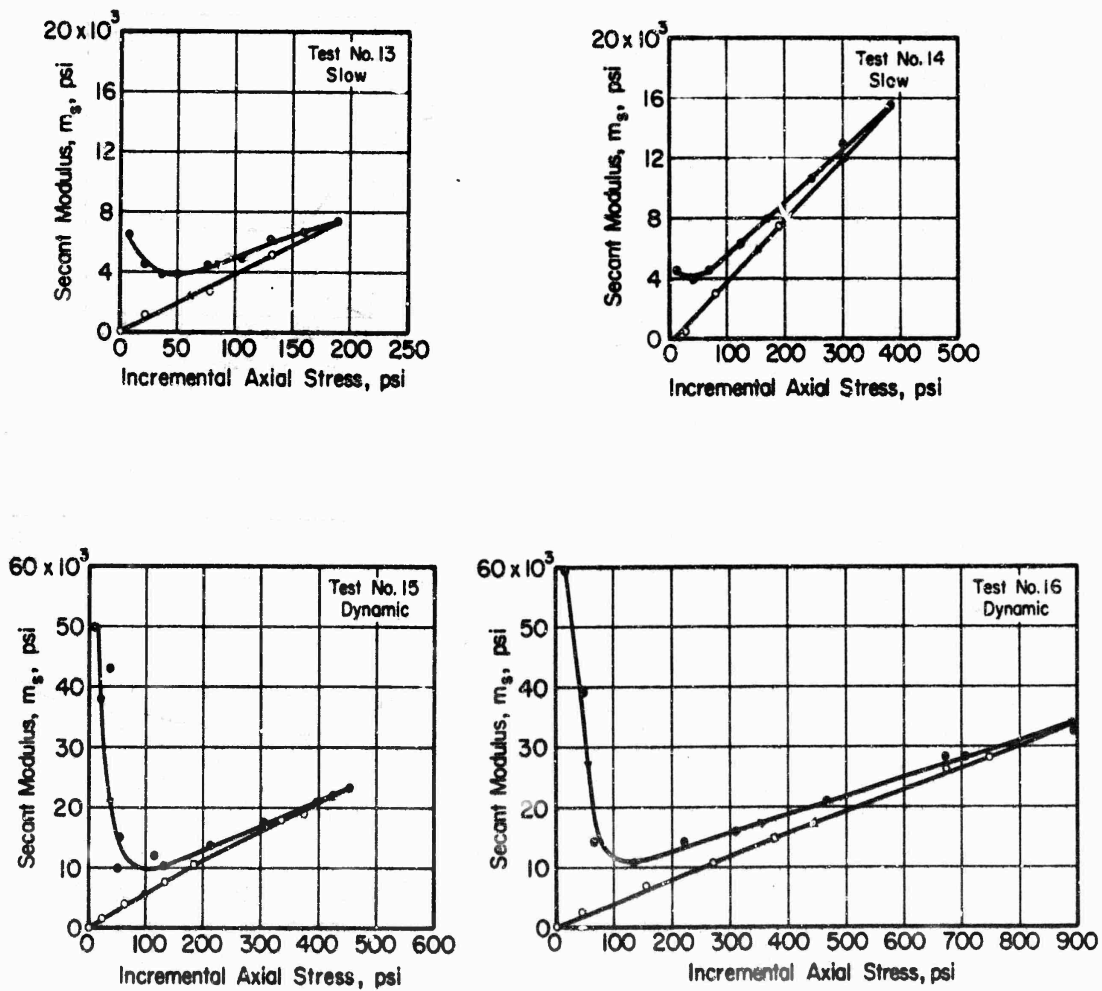
Figure 45. Relationship Between Secant Modulus and Incremental Axial Stress for Specimens Compacted at a Water Content of 16 Percent
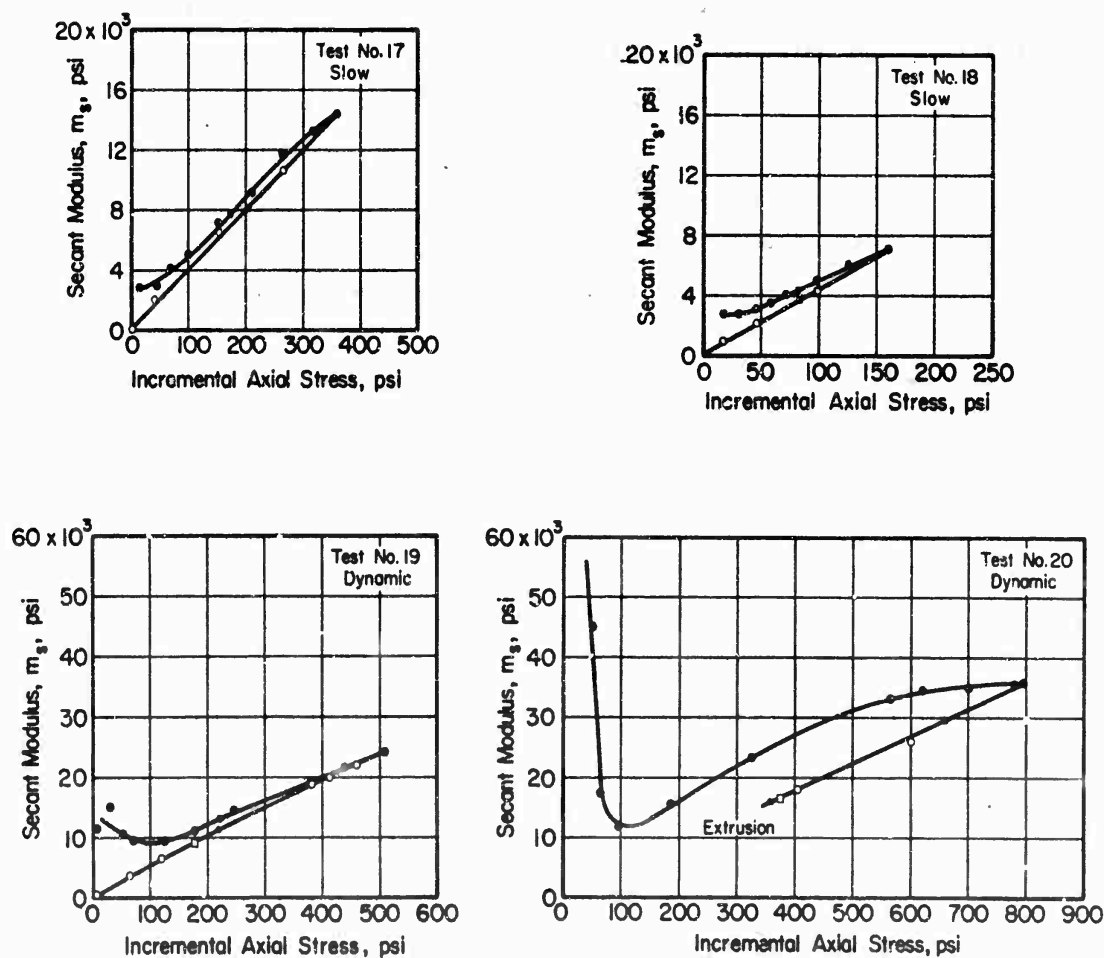
Figure 46. Relationship Between Secant Modulus and Incremental
Axial Stress for Specimens Compacted at a Water
Content of 18 Percent

97

be reiterated that the high moduli obtained from the dynamic tests at low strains probably resulted from errors in the instrumentation system.

It is difficult to reduce the secant moduli to a few diagrams, or to tabular form, because the moduli depend on the compaction water content, the stress (or strain) level, and the loading rate, and are not the same for the unloading curve as for the initial loading curve. Further, the data are not of a type that can be reduced mathematically by using dimensionless diagrams or by fitting simple equations to the curves.

One way of comparing the data is to define the secant modulus at some fixed strain. In Figure 47, the secant moduli have been defined at an axial strain of one percent, and have been plotted versus the compaction water content. The moduli are highest for the specimens compacted at the lowest water contents. This is a general observation; soils compacted at low water contents and not submerged, are quite stiff (high moduli). The much softer specimens compacted on the wet side of optimum yield lower moduli. It should be noted that the strain level used here is so small that appreciable pore pressures were probably not developed even in the specimens compacted at the highest water contents. Further, specimens compacted at water contents lower than those used during this research, would probably yield lower moduli. As expected, there is considerable scatter in the data obtained from the dynamic tests but, in general, the "dynamic" moduli exceed the "slow" moduli.

In Figure 48 the moduli have been plotted versus compaction water content for constant values of the incremental axial stress of 100, 200, 300, and 400 psi. The moduli have also been tabulated in Table VI. At an incremental axial stress of 100 psi the curves are of the same shape as those obtained using a constant axial strain of one percent (Figure 47). At an incremental axial stress of 200 psi the secant moduli minimize at a water content just dry of optimum, and then increase markedly with increasing water content. Apparently, an incremental axial stress of 200 psi was sufficient to generate significant pore pressures for specimens compacted wet of optimum but not for specimens compacted several percent on the dry side. This same effect is
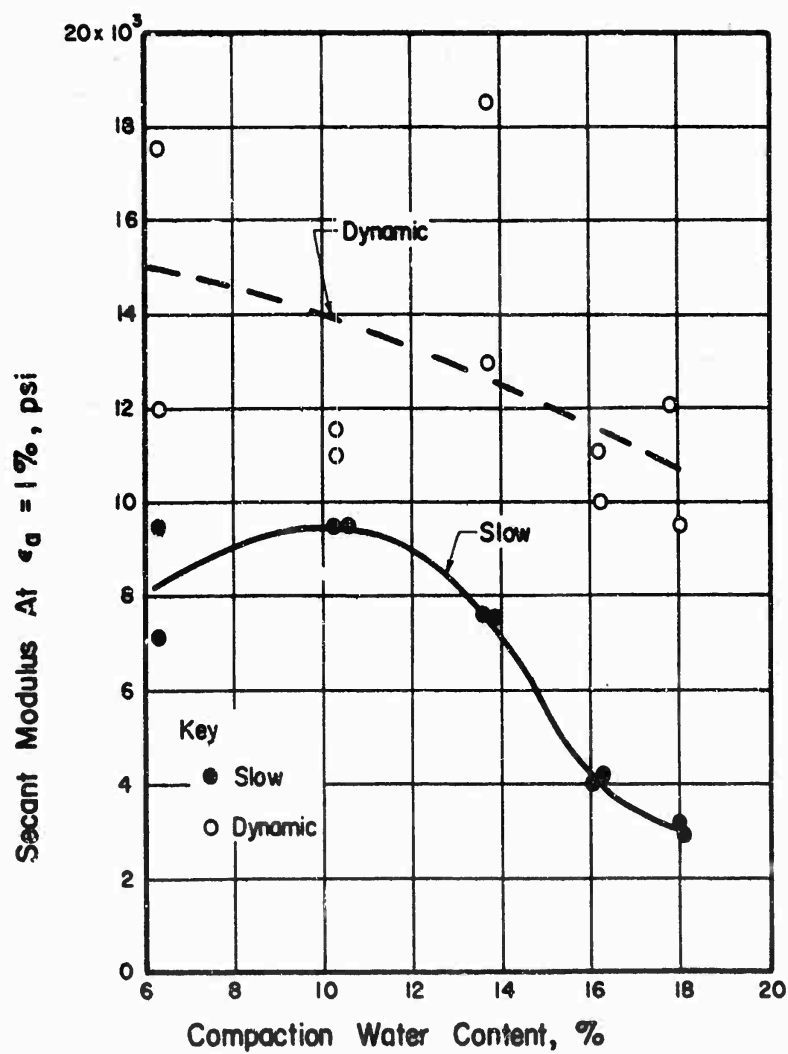
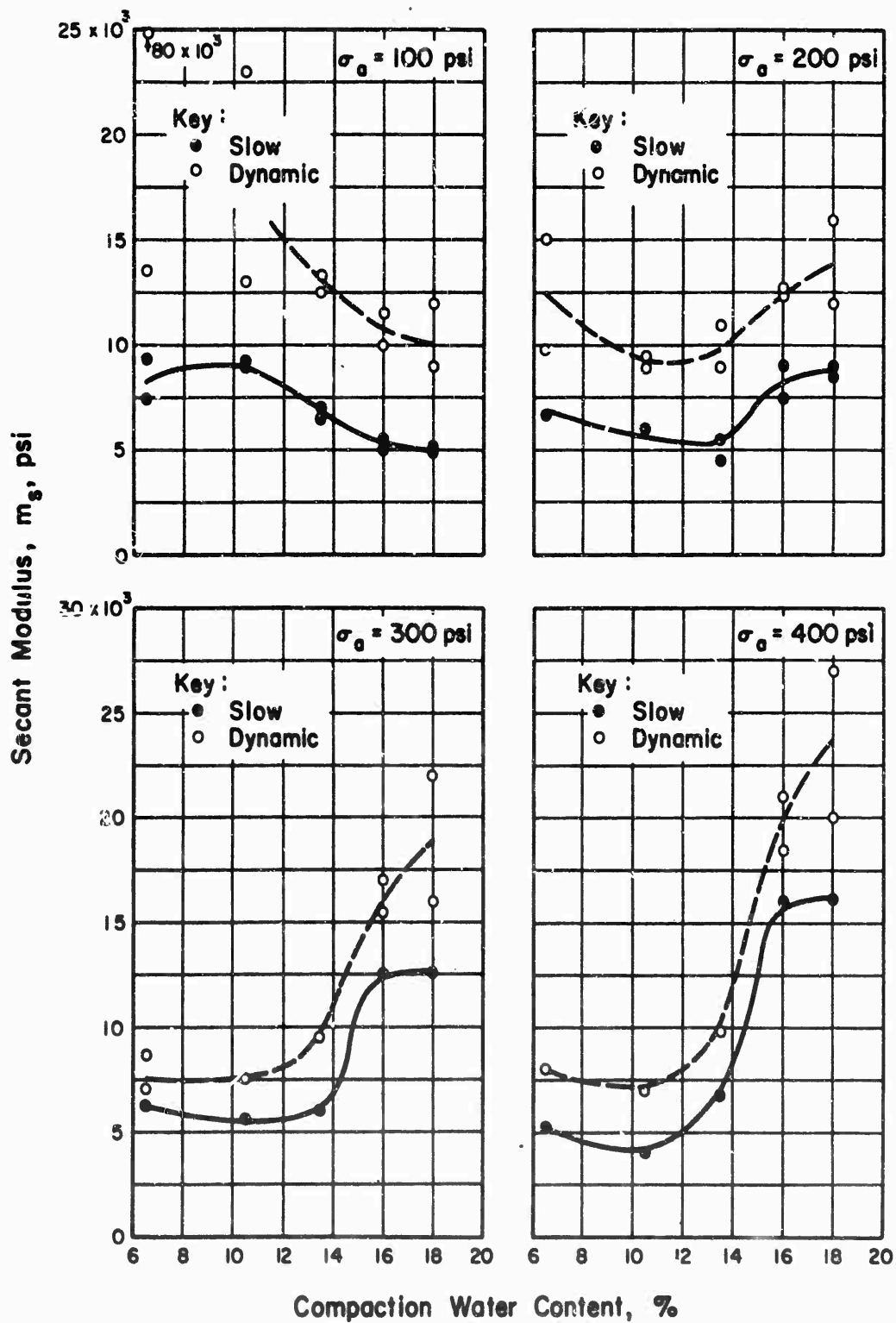Figure 47. Influence of Compaction Water Content on the Secant Modulus Defined at One Percent Axial Strain

Figure 48. Influence of Compaction Water Content
on the Secant Modulus

Table VI

SECANT MODULI DEFINED AT VARIOUS
LEVELS OF THE INCREMENTAL AXIAL STRESS

Test No.	Nominal Water Content (%)	Type of Test	σ_a=100 psi M_s (psi)	σ_a=200 psi M_s (psi)	σ_a=300 psi M_s (psi)	σ_a=400 psi M_s (psi)
1	$6\frac{1}{2}$	Slow	9,200	---	---	---
2	$6\frac{1}{2}$	Slow	7 300	6,800	6,200	5,200
3	$6\frac{1}{2}$	Dynamic	13,500	9,800	8,400	---
4	$6\frac{1}{2}$	Dynamic	30,000	15,000	7,000	8,000
5	$10\frac{1}{2}$	Slow	9,000	---	---	---
6	$10\frac{1}{2}$	Siow	9,300	6,000	4,500	4,000
7	$10\frac{1}{2}$	Dynamic	13,000	9,500	---	---
8	$10\frac{1}{2}$	Dynamic	23,000	9,000	7,500	7,000
9	$13\frac{1}{2}$	Slow	6,400	4,500	---	---
10	$13\frac{1}{2}$	Slow	7,000	5,600	6,000	6,700
11	$13\frac{1}{2}$	Dynamic	12,500	9,000	---	---
12	$13\frac{1}{2}$	Dynamic	13,300	11,000	9,600	9,800
13	16	Slow	5,000	7,600	---	---
14	16	Slow	5,500	9,000	12,600	16,000
15	16	Dynamic	10,000	12,500	17,000	21,000
16	16	Dynamic	11,500	12,500	15,500	18,500
17	18	Slow	5,000	9,000	12,600	16,000
18	18	Slow	5,000	8,500	---	---
19	18	Dynamic	9,000	12,000	16,000	20,000
20	18	Dynamic	12,000	16,000	22,000	27,000

evident for specimens subjected to higher pressures. At an incremental axial stress of 400 psi, significant pore pressures were apparently developed at water contents as much as 4 percent dry of optimum. If these tests had been carried to stresses of the order of 10,000 psi, the secant moduli for specimens compacted wet of optimum should have approached the modulus of water, about 300,000 psi.

For all tests, the "dynamic" modulus exceeds the "slow" modulus. To obtain a quantitative measure of the influence of dynamic loading, the ratio of the dynamic modulus to the "slow" modulus was determined for each water content and each level of incremental axial stress, using the average curves drawn in Figure 48. These ratios have been plotted versus the incremental axial stress in Figure 49. It is remarkable, and perhaps fortuitous, that the ratio of the moduli is independent of the compaction water content, within the range studied, and varies between the relatively narrow limits of 1.3 to 2.0.

Radial stresses. Radial stresses developed in the soil specimens during loading as a result of the restraint provided by the confining ring. The measured values of the radial stress are plotted versus the axial stress, corrected for the inertia of the loading cap, in Figures 50 through 54.

For slow tests using specimens compacted at low water contents, the applied axial stress is taken mainly by the soil structure (changes in effective stress). Thus, the radial stress increases almost linearly with the axial stress upon first loading, and a hysteresis loop is formed between the loading and unloading curves. Similar curves were obtained for dynamic tests except that the dynamic loading curves start out rather flat, then steepen, then flatten again and merge into a smooth loading curve such as obtained for the slow tests. This shape of curve can be rationalized in terms of viscosity of the soil structure and breakdown of soil structure under dynamic loadings, but such interpretations seem fraught with uncertainty considering the instrumentation problems associated with the early part of the dynamic loading curves, as considered previously. Thus, pending refinement of instrumentation techniques, smooth curves have been drawn through the data.
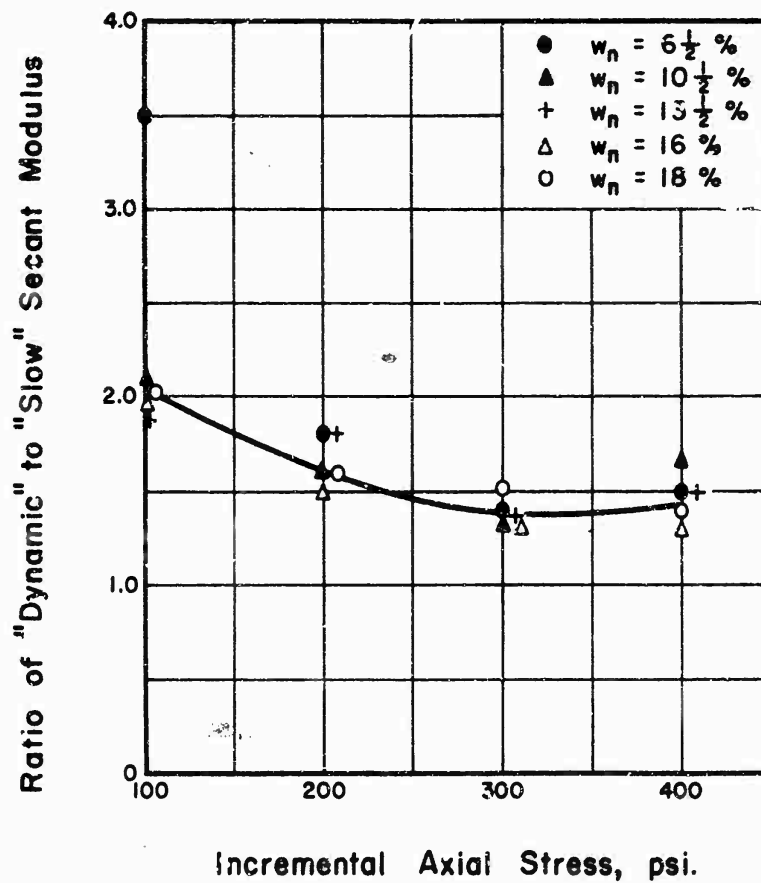
Figure 49. Relationship Between the Ratio at the "Dynamic" to the "Slow" Secant Modulus and Incremental Axial Stress
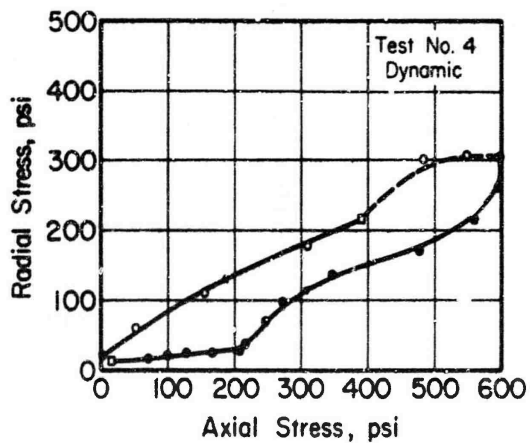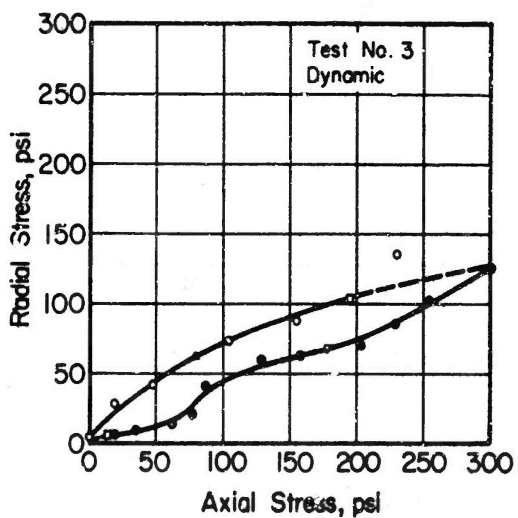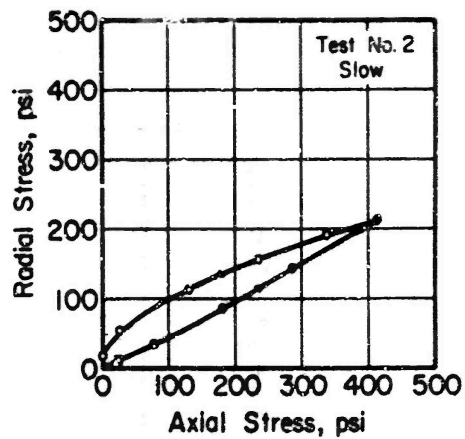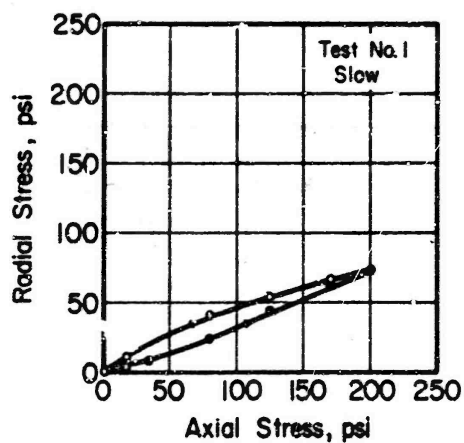
103

Figure 50. Relationship Between Radial and Axial Stress for Specimens Compacted at a Water Content of 6-1/2 Percent

Figure 51. Relationship Between Radial and Axial Stress
for Specimens Compacted at a Water Content
of 10-1/2 Percent

Figure 52. Relationship Between Radial and Axial Stress
for Specimens Compacted at a Water Content
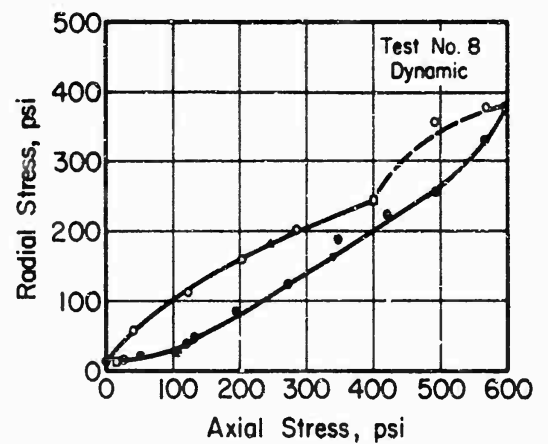of 13-1/2 Percent

Figure 53. Relationship Between Radial and Axial Stress
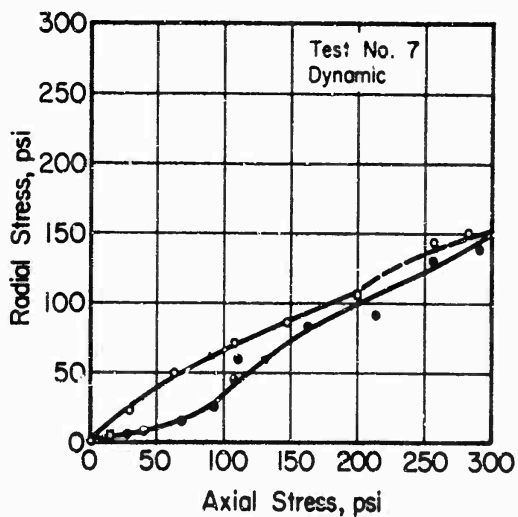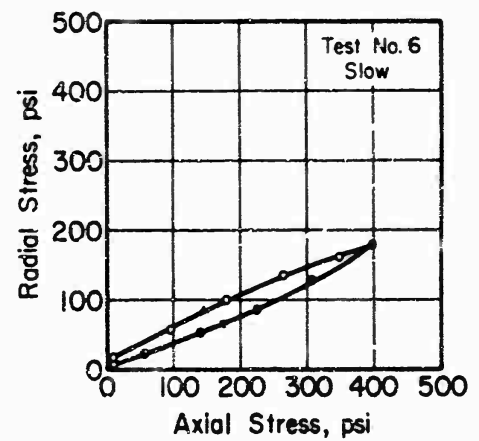for Specimens Compacted at a Water Content
of 16 Percent
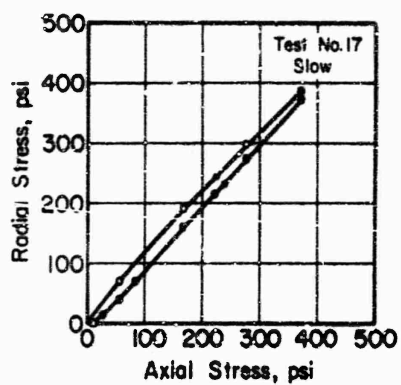
Figure 54. Relationship Between Radial and Axial Stress
for Specimens Compacted at a Water Content
of 18 Percent

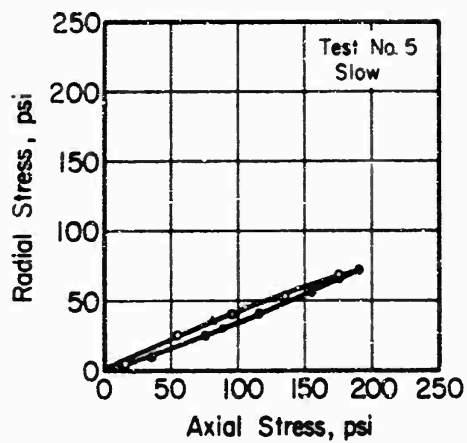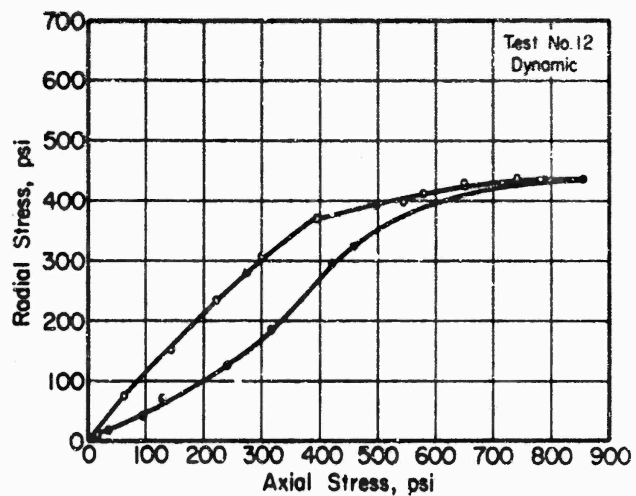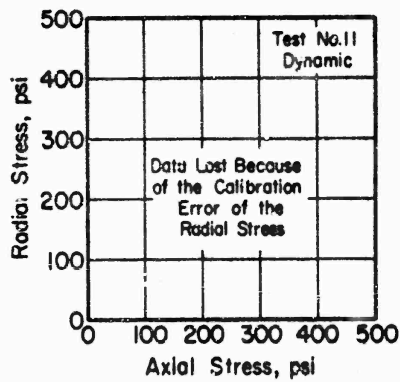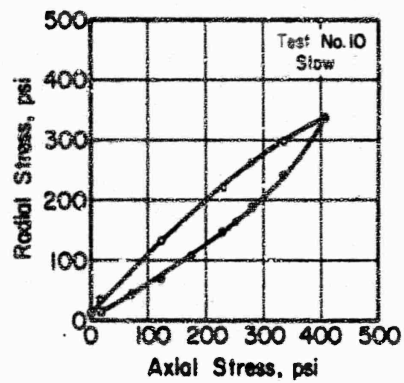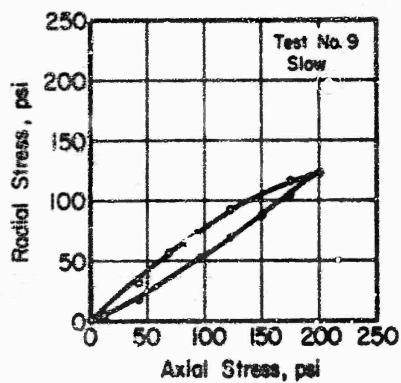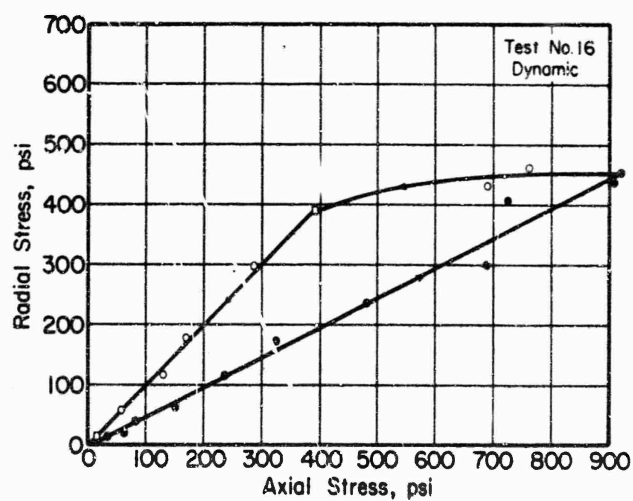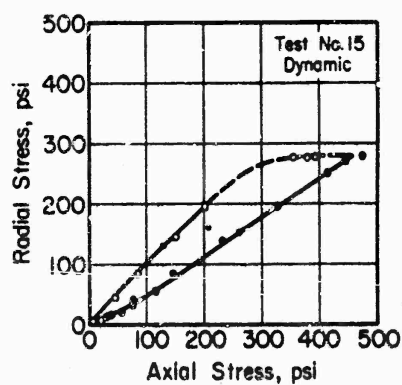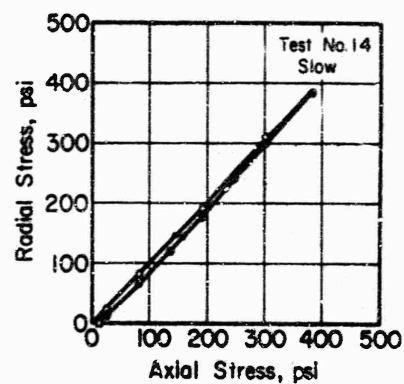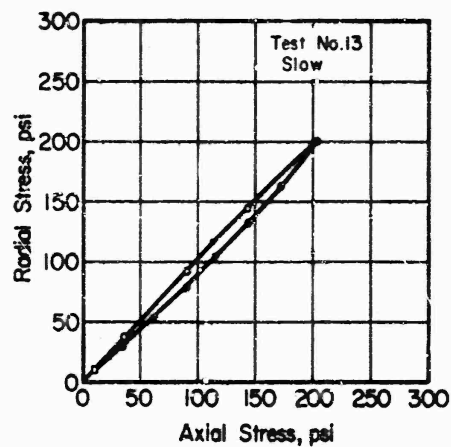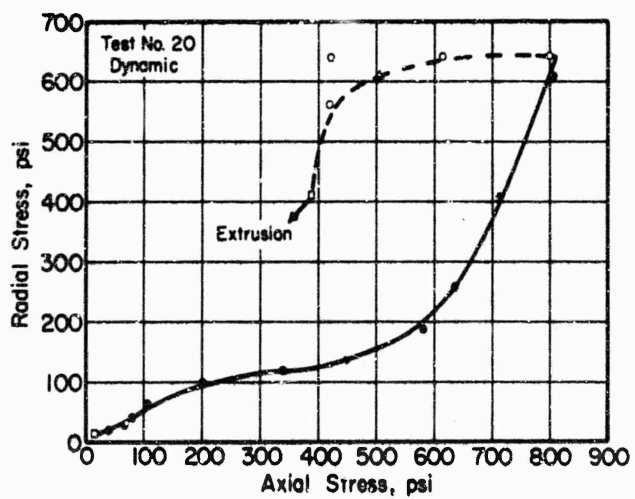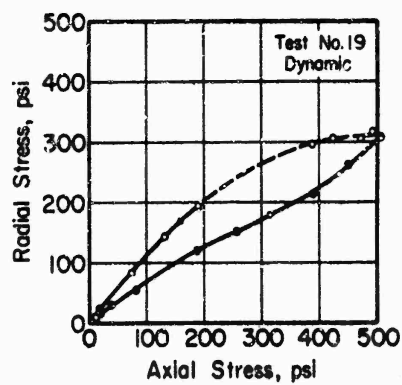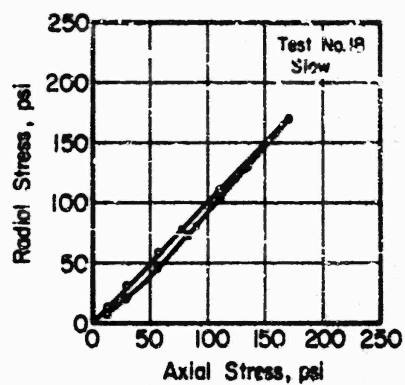As the compaction water content increases, the degree of saturation of the specimens increases and an increasing percentage of the applied axial stress is taken by the pore pressures. As a result, the slope of the radial stress versus axial stress curves steepen and approach a limit of 45 deg. corresponding to complete saturation. Further, the size of the loop between the loading and unloading curves diminishes.

The change in the "slow" curves, with increasing water content, is the direct result of the increasing degree of saturation. The dynamic curves have increasing scatter, at the higher water contents, and occasionally have rather unlikely shapes (Test 12, for example). At the present time, these odd shapes have been attributed to recording problems associated with such high speed tests.

The ratio of the radial stress to the axial stress under conditions of zero radial strain, is termed the coefficient of earth pressure at rest, and is designated by the symbols K_o or $\bar{K}_o$, depending on whether total or effective stresses are used. Only total stresses could be determined in this investigation. Values of the coefficient of earth pressure at rest are tabulated in Table VII and are plotted versus compaction water content in Figure 55. The points on these curves were taken from the average loading (as opposed to unloading) curves previously considered, and data obtained using dynamic and slow tests are considered separately.

For the slow tests at any given axial stress, K_o tends to increase with increasing compaction water content. At low water contents, where K_o probably approximates $\bar{K}_o$, K_o has a value of about 0.35 for low stress levels. At these water contents K_o increases slightly with increasing pressure. For high water contents where the initial degree of saturation exceeds 90 percent, much of the applied axial stress is taken by the pore water and K_o is nearly one at low stress levels, and is one at higher stress levels.

Throughout most of the range of compaction water content and axial pressure used during this investigation, the values of K_o were lower for dynamic tests than for slow tests. At the lowest water content, this difference might be attributed to the viscous resistance of

109

Table VII

COEFFICIENTS OF EARTH PRESSURE AT REST DEFINED AT VARIOUS LEVELS OF AXIAL STRESS

| Test No.	Nominal Water Content (%)	Type of Test	$\sigma_a = 100$ psi		$\sigma_a = 200$ psi		$\sigma_a = 300$ psi		$\sigma_a = 400$ psi	
			σ_r (psi)	K_o	σ_r (psi)	K_o	σ_r (psi)	K_o	σ_r (psi)	K_o
1	$6\frac{1}{2}$	Slow	32	0.32	72	0.36	---	--	---	--
2	$6\frac{1}{2}$	Slow	45	0.45	95	0.47	150	0.50	205	0.51
3	$6\frac{1}{2}$	Dynamic	47	0.47	75	0.37	125	0.42	---	--
4	$6\frac{1}{2}$	Dynamic	15	0.15	35	0.17	110	0.37	150	0.38
5	$10\frac{1}{2}$	Slow	35	0.35	75	0.37	---	--	---	--
6	$10\frac{1}{2}$	Slow	37	0.37	75	0.37	120	0.40	180	0.45
7	$10\frac{1}{2}$	Dynamic	35	0.35	100	0.50	---	--	---	--
8	$10\frac{1}{2}$	Dynamic	30	0.30	80	0.40	140	0.47	200	0.50
9	$13\frac{1}{2}$	Slow	55	0.55	122	0.61	---	--	---	--
10	$13\frac{1}{2}$	Slow	60	0.60	125	0.62	200	0.67	325	0.81
11	$13\frac{1}{2}$	Dynamic	--	--	---	--	---	--	---	--
12	$13\frac{1}{2}$	Dynamic	50	0.50	100	0.50	170	0.57	270	0.68
13	16	Slow	90	0.90	197	0.98	---	--	---	--
14	16	Slow	85	0.85	190	0.95	300	1.00	400	1.00
15	16	Dynamic	50	0.50	115	0.57	175	0.58	240	0.60
16	16	Dynamic	45	0.45	100	0.50	150	0.50	200	0.50
17	18	Slow	85	0.85	190	0.95	300	1.00	400	1.00
18	18	Slow	92	0.92	200	1.00	---	--	---	--
19	18	Dynamic	70	0.70	125	0.62	170	0.57	225	0.56
20	18	Dynamic	50	0.50	95	0.47	115	0.38	125	0.31
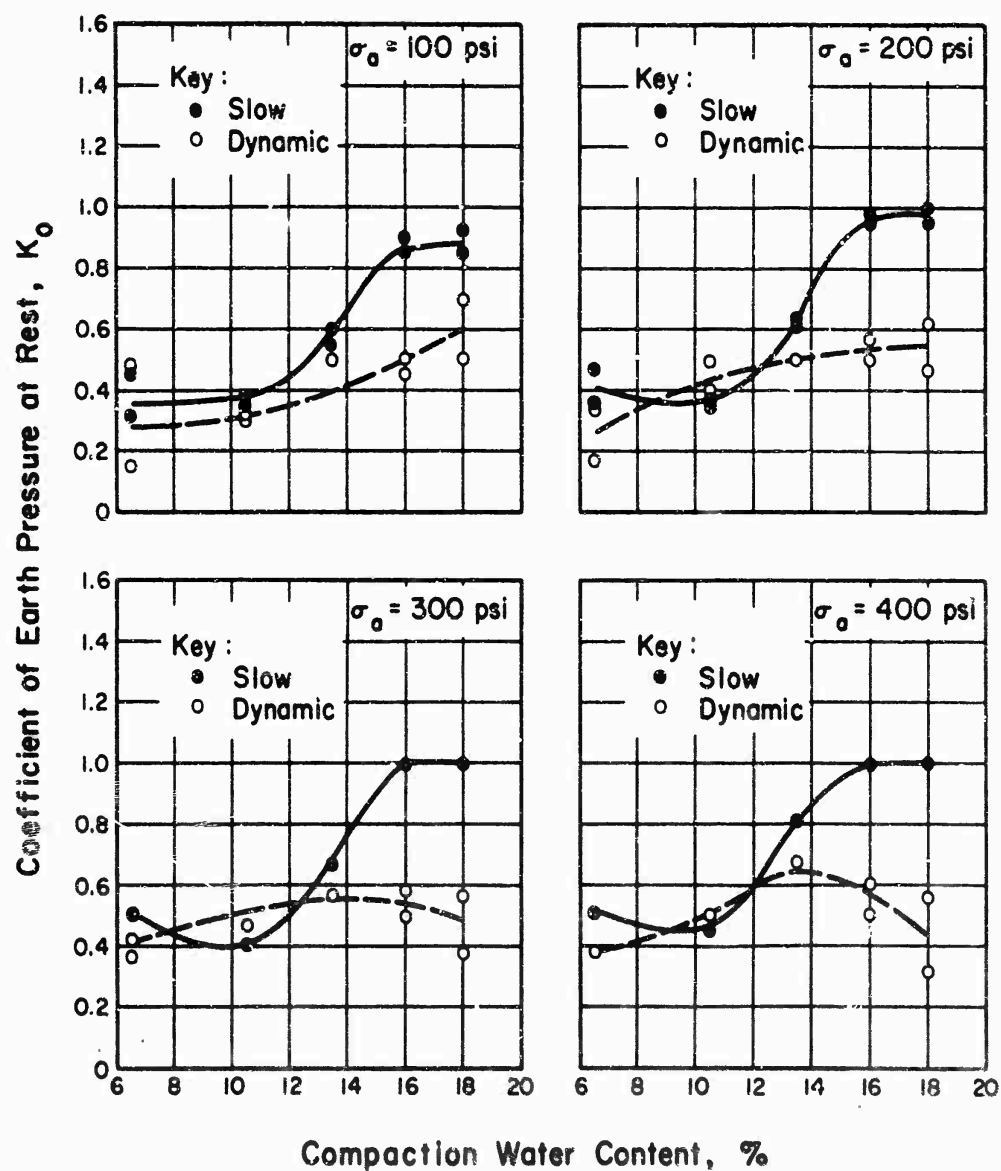
Figure 55.   Influence of Compaction Water Content on the
Coefficient of Earth Pressure at Rest

111

the soil structure to volume change. If the soil structure were to be markedly more stiff under dynamic loads than under static loads, then it would be expected that the soil could withstand given axial stresses without developing as much radial stress, and thus K_o would be lower for the dynamic tests. However, the low values of K_o at high water contents and the apparent trend of K_o to decrease at high water contents, both suggest that the data are in error. Careful examination of the magnetic tape outputs, as a function of time, indicated that the radial stresses always began to increase after the axial stresses had begun to increase. For example, in the case of Test No. 3, previously considered, the radial stresses didn't begin to increase until 0.62 ms after the axial stress first increased. It is believed that the use of a 20kc carrier system and a high speed magnetic tape system precludes the possibility of such delays in the recording system, but it seems almost certain that both the radial-stress and deformation traces were delayed.

It is possible that some part of the problem results from the fact that the rise times were only slightly in excess of the time required for a stress wave to propagate to the bottom of the specimen and return. Future experiments of this type should probably use rise times in excess of 5 milliseconds.

Residual deformation. The net deformation of the soil speci-men after the stress has been applied and then removed is termed the residual deformations have been tabulated in Table VIII and plotted versus the maximum pressure in Figure 56. The residual deformation apparently depends on the compaction water content, the maximum pressure, and whether the pressure was applied statically or dynamically.

The influence of compaction water content on the residual deformation for slow tests is shown in Figure 57. The maximum residual deformation occurs for compaction water contents on the dry side of optimum. As the maximum axial stress increases, the peak residual strain occurs at lower and lower water contents. Under undrained con-ditions, the lowest residual strains occur for compaction on the wet side of optimum because of the low percentage of air voids.

For specimens compacted at low water contents, the low dry density and low degree of saturation make large deformations possible

112

Table VIII

RESIDUAL DEFORMATIONS

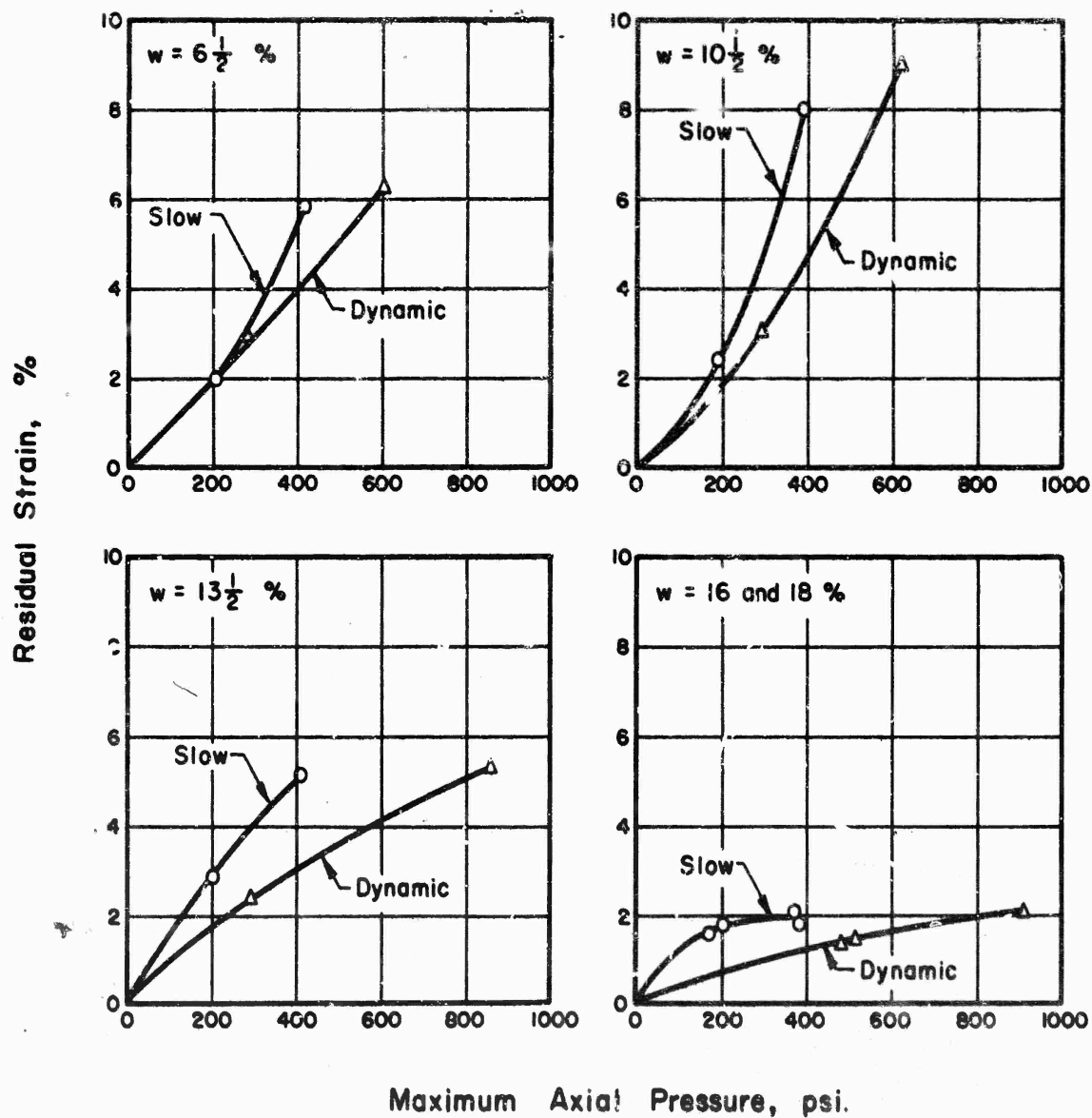| Test No.	Nominal Water Content (%)	Maximum Stress $\bar{\sigma}_a$ - max (psi)	Rise Time (S)	Maximum Strain $\epsilon_{max.}$ (%)	Residual Strain $\epsilon_{res.}$ (%)	Ratio of Residual Strain to Max. Strain $\epsilon_{res.}/\epsilon_{max.}$
1	$6\frac{1}{2}$	201	9.7	2.8	1.9	.68
2	$6\frac{1}{2}$	415	7.2	7.4	5.8	.78
3	$6\frac{1}{2}$	303	0.0024	4.2	2.8	.67
4	$6\frac{1}{2}$	600	0.0023	7.9	6.3	.80
5	$10\frac{1}{2}$	189	10.7	3.6	2.4	.67
6	$10\frac{1}{2}$	398	7.5	9.6	8.0	.83
7	$10\frac{1}{2}$	290	0.0025	4.3	3.0	.70
8	$10\frac{1}{2}$	620	0.0028	10.7	9.0	.84
9	$13\frac{1}{2}$	201	9.5	4.2	2.9	.69
10	$13\frac{1}{2}$	408	9.7	6.1	5.1	.84
11	$13\frac{1}{2}$	300	0.0025	3.5	2.4	.68
12	$13\frac{1}{2}$	857	0.0023	6.3	5.3	.84
13	16	202	12.0	2.8	1.8	.64
14	16	382	7.0	2.7	1.8	.67
15	16	475	0.0020	2.4	1.4	.58
16	16	920	0.0016	?.0	2.1	.70
17	18	370	6.0	2.9	2.0	.69
18	18	170	17.0	2.8	1.6	.57
19	18	511	0.0017	2.7	1.5	.56
20	18	893	0.0015	2.8	---	---

113

Figure 56. Relationship Between Residual Strain and Maximum Axial Pressure at Various Compaction Water Contents

in undrained tests. However, these specimens are also relatively incompressible at low stress levels. Thus, the maximum and residual strains are small for specimens subjected to low stress levels. For high stress levels, both the maximum and residual strains can be large.

As the compaction water content is increased, the soil becomes more compressible at low stress levels but the combination of higher dry densities and higher degrees of saturation results in a reduced content of air voids and thus limits the maximum and residual strains.

Thus, at low stress levels, the strains are small for specimens compacted at low water contents, because of a relatively incompressible soil structure, and at high water contents, because of a low content of air voids, and maximize for specimens compacted at intermediate water contents. At high stress levels, the maximum and residual strains are limited mainly by the content of air voids. Thus, strains are largest for specimens compacted at the lowest water contents.

The influence of loading rate on residual strain would appear anomolous at first because all specimens were allowed to creep at constant pressure for 30 to 60 seconds. The long creep time would normally be expected to eliminate any dynamic effects on residual strains. However, the pressures plotted in Figure 56 are the maximum pressures attained during the test. For dynamic tests this peak pressure exceeded the desired pressure, because of the inertia of the loading system, and was maintained for only a fraction of a millisecond. Thus, the soil was subjected to a constant stress that was significantly less than the maximum stress (Figure 41). As a result of the short duration of the peak stress, the total and residual strains were smaller than were obtained when the same stresses were applied statically.

In Figure 58 the ratio of the residual strain to the total strain at peak pressure is plotted versus the compaction water content, for ultimate pressures of 200 and 400 psi. For simplicity of discussion, the ratio of the residual strain to the total strain at the ultimate axial pressure will be termed the "residual strain ratio." The residual strain ratios are lowest for low compaction water contents, indicating large amounts of recovered deformation. For these specimens compacted at a water content of about 6 percent, 40 percent of the deformation
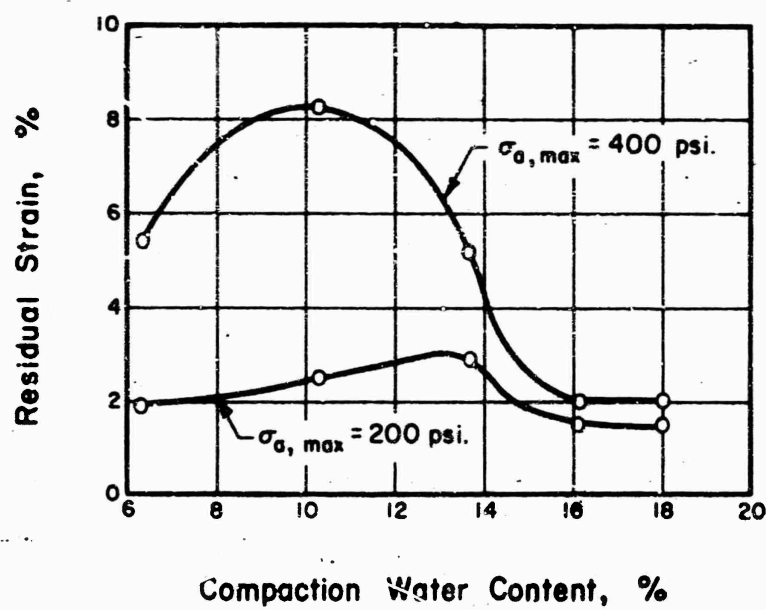
115

Figure 57. Influence of Compaction Water Content on
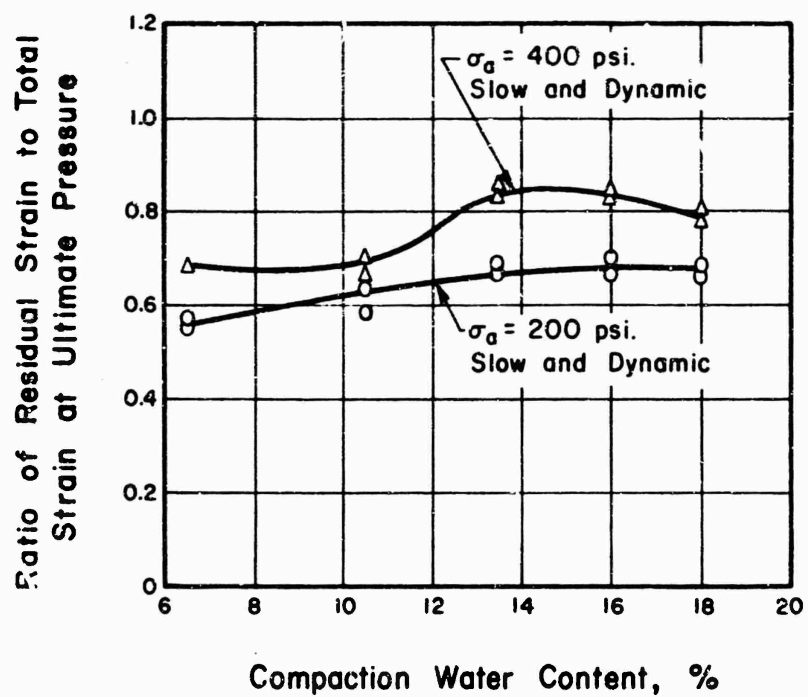the Residual Strain for Slow Tests

Figure 58. Influence of Compaction Water Content on the Ratio of Residual Strain to the Total Strain at Ultimate Pressure

117

would be recovered. For compaction at high water contents, the total
deformation is small and only 20 to 30 percent of it is recovered. The
residual strain ratio is also a function of pressure level with less
recoverable deformation at higher stress levels as expected. However,
it should be noted that at pressure saturation of the specimen, the
amount of recoverable deformation would be independent of the stress
level under undrained conditions. The residual strain ratio appears
to be independent of the loading rate at the stress levels investigated
in this program.

Conclusions Based on One-Dimensional Compression Tests

The following conclusions are drawn based on this exploratory
series of one-dimensional compression tests:

1. The specimen-preparation procedure used was successful in
preparing reasonably uniform and identical specimens. However, if the
one dimensional and triaxial tests are to be compared, a kneading com-
paction apparatus should be developed for preparation of the specimens
for the one-dimensional tests.

2. For "slow" tests, the experimental apparatus and recording
system functioned quite well; no modifications are considered necessary.
However, the system does not appear to have functioned satisfactorily
for the "dynamic" tests in which the rise time was of the order of
2 milliseconds. It does not appear that such high loading rates are
really necessary for ground motion predictions. Tests could be performed
using the same apparatus but operating the press hydraulically at its
highest rate and it is believed satisfactory results would be obtained
using rise times of perhaps 10 milliseconds. In any case, if further
high speed tests are performed, it is recommended that the one-dimen-
sional cell be redesigned to have a floating ring and to have load
cells both above and below the specimen.

3. The stress-strain curves are of the anticipated shapes.
For specimens compacted at water contents considerably less than optimum,
the soil acts very much like an overconsolidated clay subjected to a
normal consolidation test. The soil initially takes stress with only
small deformations. At some pressure, the soil structure begins to
break down and larger deformations occur. Compression causes a

118

reduction in the compressibility of the clay so that the stress-strain curves tend to become concave towards the stress axis again at high pressures (such pressures were not reached during tests on the driest specimens used in this research). For specimens compacted at high water contents, the soil is initially highly compressible but only small strains are needed to compress the air voids to nearly zero volume, and thus to cause the soil to become very incompressible under undrained conditions.

4. In accordance with the shapes of the stress-strain curves, the secant moduli vary between wide limits. For specimens compacted at low water contents, the secant moduli generally decrease with increasing stress. For slow tests on specimens at low water contents, the moduli ranged from about 20,000 psi down to about 5000 psi. Anomolously high initial moduli were obtained in the dynamic tests but these are attributed to instrumentation problems. For specimens compacted on the wet side of optimum, moduli at low strains were as low as 2000 psi. The moduli increased rapidly with increasing pressure but, for the relatively low pressures used in this investigation, did not exceed about 30,000 psi. For the range in axial pressures from 100 psi to 400 psi, the ratio of the dynamic to slow secant moduli was 1.3 to 2.0.

5. Developed radial stresses were smallest for specimens compacted at the lowest water contents. For the range of axial pressures from 100 to 400 psi, the coefficient of earth pressure at rest ranged from about 0.3 to 0.5 for specimens compacted at a water content 9 percent less than optimum. For specimens compacted on the wet side of optimum, the range was from 0.9 to 1.0.

6. Residual strains varied from 55 to 85 percent of the maximum strain. For the specimens compacted in the dry side of optimum and subjected to the pressure levels investigated herein, the residual strain varied from 55 to 70 percent of the maximum strain. The recoverable deformation for specimens compacted on the wet side of optimum was less than specimens on the dry side with the residual strains varying from 70 to 85 percent of the maximum strain.

119

SECTION VI

GENERAL CONCLUSIONS

This investigation was performed as a first phase of a model study of the interaction of a compacted cohesive soil and vertical cylinders under static and dynamic loading. The purposes of this study were first so select a soil suitable for the model study and then to obtain information on the physical properties of the compacted soil as functions of water content, stress level, and loading rate. The study was of a preliminary nature. Neither time nor funds were provided for a detailed study nor for significant alterations of available equipment.

Based mainly on a literature survey and past experience, Goose Lake clay was selected. Based on the laboratory study reported here, Goose Lake clay appears to be an ideal material for soil-structure interaction studies. The soil is available in large quantities in air dried, pulverized form. It mixes with water readily and is easily compacted. The techniques used in the preparation of the specimens used in this laboratory study yielded essentially identical specimens in any desired quantities.

As indicated by the detailed conclusions at the end of Sections IV and V, the physical properties of compacted Goose Lake clay can be varied between wide limits. Under undrained conditions, and within the stress range used in this study (up to about 1000 psi) specimens compacted at water conten.s in the vicinity of 6 percent (9 percent lower than optimum) react very much as if they were stiff clays subjected to drained tests. Thus, the shearing strength increases almost linearly with the confining pressure. At a confining pressure of 10 psi the soil acts like a highly overconsolidated clay. It expands during shear and fails at low strains on a single shear plane. As the confining pressure increases, the soil acts increasingly like a normal consolidated material. At a confining pressure of 1000 psi, the specimens fail at high strains, by bulging, with continuously decreasing volume.

When these relatively dry specimens are subjected to one dimensional compression, they withstand low pressures with little deformation.

120

As the pressure increases, the specimens pass through a point comparable to the inflection in a one dimensional consolidation curve at the maximum previous consolidation pressure. The soil structure appears to break down and larger deformations occur. However, the resulting densification causes the soil to become less and less compressible so that the rate of strain again decreases. Accordingly, the secant modulus first decreases, and then increases, as the axial pressure increases. The coefficient of earth pressure at rest is slightly less than 0.4 at low stress levels and increases to about 0.6 as the axial stress increases.

As the compaction water content increases, the strength of the soil decreases considerably, except at very low confining pressures, and the angle of internal friction, ϕ_0, approaches zero. The strains at fa   become large and independent of confining pressure.

n the case of the undrained one dimensional compression tests on specimens compacted at water contents higher than optimum, the soil is highly compressible at low stress levels but the gas voids are destroyed at relatively low strains. Thus, the soil becomes nearly incompressible at low stress levels. Accordingly, the secant modulus approaches that of water, about 300,000 psi, and the coefficient of earth pressure at rest becomes equal to one.

For the triaxial compression tests, the influence of loading rate on strength and secant modulus at one percent strain were well defined. For specimens compacted at water contents within the range of 5 percent dry of optimum to 3 percent on the wet side, the compressive strength increased at a rate varying from 2 percent per decade reduction in the time to failure, $\tau_{10t} - \tau_t/\tau_{10t}$, in the relatively slow tests to 18 percent per decade reduction in the time to failure for the dynamic tests with times to failure of the order of 3 milliseconds. Specimens compacted at lower water contents underwent smaller strength increases when the loading rates were increased. The secant modulus, defined at one percent axial strain, increased about 15 percent per decade reduction in the time to failure for the entire range of water content used during this investigation.

One dimensional compression tests were performed using rise times of about 10 seconds (termed slow) and 2 milliseconds (termed dynamic). The data indicated that the specimens subjected to the

121

highest loading rates were less compressible than the others. The
ratio of the secant moduli for the dynamic and slow tests ranged
from about 1.3 to 2.0.

If there is interest in using the Goose Lake clay in other
investigations, it would be useful to extend this laboratory program
to provide more general information on the physical properties of the
Goose Lake clay. In the case of the triaxial shear tests, experiments
should be performed using different compaction energies to determine
the variation of the soil properties with density. In the case of
the one-dimensional tests, experiments should be performed using a
variety of rise times. In particular, instrumentation problems would
be greatly reduced if rise times of the order of 10 milliseconds were
used rather than 2 milliseconds. In this study, peak pressures were
limited to the range anticipated for use in the model program. Soil
properties should be investigated at higher pressures. Also, the
effect of variable seating pressures to simulate a range in overburden
pressures in the field should be investigated to better define soil
properties for ground motion prediction.

REFERENCES

1. Olson, R. E.; Langfelder, L. J.; "Pore Water Pressures in Unsaturated Soils," _Proceedings, ASCE_, 91, SM4, 1965, pp. 127-150.

2. Perloff, W. H.; Osterberg, J. O.,; "The Effect of Strain Rate on the Undrained Shear Strength of Cohesive Soils," _Proceedings, Second PanAmerican Conference on Soil Mechanics and Foundation Engineering_, 1, 1962, pp. 103-128.

3. Skempton, A. W.; "The Colloidal 'Activity' of Clays," _Proceedings, Third Intern. Conf. on Soil Mechanics and Foundation Engineering_, 1, 1948, pp. 57-61.

4. Langfelder, L. J.; "An Investigatigation of Initial Negative Pore Water Pressure in Statically Compacted Cohesive Soils," Ph.D. thesis, University of Illinois, Urbana, Illinois, 1964, 123 pp.

5. Bishop, A. W.; Henkel, D. J., _The Triaxial Test_, Edward Arnold Ltd., London, 1957.

6. Kane, H.; Davisson, M. T.,; Olson, R. E.; Sinnamon, G. K.; _A Study of The Dynamic Soil-Structure Interaction Characteristics of Soil_, RTD-TDR-63-3116 (AF 29 60; 5535), AF Special Weapons Center, Kirtland AFB, NM, January, 1964.

7. Bishop, A. W.; "The Measurement of Pore Pressure in the Triaxial Test," _Proceedings, Conf. on Pore Pressure and Suction in Soils_, Butterworths, London, 1961, pp. 38-46.

8. Skempton, A. W.; "The Pore-Pressure Coefficients A and B," _Geotechnique_, 4, 1954, pp. 143-147.

9. Bishop, A. W.; "Discussion," _Proceedings, Conf. on Pore Pressure and Suction in Soils_, Butterworths, London, 1961, pp. 63-66.

10. Casagrande, A.; Wilson, S. D., "The Effect of Rate of Loading on Strength of Clays and Shales at Constant Water Content," _Geotechnique_, 2, 1951, pp. 251-263.

123